Near-field radiative heat transfer and noncontact friction

A. I. Volokitin*

Institut für Festkörperforschung, Forschungszentrum Jülich, D-52425, Germany and Samara State Technical University, 443100 Samara, Russia

B. N. J. Persson

Institut für Festkörperforschung, Forschungszentrum Jülich, D-52425, Germany

(Published 24 October 2007)

All material bodies are surrounded by a fluctuating electromagnetic field because of the thermal and quantum fluctuations of the current density inside them. Close to the surface of planar sources (when the distance $d \ll \lambda_T = c\hbar/k_B T$), thermal radiation can be spatially and temporally coherent if the surface can support surface modes like surface plasmon polaritons, surface phonon polaritons, or adsorbate vibrational modes. The fluctuating field is responsible for important phenomena such as radiative heat transfer, the van der Waals interaction, and the van der Waals friction between bodies. A general formalism for the calculation of the power spectral density for the fluctuating electromagnetic field is presented and applied to the radiative heat transfer and the van der Waals friction using both the semiclassical theory of the fluctuating electromagnetic field and quantum field theory. The radiative heat transfer and the van der Waals friction are greatly enhanced at short separations ($d \ll \lambda_T$) between the bodies due to the evanescent electromagnetic waves. Particularly strong enhancement occurs if the surface of the body can support localized surface modes like surface plasmons, surface polaritons, or adsorbate vibrational modes. An electromagnetic field outside a moving body can also be created by static charges which are always present on the surface of the body due to inhomogeneities, or due to a bias voltage. This electromagnetic field produces electrostatic friction which can be greatly enhanced if on the surface of the body there is a two-dimensional electron or hole system, or an incommensurate adsorbed layer of ions exhibiting acoustic vibrations. Applications of radiative heat transfer and noncontact friction to scanning probe spectroscopy are discussed. The theory gives a tentative explanation for the experimental noncontact friction data.

DOI: 10.1103/RevModPhys.79.1291 PACS number(s): 44.40.+a, 42.50.Lc, 68.35.Af, 68.37.Ps

CONTENTS

*avoli@samgtu.ru

I. INTRODUCTION

Studies of thermal radiation from materials have played an important role in the history of physics. It is enough to mention that quantum mechanics originated from attempts to explain paradoxical experimental results related to blackbody radiation. In the past, the nonradiative near-field part of electromagnetic radiation was usually ignored because it plays no role in the far-field properties of emission from planar sources. Nevertheless, recent interest in microscale and nanoscale radiative heat transfer (Pendry, 1999; Mulet *et al.*, 2001; Volokitin and Persson, 2001a, 2001b, 2003a, 2004; Joulain *et al.*, 2005), together with the development of local-probe thermal microscopy (Majumdar, 1999; Kittel *et al.*, 2005), has raised new challenges. These topics and the recent progress in detecting the noncontact friction force on a subattonewton level (Dorofeyev *et al.*, 1999; Gotsmann and Fuchs, 2001; Mamin and Rugar, 2001; Stipe *et al.*, 2001; Kuehn, Loring, and Marohn, 2006; Rast *et al.*, 2007) and the observation of coherent thermal emission from doped silicon and silicon carbide (SiC) gratings (Greffet *et al.*, 2002) have in common the substantial role of the nonradiative (evanescent) thermal field.

A. Radiative heat transfer

It is well known that the radiative heat flux per unit area between two blackbodies separated by $d \gg \lambda_T = c\hbar/k_B T$ is given by the Stefan-Boltzmann law

$$S = \frac{\pi^2 k_B^4}{60\hbar^3 c^2}(T_1^4 - T_2^4), \tag{1}$$

where T_1 and T_2 are the temperatures of solids 1 and 2, respectively, and c is the velocity of light. In this limiting case the heat transfer between two bodies is determined by the propagating electromagnetic waves radiated by the bodies and does not depend on the separation d (see Fig. 1). These propagating waves always exist outside any body due to thermal and quantum fluctuations of the current density inside the body. Quantum fluctuations are related to the uncertainty principle, and exist also at zero temperature. Thermal fluctuations are due to the irregular thermal motion of the particles in the medium, and vanish at zero temperature. The electromagnetic field created by this fluctuating current density exists not only in the form of propagating waves but also in the form of evanescent waves, which are damped exponentially with distance away from the surface of the body. This fluctuating electromagnetic field exists even at zero temperature, generated by quantum fluctuations. For an isolated body, the evanescent waves do not give any contribution to energy radiation, which is determined by the Stefan-Boltzmann law. However, for two solids separated by $d < \lambda_T$, the heat transfer may increase by many orders of magnitude due to the evanescent electromagnetic waves; this is often referred to as photon tunneling. The concept of photon tunneling can be illustrated by considering a transparent dielectric such as glass (see Fig. 2). Within the dielectric, blackbody radiation has a higher density than in the vacuum, as can be seen from Eq. (1); if the velocity of light is reduced, the density of radiation increases. The extra radiation is contained in waves that have large wave vectors q parallel to the surface. The normal component of the wave vector, which in the vacuum region is given by $\gamma = \sqrt{(\omega/c)^2 - q^2}$, will be purely imaginary for $q > \omega/c$, where ω is the electromagnetic wave frequency. This means that photons with $q > \omega/c$ cannot escape from the body and will be totally reflected from the surface. This phenomenon is known as total internal reflection. Thus the surface reflects just the right amount of radiation to ensure that the intensity of the blackbody radiation emerging into vacuum does not exceed that allowed by Eq. (1).

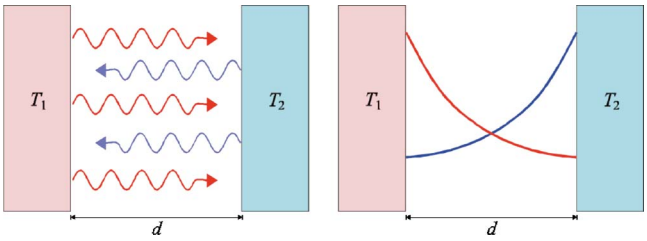

FIG. 1. (Color online) There are two modes for exchange of heat between two surfaces separated by vacuum: (a) conventional radiative heat transfer via propagating electromagnetic waves and (b) photon tunneling via evanescent waves.

It is well known that a second dielectric, if close enough to the first one, will modify the internal reflection condition so that some of the evanescent photons tunnel across into the second medium.

We consider the electromagnetic field at a distance d from a surface. The region in the q space occupied by the propagating waves is $q < k_B T/\hbar c$. The phase-space region occupied by the evanescent waves is $q < d^{-1}$. Thus, as illustrated in Fig. 3, at short distances $d \ll \lambda_T$ the number of photon states available to conduct heat may be much larger for the evanescent waves than for the propagating waves. At low temperatures (a few kelvin) it is possible for photon tunneling to dominate the heat

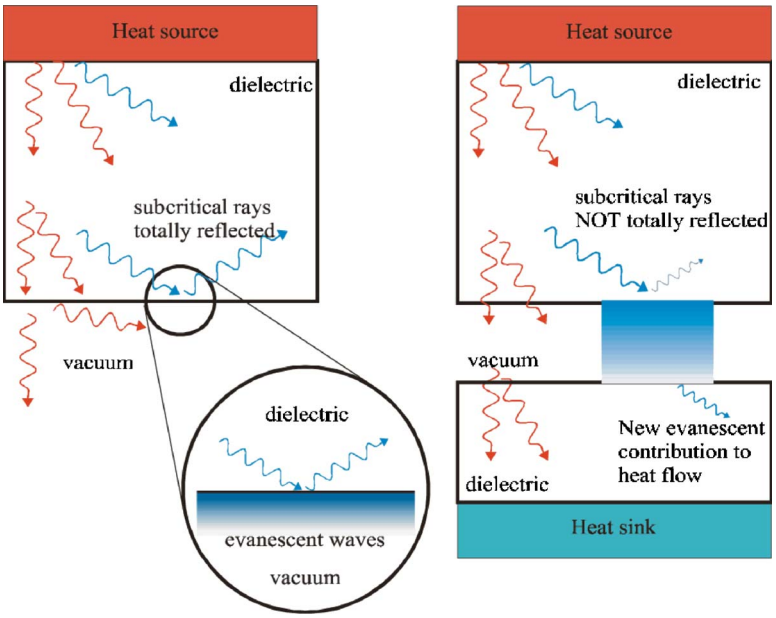

FIG. 2. (Color online) Evanescent waves play no role in thermal radiation from a hot dielectric surface to vacuum (left), but evanescent waves can carry heat from a hot to a cold dielectric surface (right).

transfer even at a spacing of a few millimeters (see Table I).

A great deal of attention has been devoted to the radiative heat transfer due to evanescent waves in connection with scanning tunneling microscopy and scanning thermal microscopy (STM) under ultrahigh-vacuum conditions (Majumdar, 1999; Pendry, 1999; Mulet *et al.*, 2001; Volokitin and Persson, 2001a, 2001b, 2003a, 2004; Joulain *et al.*, 2005; Kittel *et al.*, 2005). It is now possible to measure extremely small amounts of heat transfer into small volumes (Barnes *et al.*, 1994). STM can be used for local heating of the surface, resulting in local desorption or decomposition of molecular species, and this offers further possibilities for the control of the local chemistry at surfaces by STM.

The problem of the radiative heat transfer between two flat surfaces was considered many years ago by Polder and Van Hove (1971), Levin *et al.* (1980), and more recently by Loomis and Maris (1994), Pendry (1999), Volokitin and Persson (2001a, 2003a, 2004) and Mulet *et al.* (2002). Polder and Van Hove were the first to obtain the correct formula for the heat transfer between two flat surfaces. In their investigation, they used Rytov's theory (Rytov, 1953; Levin and Rytov, 1967; Rytov *et al.*, 1989) of the fluctuating electromagnetic field. Later this formula was rederived by Loomis and Maris (1994). However, they presented their result within the local optical approximation, where the spatial variation of the dielectric function is neglected. In the subsequent treatment, they made numerical calculations not of the heat flux itself, but of its derivative with respect to temperature, i.e., their numerical result is valid only for small temperature differences. Levin *et al.* (1980) used the generalized Kirchhoff law (Levin and Rytov, 1967) to obtain an expression for the radiative heat transfer between two good conductor surfaces. They studied the case of good conductors in detail, in both the normal and the anomalous skin effect regions. Pendry (1999) gave a more compact derivation of the formula for the heat flux between two semi-infinite bodies due to evanescent waves and calculated the heat transfer between

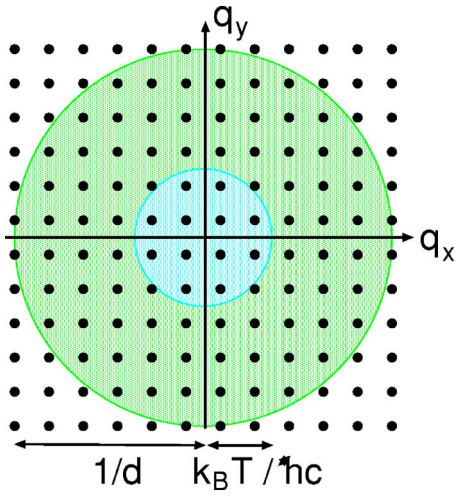

FIG. 3. (Color online) At short distances, evanescent states dominate in phase space: propagating photon modes carry heat flux within the inner circle, evanescent modes within the outer circle.

TABLE I. Critical distance λ_T as a function of temperature. For surface separation $d < \lambda_T$, the heat transfer is dominated by contribution from the evanescent electromagnetic modes. At distances of a few nanometers, radiative heat flow is almost entirely due to the evanescent modes.

T (K)	λ_T (μm)
1	2298.8
4.2	545.2
100	22.9
273	8.4
1000	2.3

a point dipole and a surface. Volokitin and Persson (2001a) considered the problem of heat transfer between two flat surfaces as a particular application of a general theory for heat transfer between bodies with arbitrary shape. They investigated numerically the dependence of the heat flux on the dielectric properties of the bodies both in the local optical approximation and using the nonlocal optical dielectric approach, and found that for good conductors, even for very small distances, the heat flux is dominated by retardation effects. The efficiency of the radiative heat transfer depends strongly on the dielectric properties of the media. It was found in these works that the heat flux diverges as the distance decreases if the temperature difference is assumed to be kept at a constant value. These results were obtained using a macroscopic theory where the spatial variation of the dielectric function was neglected. This macroscopic theory is valid only if the separation between bodies is much larger than the interatomic distances inside the bodies. Thus the precise magnitude of the heat flux between surfaces in actual contact is not yet known. However, it is possible to determine an upper limit for the heat flux, which at short separation depends only on the properties of the materials (Pendry, 1999) (see also Sec. IV.B). This result is linked to quantum information theory, which dictates that the maximal heat tunneling current in one channel is determined by the temperature alone (Pendry, 1983, 1999). The nonlocal dielectric response for the thermal electromagnetic field near a planar surface was recently discussed by Henkel and Joulain (2006).

Early pioneering measurements of the radiative heat transfer between flat chromium bodies were restricted to gap widths above 1 μm (Hargreaves, 1969). Later studies employing an indium needle in close proximity to a planar thermocouple remained inconclusive (Xu *et al.*, 1994), but an unambiguous demonstration of near-field radiative heat transfer under ultrahigh-vacuum conditions was given by Müller-Hirsch *et al.* (1999) and Kittel *et al.* (2005). It was found that for tip-sample distances below 10 nm the heat flux differs markedly from the divergent behavior predicted by macroscopic theory in which the local optical approximation is used. While the shortcomings of the local optical approximation in macroscopic theory are well known (Lifshitz and Pitaevskii, 1980; Rytov *et al.*, 1989), their manifestation in an actual experiment indicates a still unexplored potential of thermal microscopy as a new, quantitative tool for the nanometer-scale investigation of solids.

Pendry (1999) and Volokitin and Persson (2001a, 2004) showed that the heat flux can be greatly enhanced if the conductivities of the materials are chosen to maximize the heat flow due to photon tunneling. At room temperature, the heat flow is maximal at conductivities corresponding to semimetals. In fact, only a thin film ($\sim$10 Å) of a high-resistivity material is needed to maximize the heat flux. Another mechanism of enhancement for radiative heat transfer can be connected with resonant photon tunneling between states localized on the different surfaces. Recently it was discovered that resonant photon tunneling between surface plasmon modes gives rise to an enhancement of the optical transmission through subwavelength hole arrays (Krishnan *et al.*, 2001). The same coupling will enhance the radiative heat transfer [and the van der Waals friction (Volokitin and Persson, 2003b, 2003c)] if the frequency of these modes is sufficiently low to be excited by thermal radiation. At room temperature only modes with frequencies below $\sim 10^{14}\ s^{-1}$ can be excited. For normal metals, surface plasmons have much too high frequencies; at thermal frequencies, the dielectric function of normal metals becomes near purely imaginary, which excludes surface plasmon enhancement of the heat transfer for good conductors. However, surface plasmons for semiconductors are characterized by much smaller frequencies and damping constants, and can contribute to the heat transfer.

Enhancement of the heat transfer due to resonant photon tunneling between surface plasmon modes localized on the surfaces of semiconductors was predicted by Mulet *et al.* (2001) and Volokitin and Persson (2003a, 2004). In this case, multiple scattering of electromagnetic waves by the surfaces of the bodies becomes important. In particular, at sufficiently small separation d, photons go back and forth several times in the vacuum gap, building up a coherent constructive interference in the forward direction much as would occur in resonant electron tunneling. In this case, the surface plasmons on the isolated surfaces combine to form a surface plasmon molecule, in much the same way electronic states of isolated atoms combine to form molecular levels. This will result in a weak distance dependence of the heat flux because the photon transmission probability does not depend on d in this case (see below). For large d, sequential tunneling is more likely, where a surface plasmon mode decays by emitting a photon, which tunnels to other surface where it excites a plasmon, and then couples to other excitations in the media and exits. Other surface modes that can be excited by thermal radiation are adsorbate vibrational modes. Especially for parallel vibrations, these modes may have very low frequencies. Adsorbate vibrational mode enhancement of the radiative heat transfer was predicted by Volokitin and Persson (2003a, 2004) using a macroscopic approach (Volokitin and Persson, 2004) for separations $d > b$, and a microscopic approach (Volokitin and Persson, 2003a) for $d < b$, where b is the interatomic distance between adsorbates. In the latter case the heat transfer occurs through energy exchange between separate adsorbates. Persson *et al.* (2007) showed that localized photon tunneling between adsorbates can be used for vibrational heating of molecules adsorbed on insulating surfaces. The heat transfer between two small particles (when the size of the particles is much smaller than the separation between them) was first studied by Volokitin and Persson (2001a) and later by Domingues *et al.* (2005). It has been shown that at small separation ($d \ll \lambda_T$) the dipole-dipole interaction yields a large contribution to the heat transfer, whereas the contribution of the photon emission and absorption process is negligible. This near-field

transfer between nanoparticles is analogous to the energy transfer between molecules due to dipole-dipole coupling, known as Forster transfer (Forster, 1948).

B. Noncontact friction

The problem of radiative heat transfer is closely related to noncontact friction between nanostructures, including, for example, the frictional drag force between electrons in two-dimensional quantum wells (Gramila *et al.*, 1991, 1992, 1993, 1994; Sivan *et al.*, 1992), and the frictional force between an atomic force microscope tip and a substrate (Dorofeyev *et al.*, 1999; Gotsmann and Fuchs, 2001; Mamin and Rugar, 2001; Stipe *et al.*, 2001). A great deal of attention has been devoted to the problem of noncontact friction because of its importance for ultrasensitive force detection experiments. This is because the ability to detect small forces is inextricably linked to friction via the fluctuation-dissipation theorem. According to this theorem, the random force that makes a small particle jitter will also cause friction if the particle is dragged through the medium. For example, the detection of single spins by magnetic resonance force microscopy (Rugar *et al.*, 2004), which has been proposed for three-dimensional atomic imaging (Sidles *et al.*, 1995) and quantum computation (Berman *et al.*, 2000), will require force fluctuations (and consequently the friction) to be reduced to unprecedented levels. In addition, the search for quantum gravitation effects at short length scales (Arkani-Hamed *et al.*, 1998), and future measurements of the Casimir and van der Waals forces (Mohideen and Roy, 1998), may eventually be limited by noncontact friction effects.

In noncontact friction, the bodies are separated by a potential barrier thick enough to prevent electrons or other particles with a finite rest mass from tunneling across it, but allowing interaction via the long-range electromagnetic field, which is always present in the gap between bodies. The presence of an inhomogeneous tip-sample electric field is difficult to avoid, even under the best experimental conditions (Stipe *et al.*, 2001). For example, even if both the tip and the sample were metallic single crystals, the tip would still have corners, and more than one crystallographic plane would be exposed. The presence of atomic steps, adsorbates, and other defects will also contribute to the spatial variation of the surface potential. This is referred to as the "patch effect." The surface potential can also be easily changed by applying a voltage between the tip and the sample. An inhomogeneous electric field can also be created by charged defects embedded in a dielectric sample. The relative motion of the charged bodies will produce friction, which is denoted as *electrostatic friction*.

An electromagnetic field can also be created from the fluctuating current density. This fluctuating electromagnetic field gives rise to the well-known long-range attractive van der Waals interaction between two bodies (Dzyaloshinskii *et al.*, 1961) and is responsible for radiative heat transfer. If the bodies are in relative motion, the same fluctuating electromagnetic field will give rise to a friction, which is denoted as the *van der Waals friction*.

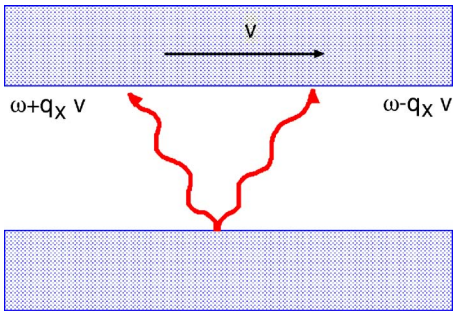

FIG. 4. (Color online) The electromagnetic waves emitted in the opposite direction from the body at the bottom will experience an opposite Doppler shift in the reference frame in which the body at the top is at rest. Due to the frequency dispersion of the reflection amplitude these electromagnetic waves will reflect differently from the surface of the body at the top, which gives rise to momentum transfer between the bodies. This momentum transfer is the origin of van der Waals friction.

The origin of the van der Waals friction is closely connected with the van der Waals interaction. The van der Waals interaction arises when an atom or molecule spontaneously develops an electric dipole moment due to quantum fluctuations. The short-lived atomic polarity can induce a dipole moment in a neighboring atom or molecule some distance away. The same is true for extended media, where thermal and quantum fluctuations of the current density in one body induce a current density in the other body; the interaction between these current densities is the origin of the van der Waals interaction. When two bodies are in relative motion, the induced current will lag slightly behind the fluctuating current inducing it, and this is the origin of the van der Waals friction.

The van der Waals interaction is mostly determined by exchange of virtual photons between the bodies (connected with quantum fluctuations), and does not vanish even at zero temperature. On the other hand, the van der Waals friction, at least to lowest order of perturbation theory, and to linear order in the sliding velocity, is determined by exchange of real photons and vanishes at zero temperature.

To clarify the origin of the van der Waals friction consider two flat parallel surfaces, separated by a sufficiently wide vacuum gap, which prevents electrons from tunneling across it. If the surfaces are in relative motion (velocity v), a frictional stress will act between them. This frictional stress is related to an asymmetry of the reflection amplitude along the direction of motion; see Fig. 4. If one body emits radiation, then in the rest reference frame of the second body these waves are Doppler shifted, resulting in different reflection amplitudes. The same is true for radiation emitted by the second body. The exchange of "Doppler-shifted photons" is the origin of van der Waals friction.

From the point of view of quantum mechanics, the van der Waals friction originates from two types of pro-

cesses. (a) Photons are created in each body with opposite momentum and the frequencies of these photons are connected by $vq_x=\omega_1+\omega_2$, where q_x is the momentum transfer. (b) A photon is annihilated in one body and created in another. The first process (a) is possible even at zero temperature, and it gives rise to a friction force which depends cubically on sliding velocity (Pendry, 1997; Volokitin and Persson, 1998, 1999). The second process (b) is possible only at finite temperatures, and gives rise to a friction which depends linearly on the sliding velocity. Thus process (b) will give the main contribution to the friction at sufficiently high temperatures and at not too large velocities.

In contrast to the van der Waals interaction, for which the theory is well established, the field of van der Waals friction is still controversial. As an example, many have studied the van der Waals friction between two flat surfaces in parallel relative motion using different methods, and obtained results that are in sharp contradiction with each other. The first calculation of van der Waals friction was by Teodorovich (1978). Teodorovich assumed that the friction force can be calculated as the ordinary van der Waals force between bodies at rest, whose dielectric functions depend on the velocity due to the Doppler shift. However, from the dynamical modification of Lifshitz's theory, it follows that this is not true (Volokitin and Persson, 1998, 1999). Later, the same approach was used by Mahanty (1980) to calculate the friction between molecules. Both theories predict wrong nonzero friction at the absolute zero of temperature to linear order in the sliding velocity. The same nonzero linear friction at zero temperature was predicted by Dedkov and Kyasov (1999, 2000). Volokitin and Persson (2002) showed that the basic equation in Dedkov and Kyasov (1999, 2000) is incorrect, and a correct treatment gives a vanishing linear friction at $T=0$ K. Schaich and Harris (1981) developed a theory that describes the dependence of friction on the temperature T and on the separation d. However, in their calculations they made a series of unphysical approximations, and for the Drude model their final formula for the friction for parallel relative motion gives a divergent result. The friction obtained by Levitov (1989); Polevoi (1990); and Mkrtchian (1995); vanishes in the limit of infinite light velocity $c\rightarrow\infty$. However, at least for short distances, one can neglect the retardation effects when calculating the van der Waals friction, as well as the van der Waals interaction. Pendry (1997) assumed zero temperature and neglected retardation effects, in which case the friction depends cubically on the velocity. Persson and Zhang (1998) obtained the formula for friction in the limit of small velocities and finite temperature, again neglecting retardation effects. Volokitin and Persson (1998, 1999) developed a theory of the van der Waals friction based on the dynamical modification of the well-known Lifshitz theory (Lifshitz, 1956) of van der Waals interaction. In the nonretarded limit and for zero temperature, this theory agrees with the results of Pendry (1997). Similarly, in the nonretarded limit and for small sliding velocity, this theory agrees with the study of Persson and Zhang (1998). Volokitin and Persson (2003b, 2003c) extended the theory to two flat surfaces in normal relative motion. For resonant photon tunneling between surface-localized states, normal motion has very different effects from parallel relative motion. It was shown that the friction may increase by many orders of magnitude when the surfaces are covered by adsorbates or can support low-frequency surface plasmons. In this case the friction is determined by resonant photon tunneling between adsorbate vibrational modes or surface plasmon modes. When one of the bodies is sufficiently rarefied, this theory gives the friction between a flat surface and a small particle, which in the nonretarded limit agrees with the results of Tomassone and Widom (1997). A theory of the van der Waals friction between a small particle and a flat surface, which takes into account screening, nonlocal optical effects, and retardation effects, was developed by Volokitin and Persson (2002). A quantum field theory of the van der Waals friction between two semi-infinite solids, and between a small neutral particle and a semi-infinite solid, was developed by Volokitin and Persson (2006). The calculated friction agrees with the friction obtained using a dynamical modification of the Lifshitz theory (Volokitin and Persson, 1999, 2002, 2003c).

Gotsmann and Fuchs (2001) reported measurements of a long-range noncontact friction between an aluminum tip and a gold (111) surface. The friction force F acting on the tip was found to be proportional to the velocity v, $F=\Gamma v$. For motion of the tip normal to the surface the friction coefficient is $\Gamma(d)=Cd^{-3}$, where d is the tip-sample spacing and $C=(8.0^{+5.5}_{-4.5})\times10^{-35}$ N s m^2 (Gotsmann and Fuchs, 2001). Later Stipe *et al.* (2001) studied noncontact friction between a gold surface and a gold-coated cantilever as a function of tip-sample spacing d, temperature T, and the bias voltage V. For vibration of the tip parallel to the surface they found $\Gamma(d)=\alpha(T)(V^2+V_0^2)/d^n$, where $n=1.3\pm0.2$ and $V_0\sim0.2$ V. At 295 K, for a spacing $d=100$ Å, they found $\Gamma=1.5\times10^{-13}$ kg s^{-1}, which is ~500 times smaller than the value reported by Gotsmann and Fuchs (2001) at the same distance using a parallel cantilever configuration. An applied voltage of 1 V resulted in a friction $\Gamma=3\times10^{-12}$ kg/s at 300 K and $d=20$ nm. Using the fluctuation-dissipation theorem, the force fluctuations were interpreted in terms of near-surface fluctuating electric fields interacting with static surface charge. Recently, Kuehn, Loring, and Marohn (2006) observed a large noncontact friction over polymer thin films.

Stipe *et al.* (2001) also measured the noncontact friction for fused silica samples. Near the silica surface the friction was found to be an order of magnitude larger than for the gold sample. The silica sample had been irradiated with γ rays which produce E' centers (Si dangling bonds) at a density of 7×10^{17} cm^{-3}. Although the sample is overall electrically neutral, the E' centers are known to be positively charged, creating enhanced field inhomogeneity and causing the noncontact friction to rise by another order of magnitude.

Dorofeyev *et al.* (1999) claimed that the noncontact friction observed by Dorofeyev *et al.* (1999) and Gotsmann and Fuchs (2001) is due to Ohmic losses mediated by the fluctuating electromagnetic field. This claim is controversial, however, since the van der Waals friction for good conductors like copper has been shown (Volokitin and Persson, 1999, 2001a, 2002; Persson and Volokitin, 2000), to be many orders of magnitude smaller than the friction observed by Dorofeyev *et al.* Zurita-Sánchez *et al.* (2004) proposed that the van der Waals friction may be strongly enhanced between the high-resistivity mica substrate and the silica tip. However, the mica substrate and silica tip were coated by gold films thick enough to completely screen the electrodynamic interaction between the underlying dielectrics.

At small separation $d \sim 1$ nm, resonant photon tunneling between adsorbate vibrational modes on the tip and the sample may increase the van der Waals friction by seven orders of magnitude in comparison with that for good conductors with clean surfaces (Volokitin and Persson, 2003b, 2003c). However, the distance dependence ($\sim 1/d^6$) is stronger than observed experimentally (Stipe *et al.*, 2001).

Recently, a theory of noncontact friction was suggested where the friction arises from Ohmic losses associated with the electromagnetic field created by moving charges induced by the bias voltage (Chumak *et al.*, 2004). In the case of a spherical tip this theory predicts the same weak distance dependence of the friction as observed in the experiment, but the magnitude of the friction is many orders of magnitude smaller than found experimentally. Recently (Volokitin and Persson, 2005; Volokitin *et al.*, 2006) we have shown that the electrostatic friction can be greatly enhanced if there is an incommensurate adsorbate layer which can exhibit acoustic vibrations. This theory gives a tentative explanation for the experimental noncontact friction data (Stipe *et al.*, 2001). The large noncontact friction observed by Kuehn, Loring, and Marohn (2006) over thin films of polymers can also be explained by the electrostatic friction (Kuehn, Marohn, and Loring, 2006).

This review is organized as follows. In Sec. II we present a short overview of the basic idea of Rytov's theory of the fluctuating electromagnetic field (Rytov, 1953). This theory was originally developed for calculating the thermal electromagnetic field, but is now the basis for theoretical studies of the van der Waals interaction (Lifshitz, 1956), radiative heat transfer (Polder and Van Hove, 1971; Loomis and Maris, 1994; Volokitin and Persson, 2001a), and van der Waals friction (Volokitin and Persson, 1999, 2003c). In this paper, the theory is applied to the problems of coherent thermal emission from planar sources (Sec. III), radiative heat transfer (Sec. IV), and van der Waals friction (Sec. V). Special attention is paid to the possible mechanism of enhancement of the radiative heat transfer and the van der Waals friction. In Sec. VI we consider electrostatic friction and discuss noncontact friction experiments. In Sec. VII we consider friction resulting from phonon emission and from the internal friction. Section VIII presents the conclusions and the outlook. For another recent review of the coherence properties of thermal radiation and radiative heat transfer in the near-field regime, see Joulain *et al.* (2005). In comparison to this review we present a more general theory of radiative heat transfer, which can be used to study nonlocal optical effects. For further reading on dissipative effects at very small scales in actual devices, see Cleland (2002).

II. THEORY OF FLUCTUATING ELECTROMAGNETIC FIELD

There are two approaches for studying a fluctuating electromagnetic field. The first, due to Rytov (1953), assumes that the fluctuating electromagnetic field is created by thermal and quantum fluctuations of the current density $\mathbf{j}^f$ inside the medium. The average $\langle \mathbf{j}^f \rangle = 0$ but $\langle \mathbf{j}^f \mathbf{j}^f \rangle \neq 0$. The electromagnetic field can be calculated using the Maxwell equations with the fluctuating current density as the source. Knowing the fluctuating electromagnetic field, one can calculate the Poynting vector, the stress tensor, etc., and obtain the heat transfer between bodies (Polder and Van Hove, 1971; Levin *et al.*, 1980; Pendry, 1999; Volokitin and Persson, 2001a), the van der Waals interaction (Lifshitz, 1956; Dzyaloshinskii *et al.*, 1961), and the van der Waals friction (Volokitin and Persson, 1999, 2003c). Of these problems the calculation of van der Waals friction is the most complex because it requires the solution of a complex electrodynamic problem involving moving boundaries (Volokitin and Persson, 1999, 2003c).

In the second approach, the electromagnetic field is described by Green's functions (Dzyaloshinskii *et al.*, 1961), which can be calculated using quantum electrodynamics (Abrikosov *et al.*, 1965). For equilibrium problems like the van der Waals interaction, the two approaches give the same results (Dzyaloshinskii *et al.*, 1961), though the Green's function method is more general. For nonequilibrium problems, Rytov's approach is simpler, and for this reason the correct results for the radiative heat flux (Polder and Van Hove, 1971) and the van der Waals friction between two semi-infinite solids with parallel surfaces (Volokitin and Persson, 1999, 2003c) were first obtained using this approach.

Rytov's theory is based on the introduction of a random current in the Maxwell equations (just as, for example, one introduces a random force in the theory of Brownian motion of a particle). For a monochromatic field [time factor $\exp(-i\omega t)$] in a dielectric, nonmagnetic medium, these equations are

$$\nabla \times \mathbf{E} = i\frac{\omega}{c}\mathbf{B}, \tag{2}$$

$$\nabla \times \mathbf{H} = -i\frac{\omega}{c}\mathbf{D} + \frac{4\pi}{c}\mathbf{j}^f, \tag{3}$$

where $\mathbf{E}$, $\mathbf{D}$, $\mathbf{H}$, and $\mathbf{B}$ are the electric and the electric displacement field, and the magnetic and the magnetic induction fields, respectively. For a nonmagnetic me-

dium $\mathbf{B}=\mathbf{H}$ (the Gaussian system of units is used) and

$$\mathbf{D}(\mathbf{r}) = \int d^3\mathbf{r}' \vec{\vec{\varepsilon}}(\mathbf{r},\mathbf{r}',\omega)\mathbf{E}(\mathbf{r}'), \tag{4}$$

where $\vec{\vec{\varepsilon}}(\mathbf{r},\mathbf{r}',\omega)$ is the dielectric dyadic of the surrounded medium. According to the fluctuation-dissipation theorem (Callen and Welton, 1951; Landau and Lifshitz, 1970; Agarwal, 1975) the average value of the symmetrized correlation functions of the components of $\mathbf{j}^f$ is given by

$$\langle j_i^f(\mathbf{r},\omega) j_k^{f*}(\mathbf{r}',\omega')\rangle = \langle j_i^f(\mathbf{r}) j_k^{f*}(\mathbf{r}')\rangle_\omega \delta(\omega-\omega'), \tag{5}$$

$$\langle j_i^f(\mathbf{r}) j_k^{f*}(\mathbf{r}')\rangle_\omega = \frac{\hbar}{(2\pi)^2}\left(\frac{1}{2}+n(\omega)\right)\omega^2 \,\mathrm{Im}\,\varepsilon_{ik}(\mathbf{r},\mathbf{r}',\omega), \tag{6}$$

$$n(\omega) = \frac{1}{e^{\hbar\omega/k_BT}-1}. \tag{7}$$

From the Maxwell equations it follows that the components of the electric field, produced by the random current density $\mathbf{j}^f$, are given by

$$E_i(\mathbf{r}) = \frac{i}{\omega}\int d^3\mathbf{r}' D_{ik}(\mathbf{r},\mathbf{r}',\omega) j_k^f(\mathbf{r}'), \tag{8}$$

where summation over repeated indices is assumed. The Green's functions of the electromagnetic field $D_{ij}(\mathbf{r},\mathbf{r}',\omega)$ obey the equations

$$(\nabla_i\nabla_k - \delta_{ik}\nabla^2)D_{kj}(\mathbf{r},\mathbf{r}',\omega) - (\omega/c)^2\int d^3x'' \varepsilon_{ik}(\mathbf{r},\mathbf{r}'',\omega)D_{kj}(\mathbf{r}'',\mathbf{r}',\omega) = (4\pi\omega^2/c^2)\delta_{ij}\delta(\mathbf{r}-\mathbf{r}'), \tag{9}$$

$$(\nabla'_j\nabla'_k - \delta_{jk}\nabla'^2)D_{ik}(\mathbf{r},\mathbf{r}',\omega) - (\omega/c)^2\int d^3x'' \varepsilon_{kj}(\mathbf{r}'',\mathbf{r}',\omega)D_{ik}(\mathbf{r},\mathbf{r}'',\omega) = (4\pi\omega^2/c^2)\delta_{ij}\delta(\mathbf{r}-\mathbf{r}'). \tag{10}$$

Using Eqs. (6)–(10), we obtain the cross-spectral density of the electric field emitted by the body at temperature T (Volokitin and Persson, 2001a) (see also Appendix A):

$$\begin{aligned}\langle E_i(\mathbf{r})E_j^*(\mathbf{r}')\rangle_\omega &= \frac{\hbar}{8\pi^2}\coth(\hbar\omega/2k_BT)\int d\mathbf{r}''\int d\mathbf{r}''' \\ &\times \mathrm{Im}\,\varepsilon_{kl}(\mathbf{r}'',\mathbf{r}''',\omega)D_{ik}(\mathbf{r},\mathbf{r}'')D_{jl}^*(\mathbf{r}',\mathbf{r}''') \\ &= \frac{\hbar c^2}{16\pi^2 i\omega^2}\coth(\hbar\omega/2k_BT)\int dS''_{1l} \\ &\times[D_{ik}(\mathbf{r},\mathbf{r}'')\nabla''_l D^*_{jk}(\mathbf{r}',\mathbf{r}'') \\ &- D^*_{jk}(\mathbf{r}',\mathbf{r}'')\nabla''_l D_{ik}(\mathbf{r},\mathbf{r}'')],\end{aligned} \tag{11}$$

where the points $\mathbf{r}$ and $\mathbf{r}'$ are outside the body. Here we have transformed an integral over the volume of the body into an integral over the surface of the body. For evanescent waves the surface of integration can be moved to infinity. Thus, using Eqs. (9) and (10) and taking into account that the surface integral vanishes in this case, we get

$$\langle E_i(\mathbf{r})E_j^*(\mathbf{r}')\rangle_\omega^{\mathrm{evan}} = \frac{\hbar}{2\pi}\coth(\hbar\omega/2k_BT)\,\mathrm{Im}\,D_{ij}(\mathbf{r},\mathbf{r}'). \tag{12}$$

III. COHERENT THERMAL EMISSION FROM PLANAR SOURCES

A particularly important limiting case is radiation from a flat surface, where the cross-spectral density can be written in the form (Volokitin and Persson, 2003c) (see also Appendix A)

$$\langle \mathbf{E}(\mathbf{r})\mathbf{E}^*(\mathbf{r}')\rangle_\omega = \coth(\hbar\omega/2k_BT) \times \int \frac{d^2q}{(2\pi)^2}(\hat{n}w_{ss}\hat{n} + \mathbf{K}w_{pp}\mathbf{K}^*) \times e^{i\mathbf{q}\cdot(\mathbf{x}-\mathbf{x}')}e^{i(\gamma z-\gamma^* z')}, \tag{13}$$

where

$$w_{ss} = \frac{\hbar\omega^2}{4c^2|\gamma|^2}[(\gamma+\gamma^*)(1-|R_s|^2)+(\gamma-\gamma^*)(R_s^*-R_s)], \tag{14}$$

$$w_{pp} = \frac{\hbar}{4|\gamma|^2}[(\gamma+\gamma^*)(1-|R_p|^2)+(\gamma-\gamma^*)(R_p^*-R_p)]. \tag{15}$$

Here $\mathbf{r}=(\mathbf{x},z)$, $\gamma=\sqrt{(\omega/c)^2-q^2}$, $\hat{q}=\mathbf{q}/q$, $\hat{n}=\hat{z}\times\hat{q}$, $\mathbf{K}=q\hat{z}-\gamma\hat{q}$, and R_s and R_p are the reflection amplitudes for s- and p-polarized electromagnetic waves.

Equation (13) describes the temporal and spatial coherence of thermal radiation of the near field emitted into free space by a plane surface. Thermal radiation is often presented as a typical example of an incoherent light source and is in marked contrast to a laser. Whereas a laser is highly monochromatic and a very directional light source, a thermal source has a broad spectrum and is usually quasi-isotropic. However, as is often the case, different behavior can be expected on a microscopic scale. Thus, it has been shown (Carminati and Greffet, 1999; Shchegrov *et al.*, 2000; Greffet *et al.*, 2002) that the field emitted by a thermal source made of a polar material is enhanced by more than four orders of magnitude and is partially coherent at a distance of the order of 10–100 nm. This phenomenon is due to surface electromagnetic waves and can be observed only on materials supporting them. Surface electromagnetic waves are modes that propagate along an interface and decrease exponentially in the perpendicular direction (evanescent waves). The propagation length of these surface waves is typically hundreds of wavelengths, resulting in a long-range spatial correlation of the electromagnetic field along the interface (Carminati and Greffet, 1999; Shchegrov *et al.*, 2000; Greffet *et al.*, 2002). The near-

field properties of the thermal electromagnetic field in the presence of surface electromagnetic waves were reviewed recently by Joulain *et al.* (2005).

There are different types of optically active surface wave. Surface phonon polaritons are observed for polar material such as silicon carbide (SiC), glass, and II-IV and III-V semiconductors. The polaritons are mechanical vibrations (phonons) propagating in a partially ionic material so that each unit cell becomes an oscillating electric dipole. Surface plasmon polaritons are longitudinal electron oscillations (an acoustic-type wave in an electron gas) that can be observed for metals and doped semiconductors, which generate electromagnetic fields with longitudinal polarization. Surface waves due to excitons and vibrations of alkali-metal ions in adlayers have also been observed.

Recent studies have shown that surface phonon polaritons can couple to a propagating wave through a grating (Greffet *et al.*, 2002). Through this coupling, the near-field coherence modifies the far-field emission. The spatial coherence leads to a high directionality of the thermal source—the radiation is emitted in angular lobes as from an antenna. The same effects can be produced with surface plasmon polaritons excited on doped silicon (Marquier *et al.*, 2004). Thermal emission mediated by surface plasmons has been demonstrated for gold (Kreiter *et al.*, 1999). Thermal emission by surface plasmons on tungsten has also been demonstrated experimentally (Laroche *et al.*, 2005). The degree of spatial coherence is extremely high in this case. Pralle (2002) developed a thermally stimulated mid-infrared source that emits radiation within a narrow range of wavelengths ($\delta\lambda/\lambda \leqslant 0.2$). In this experiment the silicon wafer was covered by a metal film. A lattice of holes in the metal mediated the coupling of the surface plasmon states to the emitted light. This technology will afford tunable infrared emitters with high power in a narrow spectral band, which are critical for sensing, spectroscopy, and thermophotovoltaic applications.

The existence of evanescent waves gives rise to a difference in the spectra of electromagnetic emission in the near- and far-field zones. In the far-field zone the Planck energy spectral density $u_{\mathrm{BB}}(\omega)$ of such radiation is obtained by multiplying the thermal energy $\Pi(T,\omega) = \hbar\omega/[\exp(\hbar\omega/k_BT)-1]$ of a quantum oscillator by the density of oscillations (modes) per unit volume, $N(\omega) = \omega^2/\pi^2c^3$:

$$u_{\mathrm{BB}} = \Pi(T,\omega)N(\omega) = \frac{\hbar}{\pi^2c^3}\frac{\omega^3}{\exp(\hbar\omega/k_BT)-1}. \tag{16}$$

According to Eq. (12) the energy density $u(\mathbf{r},\omega)$ of the emitted electric field in the near zone is defined by

$$u(\mathbf{r},\omega) = \frac{1}{8\pi}\langle E_i(\mathbf{r})E_i(\mathbf{r})\rangle_\omega = \frac{\Pi(T,\omega)}{8\pi^2\omega}\,\mathrm{Im}\,D_{ii}(\mathbf{r},\mathbf{r},\omega). \tag{17}$$

For the local optical case, the reflection amplitudes for the interface between vacuum and medium i are determined from well-known Fresnel formulas [see Eq. (B17) in Appendix B]. Using the Fresnel reflection amplitude for s-polarized electromagnetic waves in Eqs. (13) and (17), we get the following distance-independent contribution to the energy density in the near zone ($d < c/\omega\sqrt{|\varepsilon|}$):

$$u_s(\mathbf{r},\omega) = \frac{1}{6\sqrt{2}}u_{\mathrm{BB}}\sqrt{|\varepsilon| + |\varepsilon'|}. \tag{18}$$

Similarly, the p-polarized electromagnetic wave contribution is

$$u_p(\mathbf{r},\omega) = \frac{1}{8}u_{\mathrm{BB}}\left(\frac{c}{\omega d}\right)^3\frac{\varepsilon''}{|\varepsilon+1|^2}, \tag{19}$$

where ε' and ε'' are the real and imaginary parts of the dielectric function $\varepsilon = \varepsilon' + i\varepsilon''$.

For p-polarized electromagnetic waves and $\varepsilon'' \ll 1$, the near-field emission spectrum has a strong peak near the frequency ω_0 defined by the condition $\varepsilon'(\omega_0) = -1$. This effect results from the existence of a large number of surface modes with different wave numbers but with frequencies $\omega \approx \omega_0$ that are very close to each other. Therefore, if ε'' is not very large at $\omega = \omega_0$, the density of surface modes will necessarily display a strong peak at $\omega = \omega_0$. The presence of surface waves is the origin of the peak in the near-field spectrum of SiC at $\omega = 1.78 \times 10^{14}\ \mathrm{s}^{-1}$. However, since surface waves decay exponentially away from the surface, this peak will vanish in the far zone. The presence of a resonance in the density of modes $N(z,\omega)$ is, however, not required for observing spectral changes caused by the loss of evanescent modes. Indeed, in the short-distance regime, the spectrum is given by Eqs. (18) and (19), whereas in the far field, the spectrum is given by Eq. (16) multiplied by the emissivity of the surface. Thus, even in the absence of resonant surface waves, the near-field spectrum is different from the far-field spectrum, but the changes are less dramatic.

Equations (13)–(15) also suggest a new application for near-field spectroscopy. The near-field spectrum at a given distance to the interface gives access to $\mathrm{Im}\,R_{p(s)}$, and one can hope to gain information on the reflection amplitude for large wave vectors, similar to the method usually used to obtain $R_{p(s)}$ for propagating electromagnetic waves from reflectivity measurements. With the rapid development of near-field optical microscopy, such near-field spectra can be measured. This could open the way for a new technique of local solid-state spectroscopy. Measurement of the thermal near field using a scanning near-field microscope has been demonstrated recently (Wilde *et al.*, 2006). This is an important step toward the concept of local spectroscopy.

IV. RADIATIVE HEAT TRANSFER

A. General theory

The theory of electromagnetic fluctuations presented in Sec. II can be used to calculate the heat transfer between any two macroscopic bodies with different tem-

peratures T_1 and T_2, whose surfaces are separated by a distance d, much larger than the lattice constant of the solids. In this case the problem can be treated macroscopically.

In order to calculate the radiative energy transfer between the bodies, we need the ensemble average of the Poynting's vector,

$$\langle \mathbf{S}(\mathbf{r})\rangle_\omega = (c/8\pi)\langle \mathbf{E}(\mathbf{r})\times \mathbf{B}^*(\mathbf{r})\rangle_\omega + \text{c.c.}$$
$$= \frac{ic^2}{8\pi\omega}\{\nabla'\langle \mathbf{E}(\mathbf{r})\cdot\mathbf{E}^*(\mathbf{r}')$$
$$- [\mathbf{E}(\mathbf{r})\cdot\nabla']\mathbf{E}^*(\mathbf{r}')\rangle - \text{c.c.}\}_{\mathbf{r}=\mathbf{r}'}. \quad (20)$$

Thus the Poynting's vector can be expressed through the average of the product of the components of the electric field. According to the theory of fluctuating electromagnetic field, the cross-spectral density of the electric field in the vacuum gap between the bodies 1 and 2 is given by Eqs. (11) and (12) (Volokitin and Persson, 2001a) (see also Appendix A),

$$\langle E_i(\mathbf{r})E_j^*(\mathbf{r}')\rangle_\omega = \frac{[\Pi_1(\omega)-\Pi_2(\omega)]c^2}{8\pi^2 i\omega^3}$$
$$\times \int d\mathbf{S}_1''\cdot\{D_{ik}(\mathbf{r},\mathbf{r}'')\nabla''D_{kj}^*(\mathbf{r}'',\mathbf{r}')$$
$$- D_{kj}^*(\mathbf{r}'',\mathbf{r}')\nabla''D_{ik}(\mathbf{r},\mathbf{r}'')\}$$
$$+ \frac{\Pi_2(\omega)}{\pi\omega}\,\mathrm{Im}\,D_{ij}(\mathbf{r},\mathbf{r}'), \quad (21)$$

where the integration is over the surface of the body 1. The Planck's function of solid 1 is

$$\Pi_1(\omega) = \hbar\omega(e^{\hbar\omega/k_BT_1}-1)^{-1}, \quad (22)$$

and is similar for Π_2. The Green's functions $D_{ik}(\mathbf{r},\mathbf{r}')$ in the space between the bodies can be found by solving Eqs. (9) and (10) with appropriate boundary conditions (Volokitin and Persson, 2001a) (see also Appendix B).

The case of the heat transfer between two semi-infinite bodies with plane parallel surfaces a distance d apart has been studied by many (Polder and Van Hove, 1971; Loomis and Maris, 1994; Pendry, 1999; Volokitin and Persson, 2001a). Polder and Van Hove (1971) were the first to obtain the correct solution of this problem in the local optical approximation, where the spatial dispersion of the dielectric function is neglected. Thus material for which nonlocal optical properties (such as the anomalous skin effect) are important are excluded from their treatment. In general, nonlocal optical effects become important for short separation between bodies when

$$d < v_F\hbar/k_BT, l,$$

where v_F is the Fermi velocity and l is the electron mean free path (Landau and Lifshitz, 1960; Lifshitz and Pitaevskii, 1981). In typical cases nonlocal optical effects become important for $d<1000$ Å (Volokitin and Persson, 2001a). The first theory that included nonlocal optical effects was developed by Volokitin and Persson (2001a), who used the general theory described above. For the plane geometry the solution of Eqs. (9) and (10) is conveniently obtained by representing the Green's functions as Fourier integrals with respect to the transverse coordinates x, y (the z axis being normal to the surfaces); this gives a system of linear inhomogeneous ordinary differential equations from which the Green's functions can be obtained as functions of z (Abrikosov *et al.*, 1965; Volokitin and Persson, 2001a). The solution of these equations, and the calculation of Poynting's vector from the Green's function, are described in Appendix B. Here we present the final result for the heat flux between two semi-infinite bodies, separated by a vacuum gap (width d) (Volokitin and Persson, 2001a):

$$S_z = \int_0^\infty \frac{d\omega}{2\pi}[\Pi_1(\omega)-\Pi_2(\omega)]\Bigg\{\int_{q<\omega/c}\frac{d^2q}{(2\pi)^2}$$
$$\times\left[\frac{[1-|R_{1p}(\mathbf{q},\omega)|^2][1-|R_{2p}(\mathbf{q},\omega)|^2]}{|1-e^{2i\gamma d}R_{1p}(\mathbf{q},\omega)R_{2p}(\mathbf{q},\omega)|^2}\right]$$
$$+ 4\int_{q>\omega/c}\frac{d^2q}{(2\pi)^2}e^{-2|\gamma|d}$$
$$\times\frac{\mathrm{Im}\,R_{1p}(\mathbf{q},\omega)\mathrm{Im}\,R_{2p}(\mathbf{q},\omega)}{|1-e^{-2|\gamma|d}R_{1p}(\mathbf{q},\omega)R_{2p}(\mathbf{q},\omega)|^2} + [p\to s]\Bigg\}, \quad (23)$$

where the symbol $[p\to s]$ stands for terms that are obtained from the first two terms by replacing the reflection amplitude R_p for the p-polarized electromagnetic waves with the reflection amplitude R_s for the s-polarized electromagnetic waves, and where $\gamma = [(\omega/c)^2 - q^2]^{1/2}$. Contributions to the heat transfer from the propagating ($q<\omega/c$) and evanescent ($q>\omega/c$) electromagnetic waves are determined by the first and second terms in Eq. (23), respectively. Because of the presence of an exponential factor in the integrals in Eq. (23), the q integration is effectively limited by $q<\lambda_T^{-1}$ for propagating waves and $q<d^{-1}$ for evanescent waves. Thus from phase-space arguments it follows that the number of available channels for heat transfer for evanescent waves will be larger by a factor of $(\lambda_T/d)^2$ than the number of available channels for propagating waves. For $d=1$ nm and $T=300$ K, this ratio is of the order of $\sim 10^8$.

In the local optical approximation and in the nonretarded limit, Eq. (23) reduces to the results obtained by Polder and Van Hove (1971) and Pendry (1999), respectively.

Equation (23) can be understood qualitatively as follows. The heat flux per unit frequency is (thermal energy) × (transmission coefficient). The transmission coefficient can be written as

$$|A|^2 = |A_1A_2e^{i\gamma d}[1+R_1R_2e^{2i\gamma d}+(R_1R_2e^{2i\gamma d})^2+\cdots]|^2$$
$$= \frac{|A_1|^2|A_2|^2e^{-2\,\mathrm{Im}(\gamma)d}}{|1-R_1R_2e^{2i\gamma d}|^2}, \quad (24)$$

where A_1 and A_2 are the transmission amplitudes for

surfaces 1 and 2, respectively. The transmission amplitudes A for two interfaces with reflection amplitudes R_1 and R_2 is obtained by geometrical progression of subsequent reflections of electromagnetic waves between two surfaces while keeping proper track of the accumulated phase. Finally, one integrates over ω and the allowed q, and subtracts the opposite fluxes.

B. General formulas and limiting cases

We first consider some general consequences of Eq. (23). In the case of heat transfer through propagating photons ($q \leqslant \omega/c$), heat transfer is maximal for blackbodies with zero reflection amplitude, $R=R_r+iR_i=0$. Now, what is the photon-tunneling equivalent of a blackbody? For $q>\omega/c$ there are no constraints on the reflection amplitude $R(q,\omega)$ other than that $\mathrm{Im}\, R(q,\omega)$ is positive, and R_r and R_i are connected by the Kramers-Kronig relation. Therefore, assuming identical surfaces, we are free to maximize the transmission coefficient corresponding to the photon tunneling

$$|A|^2 = \frac{R_i^2 e^{-2kd}}{|1-e^{-2kd}R^2|^2}, \tag{25}$$

where A is a transmission amplitude and $k=|\gamma|$. This function is maximal when (Pendry, 1999)

$$R_r^2 + R_i^2 = e^{2kd}, \tag{26}$$

so that $|A|^2=1/4$. Substituting this result in Eq. (23) gives the maximal contribution from evanescent waves:

$$(S_z)_{\max}^{\mathrm{evan}} = \frac{k_B^2 T^2 q_c^2}{24\hbar}, \tag{27}$$

where q_c is a cutoff in q determined by the properties of the material. It is clear that the largest possible $q_c \sim 1/b$, where b is the interatomic distance. Thus from Eqs. (27) and (1) we get the ratio of the maximal heat flux connected with evanescent waves to heat flux due to blackbody radiation $(S_z)_{\max}/S_{\mathrm{BB}} \approx 0.25(\lambda_T/b)^2$, where $\lambda_T=c\hbar/k_BT$. At room temperature the contribution to the heat flux from evanescent waves will be roughly eight orders of magnitude larger than the contribution from blackbody radiation, and the upper boundary for the radiative heat transfer at room temperature $(S_z)_{\max} \sim 10^{11}$ W m^{-2}. The result that there is a maximum heat flow in a given channel connects with more profound ideas of entropy flow. It has been shown (Pendry, 1983) from general arguments that the maximum flow in a single channel is linked to the flow of energy. Briefly, the arguments were as follows. The flow of information in a channel is limited by

$$\dot{E} \geqslant \frac{3\hbar \ln^2 2}{\pi}\dot{I}^2, \tag{28}$$

where $\dot{E}$ is the energy flow and $\dot{I}$ the information flow. Identifying the energy flow with heat flow S,

$$\dot{E}=S, \quad \dot{I}=\frac{S}{k_BT\ln 2}, \tag{29}$$

we have

$$S \leqslant \frac{\pi k_B^2 T^2}{3\hbar}; \tag{30}$$

hence

$$S \leqslant S_{\max} = 2\sum_{\mathbf{q}} \frac{\pi k_B^2 T^2}{3\hbar}, \tag{31}$$

where the factor of 2 takes into account two possible polarizations. Therefore the maximum in the heat flux per channel is interpreted as conducting the maximal allowed amount of entropy per channel. Naturally, if we sum over all channels, there is a divergence unless there is a cutoff in q, which would be given by the properties of the material.

We apply the general theory to concrete materials. For the local optical case the reflection amplitudes are determined by the Fresnel formulas (B17). For metals the dielectric function can be written as

$$\varepsilon = 1 + 4\pi i\sigma/\omega, \tag{32}$$

where σ is the conductivity, which can be considered as constant in the mid- and far-infrared regions. For good conductors, when $k_BT/4\pi\hbar\sigma \ll 1$ and $\lambda_T|\varepsilon(\omega_T)|^{-3/2} < d < \lambda_T|\varepsilon(\omega_T)|^{1/2}$, where $\omega_T=c/\lambda_T=k_BT/\hbar$, the contribution to the heat transfer from p-polarized waves is determined by

$$S_p \approx 0.2\frac{(k_BT)^2}{\hbar\lambda_T d}\left(\frac{k_BT}{4\pi\hbar\sigma}\right)^{1/2}, \tag{33}$$

while the s-wave contribution for $d<\lambda_T|\varepsilon(\omega_T)|^{-1/2}$ is distance independent:

$$S_s \approx 0.02\frac{4\pi\sigma k_BT}{\lambda_T^2}. \tag{34}$$

For good conductors the heat flux associated with p-polarized electromagnetic waves decreases with the separation as $\sim d^{-1}$, and increases with decreasing conductivity as $\sigma^{-1/2}$. When $k_BT/4\pi\hbar\sigma \geqslant 1$ the heat flux decreases with increasing separation as d^{-2}. Figure 5(a) shows the heat transfer between two semi-infinite silver bodies separated by distance d and at the temperatures $T_1=273$ K and $T_2=0$ K. The s- and p-wave contributions are shown separately, and the p-wave contribution has been calculated using nonlocal optics, i.e., spatial dispersion of the dielectric function was taken into account (the dashed line shows the result using local optics). It is remarkable how important the s contribution is even for short distances. The nonlocal optical contribution to $(S_z)_p$, which is important only for $d<l$ (where l is the electron mean free path in the bulk), is easy to calculate for free-electron-like metals. The nonlocal surface contribution to $\mathrm{Im}\, R_p$ is given by (Persson and Zhang, 1998)

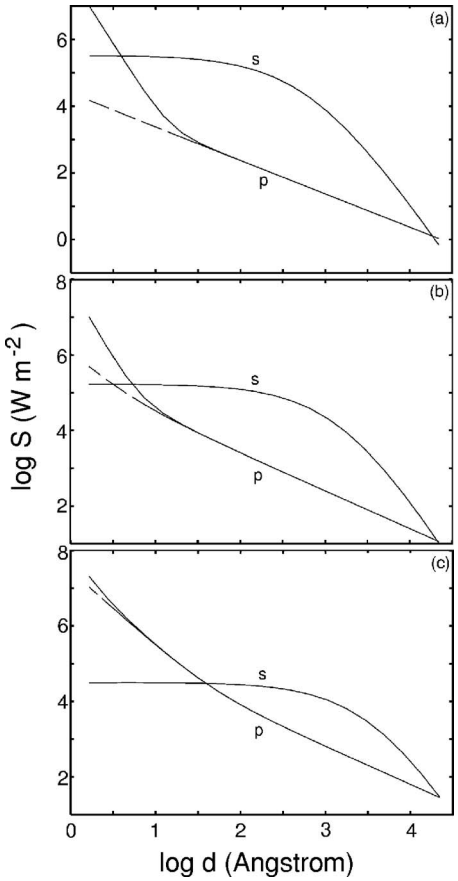

FIG. 5. The heat transfer flux between two semi-infinite silver bodies as a function of the separation d. One body is at temperature $T_1=273$ K and another at $T_2=0$ K. (a) The Drude electron relaxation time τ corresponds to a mean free path $v_F\tau=l=560$ Å. (b) The same as (a) except that l for solid 1 is reduced to 20 Å. (c) The same as (a) except that l is reduced to 3.4 Å. The dashed lines correspond to the results obtained within local optical approximation. (The base of the logarithm is 10.)

$$(\mathrm{Im}\, R_p)_{\mathrm{surf}} = 2\xi \frac{\omega}{\omega_p}\frac{q}{k_F}, \tag{35}$$

where $\xi(q)$ depends on the electron-density parameter r_s but typically $\xi(0)\sim 1$. Using this expression for Im R_p in Eq. (23) gives the (surface) contribution:

$$S_{\mathrm{surf}} \approx \frac{\xi^2 k_B^4}{\omega^2 k_F^2 d^4 \hbar^3}(T_1^4 - T_2^4).$$

Note from Fig. 5(a) that the local optical contribution to $(S_z)_p$ depends nearly linearly on $1/d$ in the distance interval studied, and that this contribution is much smaller than the s-wave contribution. Both these observations are in agreement with the analytical formulas presented above. However, for very high-resistivity materials, the p-wave contribution becomes more important, and a crossover to a $1/d^2$ dependence of $(S_z)_p$ is observed at short separations d. This is illustrated in Figs. 5(b) and 5(c), which have been calculated with the same parameters as in Fig. 5(a), except that the electron mean free path has been reduced from $l=560$ Å (the electron mean free path for silver at room temperature) to 20 Å (roughly the electron mean free path in lead at room temperature) [Fig. 5(b)] and 3.4 Å (of the order of the lattice constant, representing the minimal possible mean free path) [Fig. 5(c)]. Note that when l decreases, the p-wave contribution to the heat transfer increases while the s-wave contribution decreases. Since the mean free path cannot be much smaller than the lattice constant, the result in Fig. 5(c) represents the largest possible p-wave contribution for normal metals. However, the p-wave contribution may be even larger for other materials, e.g., semimetals, with lower carrier concentration than normal metals. For high-resistivity material, when $k_BT/4\pi\hbar\sigma>1$ the heat flux is proportional to the conductivity:

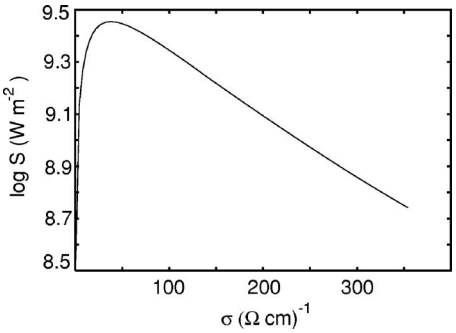

FIG. 6. The thermal flux as a function of the conductivity of the solids. The surfaces are separated by $d=10$ Å. The heat flux for other separations can be obtained using scaling $\sim 1/d^2$, which holds for high-resistivity materials. (The base of the logarithm is 10.)

$$S_p \approx 0.2\frac{k_BT\sigma}{d^2}. \tag{36}$$

By tuning the resistivity of the material we can optimize the photon transmission coefficient across the vacuum gap and hence the potential for heat transport by tunneling. The transmission coefficient $|T(\omega,q)|^2$ is proportional to the energy density of the electromagnetic field associated with evanescent waves:

$$|A(\omega,q)|^2 \sim [\mathrm{Im}\, R_p(\omega,q)e^{-qd}]^2, \tag{37}$$

where $R_p(\omega,q)$ is the reflection amplitude of the surface at wave vector q and frequency ω. For $q \gg |\varepsilon(\omega)|^{1/2}\omega/c$,

$$\mathrm{Im}\, R_p(\omega,q) \approx \mathrm{Im}\,\frac{\varepsilon-1}{\varepsilon+1} \approx \frac{8\pi\sigma/\omega}{4+(4\pi\sigma/\omega)^2}. \tag{38}$$

Assuming that the conductivity σ is independent of ω and q the energy density is maximal when

$$\sigma_{\max} = \frac{\omega}{2\pi} \approx \frac{k_BT}{2\pi\hbar} = 2.3\ T(\Omega\,\mathrm{m})^{-1}, \tag{39}$$

where we have replaced $\hbar\omega$ with the typical thermal energy k_BT. At room temperature the optimum electrical conductivity is 690 $(\Omega\,\mathrm{m})^{-1}$.

To illustrate this case, Fig. 6 shows the thermal flux as

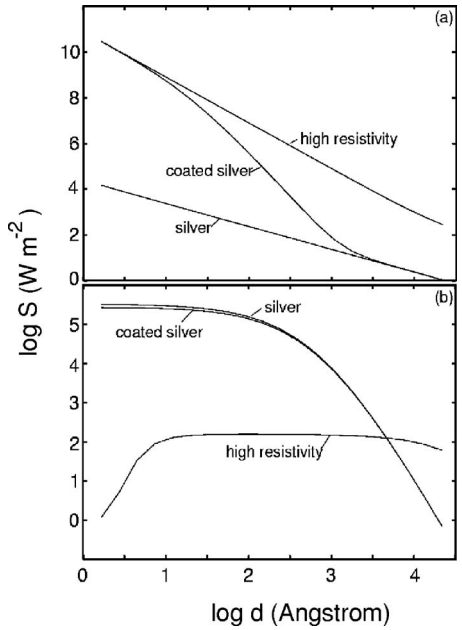

FIG. 7. The heat flux between two semi-infinite silver bodies coated with 10 Å of high resistivity ($\rho=0.14\ \Omega$ cm) material. Also shown is the heat flux between two silver bodies and two high-resistivity bodies. One body is at zero temperature and the other at $T=273$ K. (a), (b) The p- and s-wave contributions, respectively. (The base of the logarithm is 10.)

a function of the conductivity of solids. Again we assume that one body is at zero temperature and the other at $T=273$ K. The solid surfaces are separated by $d=10$ Å. The heat flux for other separations can be obtained using scaling $\sim 1/d^2$ which holds for high-resistivity materials. The heat flux is maximal when $\sigma \approx 920\ (\Omega\ \mathrm{m})^{-1}$.

Finally, we note that a thin high-resistivity coating can drastically increase the heat transfer between two solids. Figure 7 shows the heat flux when thin films (~10 Å) of a high-resistivity material $\rho=0.14\ \Omega$ cm are deposited on silver surfaces. One body is at zero temperature and the other at $T=273$ K. Figures 7(a) and 7(b) show the p and s contributions, respectively. Also shown are the heat fluxes when the two bodies are made from silver and from a high-resistivity material. It is interesting to note that, while the p-wave contribution to the heat flux for coated surfaces is strongly influenced by the coating, the s contribution is nearly unaffected.

C. Resonant photon tunneling enhancement of the radiative heat transfer

Another case when the transmission coefficient can be close to unity is connected with resonant photon tunneling between surface states localized on different surfaces. The resonant condition corresponds to the case when denominators in Eq. (23) are small. For two identical surfaces and $R_i \ll 1 \leqslant R_r$, where R_i and R_r are the imaginary and real parts of the reflection amplitude, this corresponds to the resonant condition $R_r^2 \exp(-2qd)=1$. The resonance condition can be satisfied even for the case when $\exp(-2qd) \ll 1$, since for evanescent electromagnetic waves there is no restriction on the magnitude of the real part or the modulus of R. This opens up the possibility of resonant denominators for $R_r^2 \gg 1$. Close to the resonance we can use the approximation

$$R = \frac{\omega_a}{\omega - \omega_0 - i\eta}, \tag{40}$$

where ω_a is a constant. Then from the resonant condition ($R_r = \pm e^{qd}$) we get the positions of the resonance

$$\omega_\pm = \omega_0 \pm \omega_a e^{-qd}. \tag{41}$$

For the resonance condition to be valid the separation $\Delta\omega = |\omega_+ - \omega_-|$ between two resonances in the transmission coefficient must be greater than the width η of the resonance. This condition is valid only for $q \leqslant q_c \approx \ln(2\omega_a/\eta)/d$.

For $\omega_0 > \omega_a$ and $q_c d > 1$, we get

$$S_{p\pm} = \frac{\eta q_c^2}{8\pi}[\Pi_1(\omega_0) - \Pi_2(\omega_0)]. \tag{42}$$

Note that the explicit d dependence has dropped out of Eq. (42). However, S may still be d dependent, through the d dependence of q_c. For small distances one can expect that q_c is determined by the dielectric properties of the material and thus does not depend on d. In this case the heat transfer will also be distance independent.

Resonant photon tunneling enhancement of heat transfer is possible for two semiconductor surfaces which can support low-frequency surface plasmon modes in the mid-infrared frequency region. The reflection amplitude R_p for a clean semiconductor surface at $d < \lambda_T |\varepsilon(\omega_T)|^{-1/2}$ is given by Fresnel's formula (38). As an example, consider two clean surfaces of silicon carbide (SiC). The optical properties of this material can be described using an oscillator model (Palik, 1985),

$$\varepsilon(\omega) = \varepsilon_\infty \left(1 + \frac{\omega_L^2 - \omega_T^2}{\omega_T^2 - \omega^2 - i\Gamma\omega}\right), \tag{43}$$

with $\varepsilon_\infty = 6.7$, $\omega_L = 1.8 \times 10^{14}\ \mathrm{s}^{-1}$, $\omega_T = 1.49 \times 10^{14}\ \mathrm{s}^{-1}$, and $\Gamma = 8.9 \times 10^{11}\ \mathrm{s}^{-1}$. The frequency of surface plasmons is determined by the condition $\varepsilon'(\omega_0) = -1$ and from Eq. (43) we get $\omega_0 = 1.78 \times 10^{14}\ \mathrm{s}^{-1}$. The resonance parameters are

$$\omega_a = \frac{\omega_L^2 - \omega_T^2}{\varepsilon_\infty \omega_L} = 8.2 \times 10^{12}\ \mathrm{s}^{-1}, \quad \eta = \Gamma/2, \quad q_c = 3.6/d.$$

Using these parameters in Eq. (42), and assuming that one surface is at temperature $T=300$ K and the other at 0 K, we get the heat flux $S(d)$ between two clean surfaces of silicon carbide:

$$S \approx \frac{8.4 \times 10^9}{d^2}\ \mathrm{W\ m^{-2}}, \tag{44}$$

where the distance d is in angstroms. Note that this heat flux is several orders of magnitude larger than that be-

tween two clean good conductor surfaces (see Fig. 5).

D. Adsorbate vibrational mode enhancement of the radiative heat transfer

Another mechanism for resonant photon tunneling enhancement of heat transfer is possible between adsorbate vibrational modes localized on different surfaces. If the distance between adsorbates $d \gg R$, where R is the effective radius of the adsorbate, each adsorbate is equivalent to a point dipole. As shown by Domingues *et al.* (2005), the dipole approximation is valid for distances larger than a few diameters. We consider two particles with dipole polarizabilities $\alpha_1(\omega)$ and $\alpha_2(\omega)$ and with fluctuating dipole moments p_1^f and p_2^f normal to the surfaces. According to the fluctuation-dissipation theorem (Callen and Welton, 1951; Landau and Lifshitz, 1970), the power spectral density for the fluctuating dipole moment is

$$\langle p_i^f p_j^f \rangle_\omega = \frac{\hbar}{\pi}\left(\frac{1}{2} + n_i(\omega)\right) \mathrm{Im}\ \alpha_i(\omega)\delta_{ij}. \tag{45}$$

Assume that the particles are situated opposite to each other on two different surfaces, at the temperatures T_1 and T_2, respectively, and separated by the distance d. The fluctuating electric field of a particle 1 does work on a particle 2. The rate of work is

$$P_{12} = 2\int_0^\infty d\omega\omega\ \mathrm{Im}\ \alpha_2(\omega)\langle E_{12}E_{12}\rangle_\omega, \tag{46}$$

where E_{12} is the electric field created by particle 1 at the position of particle 2:

$$E_{12} = \frac{8p_1^f/d^3}{1 - \alpha_1\alpha_2(8/d^3)^2}. \tag{47}$$

From Eqs. (45)–(47) we get P_{12}, and the rate of cooling of a particle 2 can be obtained by reciprocity using the same formula. Thus the total heat power exchange between particles is

$$P = P_{12} - P_{21} = \frac{2\hbar}{\pi}\int_0^\infty d\omega\omega \frac{\mathrm{Im}\ \alpha_1\ \mathrm{Im}\ \alpha_2(8/d^3)^2}{|1 - (8/d^3)^2\alpha_1\alpha_2|^2} \times [n_1(\omega) - n_2(\omega)]. \tag{48}$$

We first consider some general consequences of Eq. (48). There are no constraints on the particle polarizability $\alpha(\omega) = \alpha' + i\alpha''$ other than that α'' is positive and α' and α'' are connected by the Kramers-Kronig relation. Therefore, assuming identical surfaces, we are free to maximize the photon tunneling transmission coefficient [for comparison see also Eq. (25)];

$$t = \frac{(8\alpha''/d^3)^2}{|1 - (8\alpha/d^3)^2|^2}. \tag{49}$$

This function has a maximum when $\alpha'^2 + \alpha''^2 = (d^3/8)^2$ so that $t = 1/4$. Substituting this result in Eq. (48) gives the upper bound for heat transfer between two particles:

$$P_{\max} = \frac{\pi k_B^2}{12\hbar}(T_1^2 - T_2^2). \tag{50}$$

At a concentration of adsorbed molecules $n_a = 10^{19}\ \mathrm{m}^{-2}$, when one surface is at zero temperature and the other is at room temperature, the maximal heat flux due to the adsorbates $S_{\max} = n_a P_{\max} = 10^{12}\ \mathrm{W\,m}^{-2}$, which is nearly ten orders of magnitude larger than the heat flux due to blackbody radiation, $S_{\mathrm{BB}} = \sigma_B T = 4 \times 10^2\ \mathrm{W\,m}^{-2}$, where σ_B is the Stefan-Boltzmann constant.

The conditions for resonant photon tunneling are determined by

$$\alpha'(\omega_\pm) = \pm d^3/8. \tag{51}$$

Close to resonance we use the approximation

$$\alpha \approx \frac{C}{\omega - \omega_0 - i\eta}, \tag{52}$$

where $C = e^{*2}/2M\omega_0$, and e^* and M are the dynamical charge and mass of the adsorbate, respectively.

For $\eta \ll 8C/d^3$, from Eq. (48) we get

$$P = \frac{\hbar\eta}{2}\{\omega_+[n_1(\omega_+) - n_2(\omega_+)] + (+ \rightarrow -)\}, \tag{53}$$

where $\omega_\pm = \omega_0 \pm 8C/d^3$. Using Eq. (53) we estimate the heat flux between identical surfaces covered by adsorbates with concentration n_a: $J \approx n_a P$. For $8C/d^3 < \eta$ we neglect multiple scattering of the photon between the particles, so that the denominator in the integrand in Eq. (48) is equal to unity. For $d \gg b$, where b is the interparticle spacing, the heat flux between two surfaces covered by adsorbates with concentration n_{a1} and n_{a2} can be obtained after integration of the heat flux between two separated particles. We get

$$S = \frac{24 n_{a1} n_{a2}}{d^4}\int_0^\infty d\omega\ \mathrm{Im}\ \alpha_1\ \mathrm{Im}\ \alpha_2[\Pi_1(\omega) - \Pi_2(\omega)]. \tag{54}$$

Assuming that α can be approximated by Eq. (52), for $\omega_0 \ll \eta$, Eq. (54) gives the heat flux between two identical surfaces:

$$S = \frac{12\pi C^2 n_a^2}{d^4\eta}[\Pi_1(\omega_0) - \Pi_2(\omega_0)]. \tag{55}$$

We note that Eq. (55) can be obtained directly from the heat flux between two semi-infinite solids [determined by Eq. (23)], since in the limit $d > b$ we can use a macroscopic approach, where all information about optical properties of the surface is included in reflection amplitude.

The reflection amplitude for p-polarized electromagnetic waves, which takes into account the contribution from an adsorbate layer, can be obtained using the approach proposed by Langreth (1989). Using this approach, we get (Volokitin and Persson, 2005; Volokitin *et al.*, 2006)

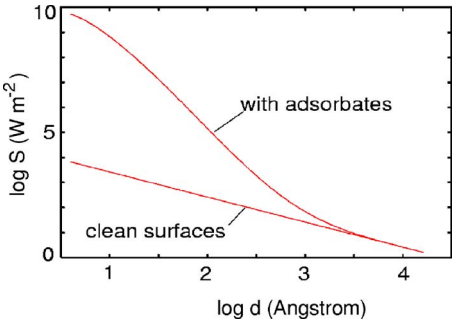

FIG. 8. (Color online) The heat flux between two surfaces covered by adsorbates and between two clean surfaces, as a function of the separation d. One body is at zero temperature and the other at $T=273$ K. For parameters corresponding to K/Cu (001) and Cu (001) (Senet *et al.*, 1999) $\omega_\perp=1.9\times10^{13}$ s^{-1}, $\omega_\parallel=4.5\times10^{12}$ s^{-1}, $\eta_\parallel=2.8\times10^{10}$ s^{-1}, $\eta_\perp=1.6\times10^{12}$ s^{-1}, and $e^*=0.88e$. (The base of the logarithm is 10.)

$$R_p=\frac{1-s/q\varepsilon+4\pi n_a[s\alpha_\parallel/\varepsilon+q\alpha_\perp]-qa(1-4\pi n_a q\alpha_\parallel)}{1+s/q\varepsilon+4\pi n_a[s\alpha_\parallel/\varepsilon-q\alpha_\perp]+qa(1+4\pi n_a q\alpha_\parallel)}, \tag{56}$$

where $s=\sqrt{q^2-(\omega/c)^2\varepsilon}$. The polarizability for ion vibrations (with dynamical charge e^*) normal and parallel to the surface is given by

$$\alpha_{\perp(\parallel)}=\frac{e^{*2}}{M(\omega_{\perp(\parallel)}^2-\omega^2-i\omega\eta_{\perp(\parallel)})}, \tag{57}$$

where $\omega_{\perp(\parallel)}$ is the frequency of the normal (parallel) adsorbate vibration, $\eta_{\perp(\parallel)}$ the corresponding damping constant, and M the adsorbate mass. In comparison with the expression obtained by Langreth (1989), Eq. (56) takes into account that the centers of the adsorbates are located at a distance a away from the image plane of the metal. Although this gives corrections of the order of $qa\ll1$ to the reflection amplitude, for parallel adsorbate vibrations on a good conductor ($|\varepsilon|\gg1$), this correction becomes important (see Sec. V.D.2). As an illustration, in Fig. 8 we compare the heat flux between two Cu(100) surfaces covered by a low concentration of potassium atoms ($n_a=10^{18}$ m^{-2}) with the heat flux between two clean Cu(100) surfaces. At separation $d=1$ nm the heat flux between adsorbate-covered surfaces is enhanced by five orders of magnitude in comparison with the heat flux between clean surfaces, and by seven orders of magnitude in comparison with the blackbody radiation. However, this enhancement of the heat flux disappears if only one of the surfaces is covered by adsorbates. For $d\gg b$ the numerical data can be approximated by

$$S\approx5.6\times10^{-24}\frac{n_a^2}{d^4}\ \mathrm{W\ m^{-2}}, \tag{58}$$

where d is in angstroms.

For $d<b$ the macroscopic approach is not valid and we sum the heat flux between each pair of adatoms. For $\eta=10^{12}$ s^{-1} and $d<10$ Å, when one surface has temperature $T=300$ K and the other $T=0$ K, from Eq. (53) we get a distance independent $P\approx10^{-9}$ W. In this case, for $n_a=10^{18}$ m^{-2} the heat flux $S\approx Pn_a\approx10^9$ W m^{-2}. Under the same conditions the s-wave contribution to the heat flux between two clean surfaces is $S_{\mathrm{clean}}\approx10^6$ W m^{-2}. Thus the photon tunneling between adsorbate vibrational states can strongly enhance the radiative heat transfer between surfaces.

It is interesting to note that in the strong coupling case ($8c/d^3\gg\eta$) the heat flux between two molecules does not depend on the dynamical dipole moments of the molecules [see Eq. (53)]. However, in the opposite case of weak coupling ($8C/d^3\ll\eta$), the heat flux is proportional to the product of the squares of the dynamical dipole moments [see Eq. (54)].

E. Vibrational heating by localized photon tunneling

The radiative heat transfer due to evanescent electromagnetic waves (photon tunneling) may be used for surface modification. Thus if a hot tip is brought ~1 nm from a surface with a thin layer of heat-sensitive polymer, one may induce local polymerization and this may be used for nanoscale lithography. This noncontact mode of surface modification may have several advantages as compared to the contact mode, e.g., no wear or contamination of the tip will occur.

We consider the radiative heat transfer between an adsorbed molecule on a tip and another molecule adsorbed on a substrate. The temperature increase at the adsorbed molecule may be large, which may induce local chemical reactions, e.g., diffusion or desorption. Heat transfer to some adsorbate vibrational mode, i.e., vibrational heating, will be important when the energy relaxation time τ_b of the adsorbate mode is long compared to the relaxation time characterizing the photon tunneling from the tip to the substrate adsorbate. High-frequency adsorbate vibrations on metals typically have short energy relaxation times (in the picosecond range) owing to the continuum of low-energy electronic excitations (Persson and Persson, 1980). However, low-frequency adsorbate vibrations, e.g., frustrated translations, have long relaxation times (typically of the order of nanoseconds for inert adsorbates on noble metals) (Persson, 1991), and in these cases photon tunneling heat transfer may be important. Adsorbate vibrational modes on insulators may have long relaxation times if the resonance frequency is above the top of the bulk phonon band. In these cases energy relaxation is caused by multiphonon processes which often are slow. One extreme example is CO adsorbed on NaCl crystals (Chang and Ewing, 1990), where $\tau_b\approx10^{-3}$ s. For this case even a weak coupling to a hot tip may result in heating of the C-O stretch vibration.

The photon tunneling energy transfer per unit time from a vibrational mode of the tip adsorbate (frequency ω_a and vibrational relaxation time $\tau_a^*=\eta_a^{-1}$) to a vibrational mode (ω_b,τ_b^*) of the substrate adsorbate (see Fig. 9) is given by Eq. (48). The molecular polarizability is given by Eq. (57). The energy transfer rate from the tip

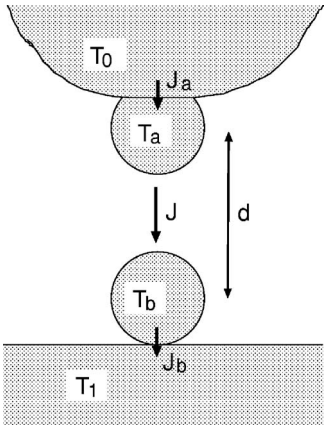

FIG. 9. The heat transfer (photon tunneling) between a tip atom (or molecule) and a substrate atom (or molecule).

to the tip adsorbate is (Volokitin and Persson, 1993)

$$J_a = \frac{\hbar\omega_a}{\tau_a}[n(\omega_a/T_0) - n(\omega_a/T_a)] \tag{59}$$

and the energy transfer rate from the substrate adsorbate to the substrate

$$J_b = \frac{\hbar\omega_b}{\tau_b}[n(\omega_b/T_b) - n(\omega_b/T_1)], \tag{60}$$

where τ_a and τ_b are the vibrational energy relaxation times. Note that in general $1/\tau_a^* > 1/\tau_a$ and $1/\tau_b^* > 1/\tau_b$ since the vibrational relaxation rate $1/\tau^*$, which enters into the polarizability, has contributions from both energy relaxation and pure dephasing. In general, the integral in Eq. (48) must be performed numerically, but as an illustration we consider the case where the relaxation time $\tau_b^* \gg \tau_a^*$. In this case Eq. (48) reduces to

$$P = r\frac{\hbar\omega_b}{\tau_b}[n(\omega_b/T_a) - n(\omega_b/T_b)], \tag{61}$$

where

$$r = \frac{(\tau_b/\tau_b^*)s}{1 + [2(\omega_a - \omega_b)\tau_a^*]^2 + 4s}, \tag{62}$$

$$s = 64\omega_a\tau_a^*\omega_b\tau_b^*\alpha_{va}\alpha_{vb}/d^6, \tag{63}$$

with $\alpha_{va} = e_a^{*2}/M_a\omega_a^2$, and similarly for mode b.

Note that the energy transfer rate J_a (and similarly for J_b) depends only on the energy relaxation rate $1/\tau_a$ and not on the relaxation rate $1/\tau_a^*$, which determines the width of the vibrational resonance state. The latter is the sum of $1/\tau_a$ and a pure dephasing contribution which reflects the fluctuation $\omega_a(t)$ in the vibrational level position due to the irregular thermal motion of atoms in the system, and which depend on the anharmonic coupling between different vibrational modes. This level fluctuation contributes to the vibrational linewidth as observed using, e.g., infrared spectroscopy, but not to the energy transfer between the adsorbate and the solid on which it is adsorbed. On the other hand, the energy transfer rate P between two adsorbates is determined by the overlap in vibrational resonance states and therefore determined by τ_a^* (and τ_b^*), and does not depend on τ_a (or τ_b). [Note that the τ_b^{-1} factor that appears in Eq. (61) cancels out against the factor τ_b in the expression for r.]

In the high-temperature limit $n(\omega/T) \approx k_B T/\hbar\omega$, and assuming that this relation holds for all modes and temperatures relevant here, we get

$$P = r\tau_b^{-1}k_B(T_a - T_b). \tag{64}$$

We also get

$$J_a = \tau_a^{-1}k_B(T_0 - T_a), \tag{65}$$

$$J_b = \tau_b^{-1}k_B(T_b - T_1). \tag{66}$$

Assuming first a steady-state situation so that $P = J_a = J_b$, we get from Eqs. (64)–(66) that $T_a \approx T_0$ and

$$T_b \approx T_1 + \frac{r}{1+r}(T_0 - T_1), \tag{67}$$

where we assumed that $\tau_b \gg \tau_a$.

The theory above can also be used to estimate the time it takes to reach the steady state where the (ensemble-averaged) adsorbate temperature is equal to Eq. (67). In general we have

$$\hbar\omega_b\frac{d}{dt}n[\omega_b/T_b(t)] = J(t) - J_b(t).$$

In the classical limit this gives

$$\frac{dT_b}{dt} = -\frac{1}{\tau_b}(1+r)T_b + \frac{1}{\tau_b}(T_1 + rT_0). \tag{68}$$

If we assume $T_b(0) = T_1$ this gives

$$T_b(t) = T_1 + \frac{r}{1+r}(T_0 - T_1)(1 - e^{-(1+r)t/\tau_b}). \tag{69}$$

Thus for $t \gg \tau$, where $\tau = \tau_b/(1+r)$, the steady-state temperature has been reached.

For adsorbates on insulating substrates τ_b will, in general, be large if the resonance frequency ω_b is well above the highest substrate phonon frequency. We now consider this case, which is equivalent to low temperature. Assume for simplicity that the temperature of the substrate vanishes ($T_1 = 0$) and assume that $\hbar\omega_a \gg k_B T_0$ and $\hbar\omega_b \gg k_B T_0$. In this case is is easy to show from Eqs. (59)–(61) that $T_a \approx T_0$ and

$$T_b \approx \frac{\omega_b T_0}{\omega_b + T_0 \ln[(1+r)/r]}, \tag{70}$$

where we measured the frequency in units of $k_B/\hbar$.

We now assume arbitrary tip and substrate temperatures but with $\tau_b \gg \tau_a$. Using Eqs. (59)–(61) we get $T_a \approx T_0$ and

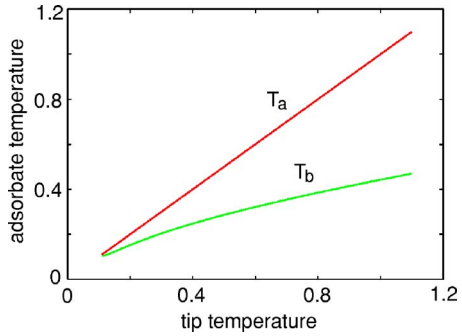

FIG. 10. (Color online) The adsorbate temperature T_a and T_b as a function of the tip temperature T_0 (all in units of $\hbar\omega_b/k_B$). For $r=9.25$ and $T_1=0.1\hbar\omega_b/k_B$.

$$\frac{\omega_b}{T_b} = \ln\left(1 + \frac{1+r}{r(e^{\omega_b/T_0}-1)^{-1} + (e^{\omega_b/T_1}-1)^{-1}}\right). \tag{71}$$

This expression reduces to Eq. (67) for high temperatures and to Eq. (70) for low temperatures. In Fig. 10 we show the effective temperature T_b as a function of the tip temperature T_0 when $T_1=0.1\hbar\omega_b/k_B$ and $r=0.25$.

The effective adsorbate temperature T_b calculated above may be used to calculate (or estimate) the rate w of an activated process: $w=w_0\exp(-E/k_BT_b)$. When the barrier height E is large, even a very small temperature increase will result in a large increase in the reaction rate. Note also that the excitation of a high-frequency mode such as the C-O stretch mode can result in reactions, e.g., diffusion, rotation, or desorption, involving other reaction coordinates. This is possible because of anharmonic coupling between the high-frequency mode and the reaction coordinate mode. This has already been observed in STM studies of several different adsorption systems (Komeda *et al.*, 2002; Pascual *et al.*, 2003).

We give an example of an adsorption system where photon tunneling may give rise to a strong temperature increase. We focus on $^{13}C^{18}O$ on NaCl(100) at $T_1=30$ K, which has been studied by Chang and Ewing (1990). In this case $\omega_b\approx 2040\ \mathrm{cm}^{-1}$, $\tau_b\approx 10^{-3}$ s [due mainly to decay via multiphonon emission (Chang and Ewing, 1990)], and the (pure-dephasing-dominated) relaxation time (Chang *et al.*, 1988) $\tau_b^*\approx 10^{-10}$ s. We assume a Pt tip at room temperature with an adsorbed $^{12}C^{18}O$ with $\omega_a\approx 2064\ \mathrm{cm}^{-1}$ and $\tau_a^*\approx 3\times 10^{-12}$ s (Beckerle *et al.*, 1990) mainly due to decay by excitation of electron-hole pairs. Using the experimentally measured vibrational polarizabilities $\alpha_{av}\approx 0.2$ Å^3 and $\alpha_{bv}\approx 0.04$ Å^3 and assuming the tip-substrate separation $d=1$ nm, we get $s\approx 20$ and $2(\omega_a-\omega_b)\tau_a^*\approx 16$. Thus from Eq. (62) we get $r\approx 10^6$ and from Eq. (71) we get $T_b\approx 300$ K where we have assumed the tip temperature $T_0=300$ K. CO/NaCl is an extreme case because of the exceptionally long vibrational energy relaxation time. However, the analysis presented above remains unchanged for any τ_b larger than 10^{-8} s so the conclusions are very general. Thus we expect strong heating effects due to photon tunneling for high-frequency modes in adsorbed layers or films on insulating substrates.

The temperature increase for the C-O stretch vibration found above is similar to the temperature increase observed (or calculated) for CO on Pd(110) during STM experiments (Komeda *et al.*, 2002). In this case the excitation of the C-O stretch vibration is caused by inelastic tunneling. The temperature increase in the C-O stretch mode resulted in CO diffusion as a result of energy transfer to the parallel frustrated translation because of anharmonic coupling. This has been observed for the CO molecule on Pd(110) (Komeda *et al.*, 2002) and on Ag(110) (Hahn and Ho, 2001). We expect similar decay processes for vibrationally excited CO on NaCl resulting, e.g., in diffusion or desorption of the CO molecule.

F. Radiative heat transfer between a small particle and a plane surface

The problem of radiative heat transfer between a small particle—considered as a pointlike dipole—and a plane surface has been considered (Pendry, 1999; Mulet *et al.*, 2001; Volokitin and Persson, 2002). The particle could be a single molecule or a dust particle, and it is modeled by a sphere with radius $R\ll d$, where d is the separation between the particle and the plane surface. The heat flux between the particle and substrate can be calculated from the rate of work of the fluctuating electromagnetic field on electrons of the particle

$$P = -\frac{dW}{dt} = -\int d^3r\langle \mathbf{j}\cdot\mathbf{E}\rangle, \tag{72}$$

where the integration is over the volume of the particle. In the case $R\ll d$ we consider the sphere as a point dipole located at $\mathbf{r}=\mathbf{r}_0$ and obtain (Volokitin and Persson, 2002)

$$P = \frac{2}{\pi}\int_0^\infty d\omega[\Pi_1(\omega)-\Pi_2(\omega)] \times \sum_{l=x,y,z}\frac{\mathrm{Im}\,\alpha(\omega)\mathrm{Im}\,D_{ll}(\mathbf{r}_0,\mathbf{r}_0)}{|1-\alpha(\omega)D_{ll}(\mathbf{r}_0,\mathbf{r}_0)|^2}, \tag{73}$$

where T_1 and T_2 are the temperatures of the particle and substrate, respectively, $D_{ll}(\mathbf{r},\mathbf{r}')$ is the Green's function of the electromagnetic field of the substrate, and the polarizability of the sphere is given by

$$\alpha = \frac{\varepsilon_p-1}{\varepsilon_p+2}R^3. \tag{74}$$

In the nonresonant case the denominator in Eq. (73) is close to unity, and for distances $R\ll d\ll\lambda_T$ we get (Volokitin and Persson, 2002)

$$P = 2\frac{\hbar}{\pi}\int_0^\infty d\omega\, \omega[n(\omega,T_1) - n(\omega,2)]\int_0^\infty dq\, q^2 e^{-2qd} \times \left\{ 2\,\mathrm{Im}\, R_p(\omega)\mathrm{Im}\,\alpha(\omega) + \left(\frac{\omega}{cq}\right)^2 \mathrm{Im}\, R_s(\omega)\mathrm{Im}\,\alpha(\omega)\right\}. \quad (75)$$

The s-wave contribution will exceed the p-wave contribution for $d > \lambda_T|\varepsilon(\omega_T)|^{-1/2}$; for metals at room temperature this typically gives $d > 30$ nm.

As pointed out by Pendry (1999), large heat transfer is expected for high-resistivity materials. In this case the heat flux between a sphere and a flat surface is given by (Pendry, 1999; Volokitin and Persson, 2002)

$$P_p \approx \frac{2\pi^2}{5}\left(\frac{R}{d}\right)^3\left(\frac{k_B^4}{16\pi^2\hbar^3\sigma_1\sigma_2}\right)(T_1^4 - T_2^4), \quad (76)$$

where $\sigma_{1(2)}$ is the conductivity of the substrate (sphere). The heat flux (76) is maximized when $k_BT/4\pi\hbar\sigma \approx 1$. In this case, for a particle at room temperature a distance $d = 2R = 10$ nm above a cold sample ($T = 0$ K) we get $P_p/d^2 \approx 10^7$ W m^{-2}. This should be compared to the heating from blackbody radiation. When the sample surface at temperature T_2 is illuminated with blackbody radiation at temperature T_1, roughly taking into account the surface reflectivity, the heat flux to the sample from blackbody radiation is approximately (Polder and Van Hove, 1971; Levin *et al.*, 1980; Volokitin and Persson, 2004)

$$S = \frac{1}{8\pi^3}\int_0^\infty d\omega[\Pi_1(\omega) - \Pi_2(\omega)] \times \int_{q<\omega/c} d^2q[1 - |R_p(\omega)|^2] + [p \to s] \approx 0.4\frac{k_B^4T_1^4}{\hbar^3c^2}\left(\frac{k_BT_1}{4\pi\hbar\sigma_1}\right)^{1/2} - [T_1 \to T_2], \quad (77)$$

where $[T_1 \to T_2]$ stands for the term obtained from the first term by replacing T_1 with T_2. For $T_2 \approx 300$ K and $T_1 \approx 0$ K, and for $k_BT/\hbar \approx 4\pi\sigma$, Eq. (77) gives $S_{\mathrm{BB}} \approx 100$ W m^{-2}. Thus, a particle may give rise to a large local enhancement of the heating of the surface, compared to uniform blackbody radiation.

When the substrate and particle are made from the same materials, which can support surface plasmons with frequencies ω_s and ω_p, respectively, in the two-pole approximation the rate of heat transfer between them is

$$P = 6\Gamma\left(\frac{R}{d}\right)^3\{[\Pi_1(\omega_p) - \Pi_2(\omega_p)] + [\omega_p \to \omega_s]\}. \quad (78)$$

For SiC with $\omega_s = 1.79\times10^{14}$ s^{-1} and $\omega_p = 1.76\times10^{14}$ s^{-1}, $d = 10$ nm, $R = 5$ nm, $T_1 = 300$ K, and $T_2 = 0$ K, Eq. (62) gives $P \approx 1.6\times10^{-10}$ W. We note that a much larger effect for the heat transfer can be achieved if the surfaces are covered with adsorbates with matched frequencies (Volokitin and Persson, 2003a, 2004) (see Sec. IV.D).

G. Local heating of the surface by an atomic force microscope tip

An atomic force microscope tip at a distance d above a flat sample surface with the radius of curvature $R \gg d$ can be approximated by a sphere with radius R. In this case the heat transfer power between the tip and surface can be estimated using the approximate formula (Hartmann, 1990, 1991; Johansson and Apell, 1997)

$$P = 2\pi\int_0^\infty d\rho\, \rho S(z(\rho)). \quad (79)$$

Here $z(\rho)$ denotes the tip-surface distance as a function of the distance ρ from the tip symmetry axis, and the heat flux per unit area $S(z(\rho))$ is determined for flat surfaces. This scheme was proposed by Hartmann (1990, 1991) for the calculation of the conservative van der Waals interaction; in this case the error is not larger than 5–10 % in an atomic force application, and 25% in the worst case situation (Johansson and Apell, 1997). We assume that the same scheme is also valid for the calculation of the heat transfer. We assume that the tip has a paraboloid shape given [in cylindrical coordinates (z,ρ)] by $z = d + \rho^2/2R$, where d is the distance between the tip and the flat surface. If

$$S = C\left(d + \frac{\rho^2}{2R}\right)^{-n}, \quad (80)$$

we get

$$P = \frac{2\pi R}{n-1}\frac{C}{d^{n-1}} = \frac{2\pi Rd}{n-1}S(d) \equiv A_{\mathrm{eff}}S(d), \quad (81)$$

where $A_{\mathrm{eff}} = 2\pi Rd/(n-1)$ is the effective surface area. In a more general case one must use numerical integration to obtain the heat transfer.

As an illustration, consider the heat flux between a SiC tip and a flat SiC surface. From Eqs. (80) and (44) we get the heat transfer power between the SiC tip at $T_1 = 300$ K and a cold SiC surface ($T_2 = 0$ K) at $R \gg d$: $P(d) = 5.2\times10^{-10}(R/d)$ W.

H. Nanoscale "heat stamp"

It has been proposed (Schmid *et al.*, 1998) that near-field optics could be exploited to write extremely fine details for integrated circuits. The basic idea of this proposal is that the components of the electromagnetic field having short wavelength (and therefore the potential for high resolution) are naturally evanescent and do not contribute to the far field. Hence fine details in any patterned mask will rapidly disappear with distance from the mask. However, if it is possible to position the wafer close to the mask then fine details can be resolved. Roughly speaking, the separation between mask and wafer must be of the same order as the lateral details to be resolved.

An extension of this idea was suggested (Pendry, 1999) in the form of "heat stamp." It is possible to imagine a mask consisting of a surface patterned alternatively

in highly reflecting (and therefore poorly emitting) material, and a second material chosen to maximize emission of heat into the evanescent modes. For adsorbate-covered structures it is possible to have a heat stamp with atomic resolution.

V. VAN DER WAALS FRICTION

A. General formalism

There are two approaches to the theories of the van der Waals interaction and the van der Waals friction. In the first approach, the fluctuating electromagnetic field is considered as a classical field which can be calculated from Maxwell's equation with the fluctuating current density as the source of the field, and with appropriate boundary conditions. This approach was used by Lifshitz in the theory of the van der Waals interaction (Lifshitz, 1956) and by Volokitin and Persson for the van der Waals friction (Volokitin and Persson, 1999, 2003c). The calculation of the van der Waals friction is more complicated than the van der Waals force because it requires determination of the electromagnetic field between moving boundaries. The solution can be found by writing the boundary conditions on the surface of each body in the rest reference frame of this body. The relation between electromagnetic fields in different reference frames is determined by the Lorenz transformation. The advantage of this approach is that, in principle, it can be used for the calculation of friction at arbitrary relative velocities. However, the calculations become complicated for bodies with complex geometry. At present the solutions are known for the van der Waals friction between two parallel plane surfaces (Volokitin and Persson, 1999, 2003c), and between a small particle and a plane surface (Volokitin and Persson, 2002).

In the second approach, the electromagnetic field is treated in the frame of the quantum field theory. This approach was used by Dzyaloshinskii *et al.* (1961) to obtain the van der Waals interaction for an arbitrary inhomogeneous medium, all parts of which are at rest.

For two bodies in slow uniform relative motion (velocity $\mathbf{v}$) the force acting on either body may be $\mathbf{F}=\mathbf{F}_0-\overleftrightarrow{\Gamma}\cdot\mathbf{v}$, where the adiabatic force $\mathbf{F}_0$ is independent of $\mathbf{v}$, and $\overleftrightarrow{\Gamma}$, the so-called friction tensor, is defined by

$$\overleftrightarrow{\Gamma}=(k_BT)^{-1}\,\mathrm{Re}\int_0^\infty dt\langle\hat{\mathbf{F}}(t)\hat{\mathbf{F}}(0)\rangle. \tag{82}$$

Here $\langle\cdots\rangle$ represents the thermal average of the force-force correlation function in the equilibrium state at fixed separation d between bodies, and $\hat{\mathbf{F}}(t)$ is the force operator in the Heisenberg representation. Equation (82) is a consequence of the fluctuation-dissipation theorem (Callen and Welton, 1951; Landau and Lifshitz, 1970). For the interaction between a localized and an extended system, Eq. (82) has been derived (Schaich, 1974a, 1974b; d'Agliano *et al.*, 1975; Nourtier, 1977) and is also valid for two extended systems. In the context of the van der Waals friction, Eq. (82) was used by Schaich and Harris (1981), but their treatment is incomplete.

In the case of extended systems the fluctuating force operator can be expressed through the operator of the stress tensor $\hat{\sigma}_{ik}$,

$$\hat{F}_i=\int dS_k\hat{\sigma}_{ik}, \tag{83}$$

where the integration is over the surface of one of the bodies and

$$\hat{\sigma}_{ik}=\frac{1}{4\pi}\left(E_iE_k+B_iB_k-\frac{1}{2}\delta_{ik}(E^2+B^2)\right), \tag{84}$$

where E_i and B_i are the electric and magnetic induction field operators, respectively. The calculation of the force-force correlation function can be done using quantum field theory (Abrikosov *et al.*, 1965; Mahan, 1990). Such calculations have been described by Volokitin and Persson (2006). The advantage of this approach is that it involves only finding the Green's functions of the electromagnetic field for the equilibrium system with fixed boundaries. Thus this approach can be easily extended to bodies with complex geometry. However, it is restricted to small relative velocities.

B. van der Waals friction between two plane surfaces in parallel relative motion at arbitrary sliding velocities

The van der Waals frictional stress $\sigma_\parallel$, which acts on the surfaces of two bodies in parallel relative motion with arbitrary sliding velocity v, is given by (Volokitin and Persson, 1999)

$$\begin{aligned}\sigma_\parallel=&\frac{\hbar}{8\pi^3}\int_0^\infty d\omega\int_{q<\omega/c}d^2q\,q_x\left\{\frac{(1-|R_{1p}|^2)(1-|R_{2p}^-|^2)}{|1-e^{2i\gamma d}R_{1p}R_{2p}^-|^2}\right.\\&\left.\times[n(\omega-q_xv)-n(\omega)]+[R_p\to R_s]\right\}\\&+\frac{\hbar}{2\pi^3}\int_0^\infty d\omega\int_{q>\omega/c}d^2q\,q_xe^{-2|\gamma|d}\\&\times\left\{\frac{\mathrm{Im}\,R_{1p}\,\mathrm{Im}\,R_{2p}^-}{|1-e^{-2|\gamma|d}R_{1p}R_{2p}^-|^2}[n(\omega-q_xv)-n(\omega)]\right.\\&\left.+[R_p\to R_s]\right\},\end{aligned} \tag{85}$$

where $n(\omega)=[\exp(\hbar\omega/k_BT)-1]^{-1}$ and $[R_p\to R_s]$ denotes the term that is obtained from the first one by replacement of the reflection amplitude $R_p(\omega)$ for p-polarized electromagnetic waves, by the reflection amplitude $R_s(\omega)$ for s-polarized electromagnetic waves, and with $R_{p(s)}^{\pm}=R_{p(s)}(\omega\pm q_xv)$. Equation (85) was obtained by Volokitin and Persson (1999) using the dynamical modification of Lifshitz theory (Lifshitz, 1956) for the van der Waals interaction. The first term in Eq. (85) represents the contribution to friction from propagating waves ($q<\omega/c$), and the second term from evanescent waves ($q>\omega/c$). It can be shown that Eq. (85) is valid even when

the spatial dispersion of the dielectric function is taken into account (Volokitin and Persson, 2003c). In the nonretarded case ($c\to\infty$), and for small velocity v, Eq. (85) reduces to the formula obtained by Persson and Zhang (1998), and in the nonretarded case and at zero temperature it reduces to the formula obtained by Pendry (1997).

From comparison of Eq. (85) with Eq. (23) for the radiative heat transfer, one can see that there is an important difference in the type of elementary excitations that play an important role in these phenomena. For radiative heat transfer all kinds of elementary excitations with frequencies that can be thermally excited are equally important. In the case of van der Waals friction, large-momentum, low-frequency excitations are particularly important. Such low-energy excitations can be associated with vibrations of massive particles. In particular, many adsorbate vibrations parallel to the metal surface are characterized by very low frequencies.

1. Discussion of general formula and limiting cases

For $d\ll\lambda_T$ we can neglect the first term in Eq. (85) and the second term can be written as

$$\sigma_\parallel=\frac{\hbar}{2\pi^3}\int_{-\infty}^{\infty}dq_y\int_0^\infty dq_x q_x e^{-2qd}\times\left\{\int_0^\infty d\omega[n(\omega)-n(\omega+q_x v)]\times\left(\frac{\mathrm{Im}\,R_{1p}^+\,\mathrm{Im}\,R_{2p}}{|1-e^{-2qd}R_{1p}^+R_{2p}|^2}+(1\leftrightarrow 2)\right)-\int_0^{q_x v}d\omega[n(\omega)+1/2]\left(\frac{\mathrm{Im}\,R_{1p}^-\,\mathrm{Im}\,R_{2p}}{|1-e^{-2qd}R_{1p}^-R_{2p}|^2}+(1\leftrightarrow 2)\right)+[p\to s]\right\}. \tag{86}$$

For zero temperature $n(\omega)=0$ for $\omega>0$, friction is given by (Pendry, 1997)

$$\sigma_\parallel=-\frac{\hbar}{4\pi^3}\int_{-\infty}^{\infty}dq_y\int_0^\infty dq_x q_x e^{-2qd}\left\{\int_0^{q_x v}d\omega\times\left(\frac{\mathrm{Im}\,R_{1p}^-\,\mathrm{Im}\,R_{2p}}{|1-e^{-2qd}R_{1p}^-R_{2p}|^2}+(1\leftrightarrow 2)\right)+[p\to s]\right\}. \tag{87}$$

In the local optical approximation the reflection amplitudes are given by Fresnel's formula (B17). For $d<\lambda_T|\varepsilon(\omega_T)|^{-1/2}$ the reflection amplitude for p-polarized electromagnetic waves can be approximated by Eq. (38). Substituting Eq. (38) in Eq. (87) and using the dielectric function (32), in the limiting cases of small and high velocities, gives

$$\sigma_\parallel=\begin{cases}\dfrac{15}{2^7\pi^2}\left(\dfrac{\hbar v}{d^4}\right)\left(\dfrac{v}{4\pi\sigma d}\right)^2 & \text{for } v\ll 4\pi\sigma/d, \quad (88)\\[2ex] \dfrac{\hbar(4\pi\sigma)^2}{2\pi^2 d^2 v}\ln\left(\dfrac{v}{4\pi\sigma d}\right) & \text{for } v\gg 4\pi\sigma/d. \quad (89)\end{cases}$$

For example, for good conductors with conductivity $\sigma=10^{17}\ \mathrm{s}^{-1}$, for $d=1$ nm and $v=1$ m/s the friction is extremely small: $\sigma_\parallel\approx 10^{-18}\ \mathrm{N\,m^{-2}}$ [in comparison the friction observed by Stipe *et al.* (2001) corresponds to $\sigma_\parallel\sim 1\ \mathrm{N\,m^{-2}}$]. The friction increases when the conductivity decreases, but there is a limit for the enhancement. Thus according to the Drude model the conductivity is given by

$$\sigma=\frac{ne^2\tau}{m}, \tag{90}$$

where the relaxation time τ cannot be shorter than $\sim 10^{-16}$ s. The lowest value of the electron concentration $n_{\min}$ is restricted by the validity of the macroscopic theory, which requires that the average separation between electrons is much smaller than the length scale of variation of the electric field, which is determined by the separation d. Thus $n_{\min}\approx d^{-3}$ so that for $d=1$ nm the conductivity cannot be smaller than $\sigma_{\min}\approx 10^{12}\ \mathrm{s}^{-1}$ and, consequently, at $v=1$ m/s for metals the friction cannot be larger than $10^{-13}\ \mathrm{N\,m^{-2}}$.

C. van der Waals friction between plane surfaces at finite temperatures and small velocities

For $v<dk_BT/\hbar$ (at $d=1$ nm and $T=300$ K for $v<10^3$ m/s) the main contribution to the friction [Eq. (85)] depends linearly on the sliding velocity v so that the frictional stress σ which acts on the surfaces of the two bodies in parallel or normal relative motion can be written as $\sigma=\gamma v$. The contribution to the friction coefficient $\gamma_\parallel=\gamma_\parallel^{\mathrm{rad}}+\gamma_\parallel^{\mathrm{evan}}$ from propagating electromagnetic waves for parallel relative motion is

$$\gamma_\parallel^{\mathrm{rad}}=\frac{\hbar}{8\pi^2}\int_0^\infty d\omega\left(-\frac{\partial n}{\partial\omega}\right)\int_0^{\omega/c}dq\,q^3\times\frac{(1-|R_{1p}|^2)(1-|R_{2p}|^2)}{|1-e^{2i\gamma d}R_{1p}R_{2p}|^2}+[p\to s], \tag{91}$$

and the contribution from evanescent electromagnetic waves is

$$\gamma_\parallel^{\mathrm{evan}}=\frac{\hbar}{2\pi^2}\int_0^\infty d\omega\left(-\frac{\partial n}{\partial\omega}\right)\int_{\omega/c}^\infty dq\,q^3e^{-2|\gamma|d}\times\mathrm{Im}\,R_{1p}\,\mathrm{Im}\,R_{2p}\frac{1}{|1-e^{-2|\gamma|d}R_{1p}R_{2p}|^2}+[p\to s]. \tag{92}$$

Similarly, for normal relative motion the contribution to the friction coefficient from propagating electromagnetic waves is

$$\gamma_\perp^{\rm rad} = \frac{\hbar}{4\pi^2}\int_0^\infty d\omega\left(-\frac{\partial n}{\partial\omega}\right)\int_0^{\omega/c} dq\, q\, \gamma^2 \times[(1-|R_{1p}R_{2p}|^2)^2 + |(1-|R_{1p}|^2)R_{2p}e^{i\gamma d} + (1-|R_{2p}|^2)R_{1p}^* e^{-i\gamma d}|^2]\frac{1}{|1-e^{2i\gamma d}R_{1p}R_{2p}|^4} + [p\to s], \quad (93)$$

and the contribution from evanescent electromagnetic waves by

$$\gamma_\perp^{\rm evan} = \frac{\hbar}{\pi^2}\int_0^\infty d\omega\left(-\frac{\partial n}{\partial\omega}\right)\int_{\omega/c}^\infty dqq\,|\gamma|^2 e^{-2|\gamma|d} \times\{(\mathrm{Im}\, R_{1p} + e^{-2|\gamma|d}|R_{1p}|^2\,\mathrm{Im}\, R_{2p}) \times(\mathrm{Im}\, R_{2p} + e^{-2|\gamma|d}|R_{2p}|^2\,\mathrm{Im}\, R_{1p}) + e^{-2|\gamma|d} \times[\mathrm{Im}(R_{1p}R_{2p})]^2\}\frac{1}{|1-e^{-2|\gamma|d}R_{1p}R_{2p}|^4} + [p\to s]. \quad (94)$$

Equations (91)–(94) were first derived by Volokitin and Persson (1999, 2003c) using the semiclassical theory of the fluctuating electromagnetic field. Volokitin and Persson (2006) gave an alternative derivation using the quantum field theory.

There is a major difference between the friction coefficients for normal and parallel relative motion, related to the denominators in the formulas for the friction coefficient. The resonant condition corresponds to the case when the denominators of the integrand in Eqs. (92)–(94), which is due to multiple scattering of electromagnetic waves from the opposite surfaces, are small. At resonance, if the imaginary part of the reflection amplitude $R_i \ll 1$ the integrand in Eq. (94) has a large factor $\sim 1/R_i^2$, in sharp contrast to the case of parallel relative motion, where there is no such enhancement factor.

For good metals ($k_BT/4\pi\hbar\sigma \ll 1$) using Eq. (94) for $\lambda_T(k_BT/4\pi\hbar\sigma)^{3/2} < d < \lambda_T(4\pi\hbar\sigma/k_BT)^{1/2}$, we get

$$\gamma_{\perp p}^{\rm evan} \approx 0.13\frac{\hbar}{d^3\lambda_T}\left(\frac{k_BT}{4\pi\hbar\sigma}\right)^{1/2} \quad (95)$$

and for $d < \lambda_T(k_BT/4\pi\hbar\sigma)^{3/2}$ we get

$$\gamma_{\perp p}^{\rm evan} \approx \frac{\hbar}{d^4}\left(\frac{k_BT}{4\pi\hbar\sigma}\right)^2\left(1+\ln\frac{\hbar\sigma}{2k_BT}\right). \quad (96)$$

The last contribution will dominate for metals without too high a conductivity ($k_BT/4\pi\hbar\sigma \simeq 1$).

For comparison, the p-wave contribution for parallel relative motion, for $d < \lambda_c = \lambda_T|\varepsilon(\omega = k_BT/\hbar)|^{-1/2}$, is (Volokitin and Persson, 1999, 2001a)

$$\gamma_{\parallel p}^{\rm evan} \approx 0.3\frac{\hbar}{d^4}\left(\frac{k_BT}{4\pi\hbar\sigma}\right)^2. \quad (97)$$

It is interesting to note that for normal relative motion, in contrast to parallel relative motion, for good conductors, for almost all $d > 0$ the main contribution to the friction comes from retardation effects. This follows because Eq. (95), in contrast to Eq. (97), contains the light velocity.

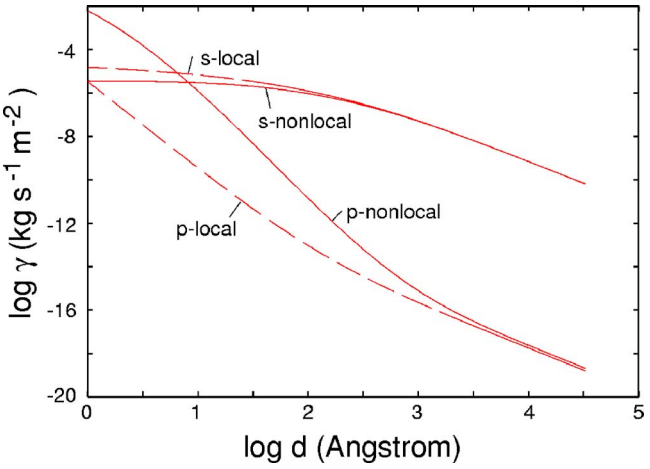

FIG. 11. (Color online) The friction coefficient for two flat surfaces in parallel relative motion as a function of separation d at $T=273$ K with parameters chosen to correspond to copper ($\tau^{-1}=2.5\times10^{13}$ s^{-1}, $\omega_p=1.6\times10^{16}$ s^{-1}). The contributions from the s- and p-polarized electromagnetic fields are shown separately. The full and dashed curves have been obtained using the nonlocal optical dielectric formalism and local optical approximation, respectively. (The base of the logarithm is 10.)

From Eq. (94) we get the s-wave contribution to the friction for $d < \lambda_c$,

$$\gamma_{\perp s}^{\rm evan} \approx 10^{-2}\frac{\hbar}{\lambda_c^4}[3 - 5\ln(2d/\lambda_c)]. \quad (98)$$

For parallel relative motion we can neglect the multiple scattering of electromagnetic waves from opposite surfaces. In this case $\gamma_{\parallel s}^{\rm evan} = 0.5\gamma_{\perp s}^{\rm evan}$.

Figure 11 shows the contribution to the friction coefficient $\gamma_\parallel$ from evanescent electromagnetic waves for two semi-infinite solids in parallel relative motion, with parameters chosen to correspond to copper ($\tau^{-1}=2.5\times10^{13}$ s^{-1}, $\omega_p=1.6\times10^{16}$ s^{-1}) at $T=273$ K. The same result for normal relative motion is shown in Fig. 12. In both cases we show the s- and p-wave contributions separately. The dashed lines show the result when the local (long-wavelength) dielectric function $\varepsilon(\omega)$ is used,

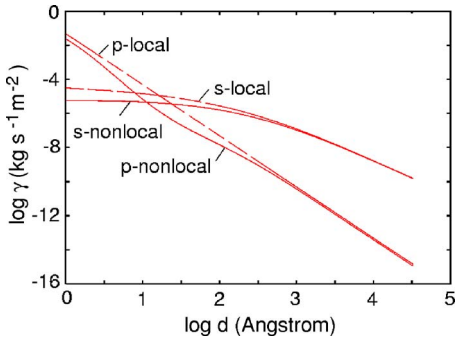

FIG. 12. (Color online) The same as Fig. 11 but for normal relative motion.

and the full lines show the result obtained using the nonlocal optical dielectric formalism, which was proposed for studying the anomalous skin effect (Kliewer and Fuchs, 1969, 1969). This formalism takes into account the spatial dispersion of the dielectric function. Figure 11 shows that, for sufficiently small separations ($d<1000$ Å), for parallel relative motion the nonlocal optical effects become important for the p-wave contribution. However, for the s-wave contribution, for both parallel and normal relative motion, the nonlocal optical effects are negligibly small for practically all separations. For normal relative motion, for the p-wave contribution the nonlocal optical effects are less important than for the parallel relative motion. The calculations presented take into account the nonlocal effects in the bulk of the solids. There is also the contribution to the nonlocal optical response from the surface region, which was investigated by Persson and Volokitin (2000) and Volokitin and Persson (2001a). For $d>10$ Å the nonlocal bulk contribution is of the same importance as the surface contribution.

For high-resistivity metals ($k_BT/4\pi\hbar\sigma>1$), for $d<\lambda_c$ we get

$$\gamma_\parallel \approx 0.05\frac{\hbar}{d^4}\frac{k_BT}{4\pi\hbar\sigma} \tag{99}$$

and $\gamma_\perp \approx 10\gamma_\parallel$. Thus, in contrast to the heat flux, van der Waals friction diverges in the limit $\sigma\to 0$. Of course, in reality the friction must vanish in this limit because the conductivity is proportional to the concentration n of free electrons, and the friction must vanish when n vanishes. The origin of the discrepancy lies in the breakdown of the macroscopic theory which is not valid at very low electron concentrations. The macroscopic approach for the electromagnetic properties of matter is valid only when the length scale of spatial variation of the electromagnetic field is much larger than the average distance between electrons. For evanescent waves, this length scale is determined by the separation d between bodies. From this condition we can estimate the maximal friction, which corresponds to high-resistivity materials. The minimal conductivity can be estimated as (see Sec. V.B.1)

$$\sigma_{\min} \sim \frac{e^2\tau}{md^3} \tag{100}$$

and the maximum friction can be estimated as

$$\gamma_{\parallel\max} \sim 0.05\frac{\hbar}{d^4}\frac{k_BT}{4\pi\hbar\sigma_{\min}} \sim 0.05\frac{mk_BT}{4\pi e^2\tau d}. \tag{101}$$

To estimate the friction coefficient Γ for an atomic force microscope tip with the radius of curvature $R\gg d$ we can use the "proximity approximation" given by Eq. (79), with the heat flux per unit area replaced by the friction coefficient per unit area. Thus, for the friction coefficient for a spherical tip we get

$$\Gamma_\parallel^s \approx 2\pi\int_0^\infty d\rho\,\rho\gamma_\parallel(d+\rho^2/2R) = 0.05\frac{2\pi R}{3d^3}\frac{k_BT}{4\pi\sigma}, \tag{102}$$

and the maximum of friction can be estimated as

$$\Gamma_{\parallel\max}^s \sim 0.05\frac{2\pi R}{3d^3}\frac{k_BT}{4\pi\sigma_{\min}} \sim 0.1\frac{mk_BTR}{4\pi e^2\tau}. \tag{103}$$

For $\tau\sim 10^{-16}$ s, $R\sim 1$ μm, and $T=300$ K we get $\Gamma_{\max}\sim 10^{-15}$ kg/s. This friction is two orders of magnitude smaller than the friction observed in a recent experiment at $d=10$ nm (Stipe *et al.*, 2001). Similarly, in the case of a cylindrical tip, we get

$$\Gamma_\parallel^c \approx 2w\int_0^\infty d\rho\,\gamma_\parallel(d+\rho^2/2R) = \frac{2^{1/2}\pi}{64}\sqrt{\frac{R}{d}}\frac{k_BTw}{4\pi\sigma d^3}, \tag{104}$$

where w is the width of the tip, and the maximum of friction can be estimated as

$$\Gamma_{\parallel\max}^c \sim \frac{2^{1/2}\pi}{64}\sqrt{\frac{R}{d}}\frac{k_BTw}{4\pi\sigma_{\min}d^3} \sim \frac{2^{1/2}\pi}{64}\sqrt{\frac{R}{d}}\frac{mk_BTw}{4\pi e^2\tau}. \tag{105}$$

For $w=7$ μm, $d=10$ nm, and with the other parameters as above, Eq. (105) gives friction of the same order of magnitude as was observed in experiment (Stipe *et al.*, 2001). Thus the van der Waals friction between high-resistivity materials can be measured with the present state-of-the-art equipment.

Recently, a large electrostatic noncontact friction has been observed between an atomic force microscope tip and thin dielectric films (Kuehn, Loring, and Marohn, 2006). The van der Waals friction will also be large for dielectrics with high absorption at low frequencies. As an example we consider the van der Waals friction between thin water films adsorbed on transparent dielectric substrates like silica or mica. Water has an extremely large static dielectric function of around 80. The low-frequency contribution to the dielectric function, responsible for this large static value, is due to relaxation of the permanent dipoles of the water molecules. It can be accurately described by the Debye (1929) theory of rotational relaxation. The theoretical fit of the experimental data is (Sernelius *et al.*, 1997)

$$\varepsilon(\omega) = 4.35 + \frac{C}{1-i\omega/\omega_0}, \tag{106}$$

where $C=72.24$ and $\omega_0=1.3\times 10^{11}$ s^{-1}. We note that water has large absorption in the radio-frequency range at $\omega\sim\omega_0$ and shows in this region of the spectrum anomalous dispersion. In this frequency range the dielectric constants ε_3 of mica or silica are nearly constant (and real) and $|\varepsilon_2|\gg\varepsilon_3$, where ε_2 denotes the dielectric function of water. For a planar film with thickness d_f and dielectric function $\varepsilon_2(\omega)$ on top of a substrate with the dielectric function $\varepsilon_3(\omega)$ the reflection amplitude

$$R_p = \frac{R_{p21} - R_{p23}\exp(-2qd_f)}{1 - R_{p21}R_{23}\exp(-2qd_f)}, \tag{107}$$

where

$$R_{pij} = \frac{\varepsilon_i - \varepsilon_j}{\varepsilon_i + \varepsilon_j}, \tag{108}$$

where the index 1 is associated with vacuum. For $qh \ll 1$ and $q^{-1} \sim d \ll |\varepsilon_2| d_f/\varepsilon_3$, the reflection amplitude can be approximated by

$$R_p \approx 1 - \frac{2}{\varepsilon_2 q d_f}. \tag{109}$$

Substituting Eq. (109) into Eq. (92) and using the proximity approximation we obtain the friction between a cylindrical atomic force microscope tip and a sample,

$$\Gamma_\parallel^c = \frac{\pi\hbar R^{1/2} w}{6\sqrt{2}C^2 d_f^2 d^{3/2}}\left(\frac{k_B T}{\hbar\omega_0}\right)^2. \tag{110}$$

For $d_f = 1$ nm and with the other parameters the same as above we get $\Gamma_\parallel^c = 4.8\times 10^{-12}$ kg/s. The friction observed in by (Stipe *et al.*, 2001) has the same weak distance dependence as predicted by Eq. (110), but is one order of magnitude smaller than predicted by (110).

D. Resonant photon tunneling enhancement of the van der Waals friction

1. Surface phonon polariton enhancement of the van der Waals friction

As in the case of radiative heat transfer, the van der Waals friction can be greatly enhanced by resonant photon tunneling between localized surface states, e.g., surface plasmon polaritons and adsorbate vibration modes. Using the same approximation as when deriving Eq. (42), we get (Volokitin and Persson 2003c)

$$\gamma_\perp = \frac{3}{128}\frac{\hbar^2\omega_a^2}{d^4 k_B T \eta}\frac{1}{\sinh^2(\hbar\omega_0/2k_B T)}, \tag{111}$$

and for parallel motion

$$\gamma_\parallel = \frac{\hbar^2\eta q_c^4}{128\pi k_B T}\frac{1}{\sinh^2(\hbar\omega_0/2k_B T)}. \tag{112}$$

Resonant photon tunneling enhancement of the van der Waals friction is possible for two semiconductor surfaces which can support low-frequency surface plasmon or surface polariton modes. As an example we consider two clean surfaces of silicon carbide (SiC). Using the parameters describing the optical properties of this material (see Sec. IV.C), we get $\gamma_\perp = 4.2\times 10^3/d^4$ kg s^{-1} m^{-2} and $\gamma_\parallel = 2.2\times 10^2/d^4$ kg s^{-1} m^{-2}, where the distance d is in angstroms. Note that the friction between two semiconductor surfaces is several orders of magnitude larger than that between two clean good conductor surfaces (see Figs. 11 and 12).

2. Adsorbate vibrational mode enhancement of the van der Waals friction

Another enhancement mechanism of the van der Waals friction is connected with resonant photon tunneling between adsorbate vibrational modes localized on different surfaces. Volokitin and Persson (2003b, 2003c) showed that resonant photon tunneling between two surfaces separated by $d = 1$ nm, and covered by a low concentration of potassium atoms, results in friction which is six orders of magnitude larger than for clean surfaces. The adsorbate-induced enhancement of the van der Waals friction is even larger for Cs adsorption on Cu (100). In this case, even for $\theta \geqslant 0.1$, the adsorbed layer exhibits an acoustic branch for vibrations parallel to the surface (Senet *et al.*, 1999). Thus $\omega_\parallel = 0$ and according to Eq. (56) at small frequencies the reflection amplitude is given by

$$R_p = 1 - \frac{2qa\omega_q^2}{\omega^2 - \omega_q^2 + i\omega\eta}, \tag{113}$$

where $\omega_q^2 = 4\pi n_a e^{*2} a q^2/M$, e^* is the ion charge, and a is the separation between an ion and the image plane. Using Eq. (113) in Eq. (92) for

$$\frac{a}{\eta d}\sqrt{\frac{4\pi n_a e^{*2} a}{M d^2}} \ll 1$$

gives

$$\gamma_\parallel \approx 0.62\frac{k_B T a^2}{\eta d^6}. \tag{114}$$

It is interesting to note that $\gamma_\parallel$ in Eq. (114) does not depend on n_a, e^*, and M. However, Eq. (113) is only valid when there are acoustic vibrations in the adsorbed layer. For Cs adsorbed on the Cu(100) surface the acoustic vibrations exist only for coverage $\theta \geqslant 0.1$ (Senet *et al.*, 1999). The friction acting on an atomic force microscope

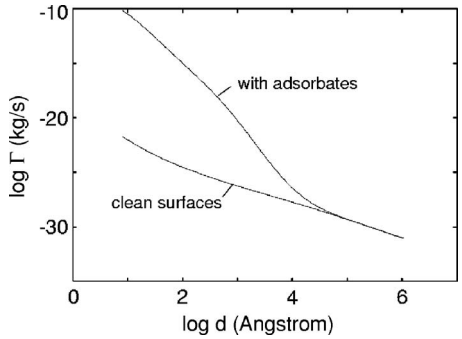

FIG. 13. The friction coefficient between the copper tip and copper substrate of surfaces which are covered by low concentration of cesium atoms, as a function of the separation d. The cylindrical tip is characterized by the radius of curvature $R = 1$ μm and the width $w = 7$ μm. The other parameters correspond to Cs adsorbed on the Cu (100) surface at coverage $\theta \approx 0.1$ (Senet *et al.*, 1999; Volokitin and Persson, 2005): $e^* = 0.28e$, $\eta = 3\times 10^9$ s^{-1}, $a = 2.94$ Å, and $T = 293$ K. (The base of the logarithm is 10.)

tip can be estimated using a similar approximation as Eq. (79). Using this approximation and Eq. (114) for a cylindrical tip we get

$$\Gamma_{\parallel}^{c} \approx 0.68 \frac{k_B T a^2 R^{0.5} w}{\eta d^{5.5}}, \tag{115}$$

where R is the radius of curvature of the tip and w its width. For Cs adsorption on Cu(100) the damping parameter η was estimated by Volokitin and Persson (2005) as $\eta \approx 3\times 10^9$ s^{-1}. Using this value of η in Eq. (115) for $a=2.94$ Å (Senet *et al.*, 1999), $R=1$ μm, $w=7$ μm, and $T=293$ K at $d=10$ nm we get $\Gamma_{\parallel}=0.5\times 10^{-13}$ kg/s, which is only three times smaller than the friction observed by Stipe *et al.* (2001) at the same distance. However, the van der Waals friction is characterized by a much stronger distance dependence ($\sim 1/d^{5.5}$) than observed in the experiment ($\sim 1/d^n$, where $n=1.3\pm 0.2$). Thus at small distances the van der Waals friction will be much larger than friction observed by Stipe *et al.* (2001), and can thus be measured experimentally. Figure 13 shows how the friction coefficient depends on the distance d between the copper tip and the copper substrate, when the surfaces of the tip and the substrate are covered by a low concentration of the Cs atoms, and for clean surfaces. In comparison, the friction between two clean surfaces at the separation $d=1$ nm is 11 orders of magnitude smaller. However, the friction between clean surfaces shown in Fig. 13 was calculated in the local optical approximation. For parallel relative motion, nonlocal optical effects are very important (see Fig. 11), and when they are taken into account the friction at $d=1$ nm between adsorbate-covered surfaces will be larger by seven orders of magnitude than the friction between clean surfaces.

E. van der Waals friction between a small particle and a plane surface

The friction force acting on a small particle during motion parallel to a flat surface can be obtained from the friction between two semi-infinite bodies in the limit when one of the bodies is sufficiently rarefied. This means that the dielectric function of this body, say body 2, is close to unity, i.e., $\varepsilon_2 - 1 \to 4\pi n \alpha_2 \ll 1$, where n is the concentration of particles in body 2 and α_2 is their polarizability. To linear order in the concentration n the reflection amplitudes are

$$R_{2p} \approx 2\pi n \,\mathrm{Im}\,\alpha_2, \quad R_{2s} \approx \pi n \,\mathrm{Im}\,\alpha_2 \left(\frac{\omega}{cq}\right)^2.$$

The friction force acting on a particle moving parallel to a plane surface can be obtained as the ratio between the change of the frictional shear stress after displacement of body 2 by small distance dz, and the number of the particles in a slab with thickness dz:

$$\begin{aligned} F_{\mathrm{fric}} = \left.\frac{d\sigma_{\parallel}(z)}{ndz}\right|_{z=d} = \frac{\hbar}{\pi^2}\int_{-\infty}^{\infty} dq_y \int_0^{\infty} dq_x q_x q e^{-2qd} \Bigg\{ \int_0^{\infty} d\omega [n(\omega) - n(\omega + q_x v)] \\ \times \Bigg(2\{\mathrm{Im}\, R_{1p}(\omega + q_x v)\mathrm{Im}\,\alpha_2(\omega) + [\omega + q_x v \leftrightarrow \omega]\} + \left(\frac{1}{cq}\right)^2 \{\omega^2 \,\mathrm{Im}\, R_{1s}(\omega + q_x v)\mathrm{Im}\,\alpha_2(\omega) \\ + [\omega + q_x v \leftrightarrow \omega]\} \Bigg) - \int_0^{q_x v} d\omega [n(\omega) + 1/2] \Bigg(2\{\mathrm{Im}\, R_{1p}(\omega - q_x v)\mathrm{Im}\,\alpha_2(\omega) + [\omega - q_x v \leftrightarrow \omega]\} \\ + \left(\frac{1}{cq}\right)^2 \{\omega^2 \,\mathrm{Im}\, R_{1s}(\omega - q_x v)\mathrm{Im}\,\alpha_2(\omega) + [\omega - q_x v \leftrightarrow \omega]\} \Bigg) \Bigg\}, \end{aligned} \tag{116}$$

where the symbols $[\omega \pm q_x v \leftrightarrow \omega]$ stand for the terms that can be obtained from the preceding terms by interchanging $\omega \pm q_x v$ and ω.

To linear order in the sliding velocity v, we get from Eq. (116) $F_{\mathrm{fric}} = -\Gamma_{\parallel} v$, where

$$\Gamma_{\parallel} = \frac{\hbar}{\pi}\int_0^{\infty} d\omega \left(-\frac{\partial n(\omega)}{\partial \omega}\right) \int_0^{\infty} dq\, q^4 e^{-2qd} \times \left[2\,\mathrm{Im}\, R_p(q,\omega) + \left(\frac{\omega}{cq}\right)^2 \mathrm{Im}\, R_s(q,\omega) \right] \mathrm{Im}\,\alpha(\omega). \tag{117}$$

In the nonretarded limit, this equation reduces to the formula obtained by Tomassone and Widom (1997).

However, Eq. (117) does not take into account screening effects, which become important at small separation between the particle and surface. General formulas for friction coefficients that take into account screening effects were obtained by Volokitin and Persson (2002) using the semiclassical theory of the fluctuating electromagnetic field. Volokitin and Persson (2006) derived the same equations using quantum field theory. For the motion of the particle parallel to the surface the friction coefficient is

$$\Gamma_{\parallel} = \frac{2\hbar}{\pi}\int_0^{\infty} d\omega\left(-\frac{\partial n}{\partial \omega}\right) \times\left\{\sum_{k=x,y,z} \mathrm{Im}\,\alpha_{kk}\frac{\partial^2}{\partial x \partial x'}\,\mathrm{Im}\,D^0_{kk}(\mathbf{r},\mathbf{r}',\omega) - 2\,\mathrm{Re}[\alpha_{xx}(\omega)\alpha^*_{zz}(\omega)] \times\left(\frac{\partial}{\partial x}\,\mathrm{Im}\,D^0_{xz}(\mathbf{r},\mathbf{r}_0,\omega)\right)^2\right\}_{\mathbf{r}=\mathbf{r}'=\mathbf{r}_0}. \quad (118)$$

For normal motion the friction coefficient is

$$\Gamma_{\perp} = \frac{2\hbar}{\pi}\int_0^{\infty} d\omega\left(-\frac{\partial n}{\partial \omega}\right)\sum_{k=x,y,z}\left\{\mathrm{Im}\,\alpha_{kk}(\omega)\frac{\partial^2}{\partial z \partial z'} \times\{\mathrm{Im}\,D^0_{kk}(\mathbf{r},\mathbf{r}',\omega) + \mathrm{Im}[\alpha_{kk}D^0_{kk}(\mathbf{r},\mathbf{r}_0,\omega)D^0_{kk}(\mathbf{r}',\mathbf{r}_0,\omega)]\} + \left(\frac{\partial}{\partial z}\,\mathrm{Im}[\alpha_{kk}(\omega)D^0_{kk}(\mathbf{r},\mathbf{r}_0,\omega)]\right)^2\right\}_{\mathbf{r}=\mathbf{r}'=\mathbf{r}_0}, \quad (119)$$

where D^0_{ij} is the Green's function of the electromagnetic field from the semi-infinite body without interaction with the particle, and

$$\alpha_{ii}(\omega) = \frac{\alpha^0(\omega)}{1-\alpha^0(\omega)D^0_{ii}(\mathbf{r}_0,\mathbf{r}_0,\omega)},$$

where $\alpha^0(\omega)$ is the polarizability of the particle without interaction with the surface.

For a spherical particle the polarizability is given by Eq. (73), and for $R \ll d \ll \lambda_T$ in the formulas for the Green's functions (Appendix B) we can put $\gamma = iq$. For good conductors ($|\varepsilon| \gg 1$), in the frequency range accessible by thermal radiation, the modulus of the reflection amplitude $|R_{p(s)}| \leqslant 1$. Thus, for $d \gg R$, we can neglect screening effects and from Eqs. (118) and (119) we get Eq. (117) and $\Gamma_{\perp} = 2\Gamma_{\parallel}$. In the limit $d < |\varepsilon(\omega = k_B T/\hbar)|^{-1/2}\lambda_T$ the p- and s-wave contributions to the friction coefficient become (Volokitin and Persson 2002)

$$\Gamma_{p\parallel} \approx 3\frac{\hbar}{d^5}\left(\frac{k_B T}{4\pi\hbar}\right)^2 \sigma_1^{-1}\sigma_2^{-1}R^3, \quad (120)$$

$$\Gamma_{s\parallel} \approx \frac{\pi^3}{10}\frac{\hbar}{d\lambda_T^4}R^3\frac{\sigma_1}{\sigma_2}, \quad (121)$$

where σ_1 and σ_2 are the conductivities of the sample and the particle, respectively. For $d = 2R = 10$ nm and $\sigma_s = \sigma_p = 4\times 10^{17}\ \mathrm{s}^{-1}$ (corresponding to gold) we get the very small friction $\Gamma \sim 10^{-29}\ \mathrm{kg\,s^{-1}}$.

However, the friction can be greatly enhanced for high-resistivity materials. Using Eq. (117) in the nonretarded limit (which can be formally obtained as a limit $c \to \infty$) and for high-resistivity material ($4\pi\sigma \ll k_B T/\hbar$) we get

$$\Gamma_{p\parallel} = 0.9\frac{k_B T}{4\pi\sigma}\frac{R^3}{d^5}, \quad (122)$$

where we have assumed that the particle and substrate have the same dielectric function $\varepsilon = 1 + 4\pi i\sigma/\omega$. As discussed above (see Sec. V.B.1), the macroscopic theory [which was used in obtaining Eq. (122)] is valid only when $\sigma \gg \sigma_{\min} \sim e^2\tau/md^3$. For $\sigma \sim \sigma_{\min}$, $d = 2R = 10$ nm, and $\tau = 10^{-15}$ s, Eq. (122) gives $\Gamma_{p\parallel\max} \sim 10^{-18}$ kg/ s.

If the particle and substrate are made from the same material, which can support surface phonon polaritons, the friction is

$$\Gamma_{\parallel} = \frac{9k_B T\eta R^3}{d^5}\left(\frac{1}{\omega_s^2}+\frac{1}{\omega_p^2}\right), \quad (123)$$

where ω_s and ω_p are the frequencies of the surface phonon polaritons for the substrate and particle, respectively. If the substrate and particle are made from SiC, $\omega_s = 1.79\times 10^{14}\ \mathrm{s}^{-1}$ and $\omega_p = 1.76\times 10^{14}\ \mathrm{s}^{-1}$. Thus for $d = 2R = 10$ nm, $\eta = 8.9\times 10^{11}\ \mathrm{s}^{-1}$, and $T = 300$ K we get $\Gamma \sim 10^{-21}\ \mathrm{kg\,s^{-1}}$. This friction coefficient is eight orders of magnitude larger than for good conductors.

F. van der Waals friction mediated by blackbody radiation

van der Waals friction also occurs when a particle moves relative to blackbody radiation, e.g., relative to the walls of an oven, or in the cosmic microwave background. This kind of friction has no position dependence, i.e., it is spatially homogeneous. The consequence is a universal dissipative drag acting on all matter in relative motion with respect to a thermalized photon gas. To calculate this universal drag we use the same approach as in Sec. V.E. Assuming that the size of the particle is smaller than λ_T we get the friction coefficient for a particle moving relative to blackbody radiation,

$$\Gamma^{\mathrm{BB}} = \frac{2\hbar}{\pi}\int_0^{\infty} d\omega\left(-\frac{\partial n}{\partial\omega}\right)\sum_{k=x,y,z}\mathrm{Im}\,\alpha_{kk}\frac{\partial^2}{\partial x\partial x'} \times\mathrm{Im}\,D^{\mathrm{BB}}_{kk}(\mathbf{r},\mathbf{r}',\omega)|_{\mathbf{r}=\mathbf{r}'}, \quad (124)$$

where α_{kk} is the polarizability of the particle and $D^{\mathrm{BB}}_{kk}(\mathbf{r},\mathbf{r}',\omega)$ is the Green's function of blackbody radiation. For a spherical particle $\alpha_{kk} = \alpha$, and using the formula [see Lifshitz and Pitaevskii (1980)]

$$\sum_{k=x,y,z} D^{\mathrm{BB}}_{kk}(\mathbf{r},\mathbf{r}',\omega) = 2\left\{\frac{\omega^2}{c^2}\frac{1}{|\mathbf{r}-\mathbf{r}'|}\exp\left(\frac{i\omega}{c}|\mathbf{r}-\mathbf{r}'|\right) - 2\pi\delta(\mathbf{r}-\mathbf{r}')\right\} \quad (125)$$

we get

$$\Gamma^{\mathrm{BB}} = \frac{\beta\hbar^2}{3\pi c^5}\int_0^{\infty} d\omega\frac{\omega^5\,\mathrm{Im}\,\alpha(\omega)}{\sinh^2\left(\frac{1}{2}\beta\hbar\omega\right)}, \quad (126)$$

where $\beta^{-1} = k_B T$. Equation (126) was first obtained by Mkrtchian *et al.* (2003) using a different approach. The

photon gas exerts a drag on any polarizable particle that moves with respect to the reference frame in which the photon gas is thermalized, and this drag is proportional to the relative velocity.

Tungsten ovens can operate at temperatures as high as 3000 K. If a beam of atoms, ions, or molecules passes through such an oven, it will be subject to drag due to the van der Waals friction mediated by the thermal radiation. For an atom or molecule the polarizability α can be characterized by a single absorption line at $\omega=\omega_0$. In this case $\mathrm{Im}\,\alpha(\omega)=\alpha_0\delta(\omega/\omega_0-1)$, where α_0 is the static polarizability at $\omega=0$.

Setting $m/\tau=\Gamma^{\mathrm{BB}}$, where m is the mass of the molecule and τ is the relaxation time, gives

$$\tau=\frac{3\pi mc^5\hbar^4}{2^6\alpha_0(k_BT)^5}\frac{\sinh^2(x)}{x^6}, \tag{127}$$

where $x=\beta\hbar\omega_0/2$. The relaxation time has a minimum at a temperature dependent frequency that coincides with the minimum of the function $f(x)=\sinh^2(x)/x^6$, at $x_m=2.98$, where $f(x_m)=0.137$. Ba^+ has a resonance near 2 eV, which is about six times the thermal energy associated with a 3000 K oven. For this resonance, the relaxation time would be near the minimum, and for the ion polarizability $\alpha_0\approx 1.0\times 10^{-30}\ \mathrm{m}^3$ one obtains the relaxation time $\approx 10^5$ s, i.e., 1 day. This relaxation time can be measured using ion traps.

For the cosmos, it is believed that hydrogen atoms condensed from protons and electrons when the radiation cooled to about 3000 K, and that the coupling of the cosmic radiation to matter due to Compton scattering becomes ineffective below this condensation temperature (Peebles, 1993). However, atoms, ions, and molecules with absorption in the appropriate frequency range should remain coupled to the cosmic radiation as its temperature drops from 3000 to perhaps 300 K. This coupling could influence the structure and anisotropies observed in recent experiments on the cosmic microwave background (Kovac *et al.*, 2002). It could also influence the behavior of molecules formed from the residue of novas and supernovas, and then subject to drag from a still hot cosmic microwave (i.e., electromagnetic) background. At much lower temperatures, macroscopic bodies can coalesce, in which geometrically determined resonances may become relevant.

G. van der Waals frictional drag force between quantum wells

The van der Waals friction can be tested not only by measuring the friction force during relative motion of the two bodies; an alternative method consists in driving an electric current in one metallic layer and registration of the effect of the frictional drag of the electrons in a second (parallel) metallic layer (Fig. 14). Such experiments were predicted by Pogrebinskii (1977) and Price (1983) and were performed for two-dimensional (2D) quantum wells (Gramila *et al.*, 1991, 1993; Sivan *et al.*, 1992). In these experiments, two quantum wells are separated by a dielectric layer thick enough to prevent

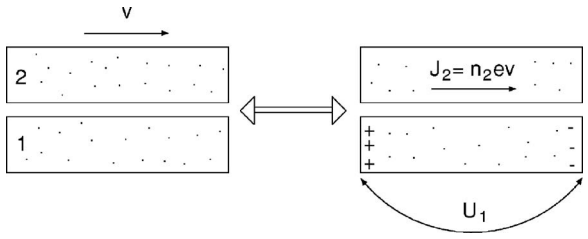

FIG. 14. Two ways for studying the van der Waals friction. Left: A metallic block sliding relative to the metallic substrate with the velocity v. An electronic frictional stress will act on the block (and on the substrate). Right: The shear stress σ can be measured if instead of sliding the upper block, a voltage U_2 is applied to the block resulting in a drift motion of the conduction electrons (velocity v). The resulting frictional stress σ on the substrate electrons will generate a voltage difference U_1 (proportional to σ) as indicated.

electrons from tunneling across it but allowing interlayer interaction between them. A current of density $J_2=n_2ev$ is driven through layer 2 (where n_2 is the carrier concentration per unit area in the second layer); see Fig. 14. Due to the proximity of the layers, the interlayer interactions will induce a current in layer 1 due to a friction stress $\sigma=\gamma v$ acting on electrons in layer 1 from layer 2. If layer 1 is an open circuit, an electric field E_1 will develop in the layer whose influence cancels the frictional stress σ between the layers. Thus the frictional stress $\sigma=\gamma v$ must equal the induced stress n_1eE_1, so that

$$\gamma=n_1eE_1/v=n_1n_2e^2E_1/J_2=n_1n_2e^2\rho_{12}, \tag{128}$$

where the *transresistivity* $\rho_{12}=E_1/J_2$ is defined as the ratio of the induced electric field in the first layer to the driving current density in the second layer. The transresistivity is often interpreted in terms of a drag rate, which, in analogy with the Drude model, is defined by $\tau_D^{-1}=\rho_{12}n_2e^2/m^*=\gamma/n_1m^*$. The most widely used approach to study the drag effect is based on the Boltzmann equation (Sivan *et al.*, 1992; Tso and Vasilopoulos, 1992; Jauho and Smith, 1993; Zheng and MacDonald, 1993), and the Kubo formalism (Hu *et al.*, 1995; Kamenev and Oreg, 1995). Volokitin and Persson (2001c) developed a theory of the drag effect based on the semiclassical theory of the fluctuating electromagnetic field. In this theory, when the separation between the quantum wells $d\ll\lambda_T$, the friction coefficient γ is given by Eq. (92) where $R_i(\omega)$ is the reflection amplitude for layer i. The retardation effects are automatically included in this approach.

For independent electrons the formulas for the reflection amplitudes for the individual quantum well for p- and s-polarized electromagnetic waves are given in Appendix C. For $d<v_F\hbar/k_BT$ the reflection amplitude for p-polarized electromagnetic waves is (Persson and Zhang, 1998; Volokitin and Persson, 2001c)

$$R_p=1+\frac{i\hbar\varepsilon\omega}{2k_Fe^2}, \tag{129}$$

where ε is the dielectric constant of the surrounding dielectric, $k_F=\sqrt{2\pi n_s}$ is the Fermi wave vector for a 2D

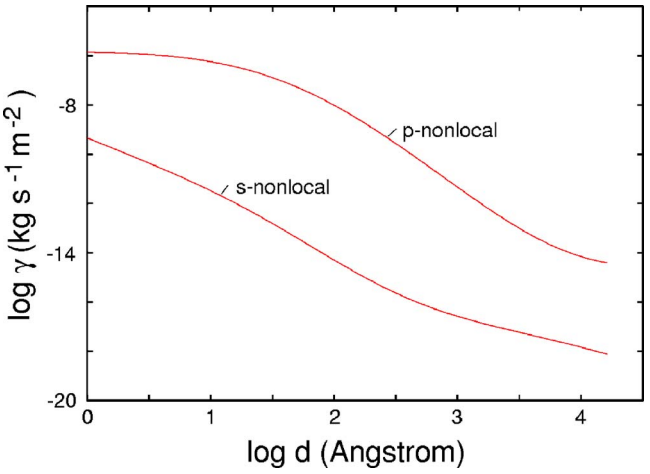

FIG. 15. (Color online) The frictional drag coefficient for two quantum wells at $T=3$ K as a function of separation d. The s- and p-wave contributions are shown separately. The calculations were performed with surface electron density $n_s=1.5\times10^{15}$ m^{-2}, damping constant $\eta=1.3\times10^{10}$ s^{-1}, effective electron mass $m^*=0.067m_e$, and dielectric constant $\varepsilon=10$. (The base of the logarithm is 10.)

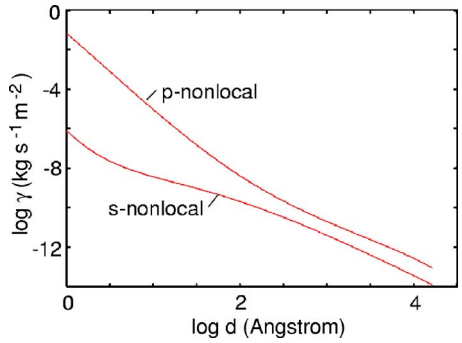

FIG. 16. (Color online) The frictional drag coefficient for two quantum wells at $T=273$ K as a function of separation d. The s- and p-wave contributions are shown separately. The calculations were performed using the surface electron density $n_s=1.05\times10^{19}$ m^{-2}, damping constant $\eta=2.5\times10^{13}$ s^{-1}, effective electron mass $m^*=m_e$, and dielectric constant $\varepsilon=1$. (The base of the logarithm is 10.)

electron gas, and n_s is the electron concentration of the 2D electron layer. Using Eq. (129) in Eq. (92) we get the contribution to the frictional drag rate from p-polarized waves,

$$\tau_{Dp}^{-1}=\gamma_p/nm^*\approx 0.2360\frac{(k_BT)^2}{\hbar\varepsilon_F(q_{TF}d)^2(k_Fd)^2}, \tag{130}$$

where $q_{TF}=2a_0^{-1}/\varepsilon$ is the single-layer Thomas-Fermi screening wave vector, $a_0=\hbar/m^*e^2$, and ε_F is the Fermi energy. Equation (130) is a factor of 2 larger than the result obtained by Gramila *et al.* using an approach based on the Boltzmann equation (Gramila *et al.*, 1993), and approximately a factor of 2 smaller than the result obtained by Persson and Zhang using a theory of the van der Waals friction (Persson and Zhang, 1998).

Figure 15 shows the friction coefficient γ as a function of distance d between two quantum wells at $T=3$ K, and with $n_s=1.5\times10^{15}$ m^{-2}, $m^*=0.067m_e$, $v_F=1.6\times10^7$ cm/s, and for the electron mean free path $l=v_F\tau=1.21\times10^5$ Å. We have also assumed $\varepsilon=10$, which corresponds to the condition of the experiment (Gramila *et al.*, 1991, 1993). In this case the s-wave contribution is negligibly small in comparison with the p-wave contribution. For $d=175$ Å we find $\gamma=3.3\times10^{-9}$ kg s^{-1} m^{-2} which corresponds to a drag rate $\tau_D^{-1}=3.3\times10^7$ s^{-1}, which is close to the experimental value $(\tau_D^{-1})_{\rm expt}=1.5\times10^7$ s^{-1} (Gramila *et al.*, 1991, 1993). Figure 16 shows the friction coefficient for 2D quantum wells with high electron density $n_s=10^{19}$ m^{-2}, $T=273$ K, $\tau=4\times10^{-14}$ s, and $\varepsilon=1$, where the result for other ε can be obtained using the scaling $\tau_{Dp}\sim\varepsilon^2$ and τ_{Ds} is independent of ε. In Figs. 15 and 16 the p- and s-wave contributions are shown separately. Calculations show that p waves give a larger contribution for friction for both low-density and high-density 2D quantum wells. Figure 17 shows the dependence of the friction coefficient on the electron density for the same parameters as in Fig. 15. In this case the boundary between degenerate and nondegenerate electron density is determined by the Fermi density $n_F=3k_BTm^*/2\pi\hbar^2=1.09\times10^{14}$ m^{-2}. From calculations we find the maximum of the frictional drag force for the electron density $n_{\rm max}\approx1\times10^{15}$ m^{-2}; this means that the experiment (Gramila *et al.*, 1991, 1993) was performed near optimum conditions.

The frictional drag between quantum wells makes it possible to probe directly the interparticle interaction. Interparticle interactions form the cornerstone of many-body physics. Many-body effects are particularly impor-

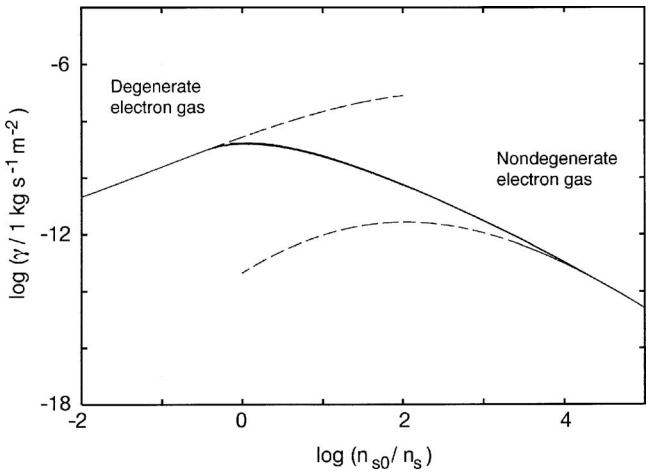

FIG. 17. The frictional drag coefficient for two quantum wells at $T=3$ T as a function of electron concentration n_s. The full curve was obtained by interpolation between the curves (dashed lines) obtained within the nonlocal optical dielectric approach, with the dielectric functions corresponding to a degenerate electron gas ($n_s>n_F\sim10^{14}$ m^{-2}), and to the nondegenerate electron gas ($n_s<n_F$). The electron density parameter $n_{s0}=1.5\times10^{15}$ m^{-2}, damping constant $\eta=1.3\times10^{10}$ s^{-1}, effective electron mass $m^*=0.067m_e$, separation $d=175$ Å, and the dielectric constant $\varepsilon=10$. (The base of the logarithm is 10.)

tant in low-dimensional systems. This leads to many intriguing phenomena, such as Luttinger liquid behavior in quantum wires, the fractional quantum Hall effect, and Wigner crystallization in two-dimensional electron gases in a magnetic field. As technology improves and semiconductor devices shrink further in size, interaction effects become even more pronounced, and it may become possible to probe these effects in novel experiments.

VI. ELECTROSTATIC FRICTION

A. Effect of a bias voltage and the spatial variation of the surface potential

The electrostatic potential at the surface of a metal relative to its interior depends on the magnitude of the surface dipole moment per unit area, which, in turn, depends on the separation of the lattice planes that are parallel to the surface (Lang and Kohn, 1971). Variation of the crystallographic direction at the surface of a clean polycrystalline metal results in a variation of the surface potential. This is referred to as the patch effect. Patch potentials are also generated and influenced by surface contamination and, in the case of alloys, by variation in the chemical composition. The surface potential can be easily changed by applying a voltage between an atomic force microscope tip and the sample. The electrostatic forces between conducting surfaces due to spatial variation of the surface potential were studied by Speake and Trenkel (2003).

Patch potential variation is specific to the particular sample and depends on environmental factors. Spatial variation of the surface potential is expected to be related to the physical size of the surface crystallites, which in the case of metal is typically of the order of 1 μm. Thin films deposited on substrates at temperatures much less than the melting point of the film are often amorphous, with nonuniform thickness and crystallite size of the same order as the thickness of the film (Liu *et al.*, 1997). Annealing of the film can produce grain structures that are substantially larger than the film thickness. The patch-potential variations have been measured under various conditions using vibrating or rotating plate electrometers (Rossi and Opat, 1992). Notably, it was shown that large-scale variations in surface potential were caused by adsorption of contaminants which was transient and found to reduce the variation of the surface potential of clean surfaces (Mohideen and Roy, 1998; Ederth, 2000).

1. General theory

We begin by considering a model in which the tip of a metallic cantilever of length L is a section of a cylindrical surface with the radius of curvature R (Fig. 18). The cantilever is perpendicular to a flat sample surface which occupies the x-y plane, with the z axis pointing away from the sample. The tip displacement $\mathbf{u}(t)=\hat{x}u_0e^{-i\omega t}$ is assumed to be parallel to the surface (along the x axis),

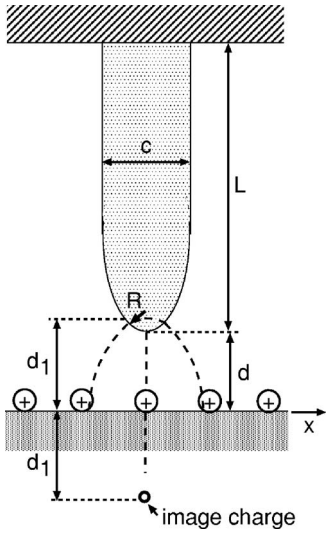

FIG. 18. Scheme of the tip-sample system. The tip shape is characterized by its length L and the tip radius of curvature R.

which will be a good approximation when the oscillation amplitude u_0 is sufficiently small. The cantilever width w, i.e., the size in the direction perpendicular to the x-z plane, is taken to be much larger than its thickness c ($w \gg c$), and d is the separation between the tip and sample surface. It is straightforward to obtain the static electric field distribution when $d \ll R$. In this case the electrostatic field of the entire cylinder is effectively the same as that due to its bottom part. The problem is then reduced to solving the two-dimensional Laplace equation with the boundary conditions that the potential has the constant values V and 0 at the metallic surfaces of the tip and sample. In this case the electric field distribution outside the conductors is equal to the field due to two charged wires passing through points at $z=\pm d_1 = \pm\sqrt{(d+R)^2-R^2}$ (Landau and Lifshitz, 1960). The wires have charges $\pm Q$ per unit length, $Q=CV$, where $C^{-1} = 2\ln[(d+R+d_1)/R]$. The electric potential at a point $\mathbf{r}$ exterior to the tip and the sample is

$$\varphi_0(\mathbf{r}) = -2Q[\ln|\mathbf{r}-\mathbf{r}_+| - \ln|\mathbf{r}-\mathbf{r}_-|] = Q\int_{-\infty}^{\infty}\frac{dq}{|q|}e^{iqx}(e^{-|q||z-z_+|} - e^{-|q||z-z_-|}), \tag{131}$$

where $\mathbf{r}_\pm = \pm\hat{z}d_1$. The attractive cantilever-surface force can be calculated straightforwardly using Eq. (131) (Chumak *et al.*, 2004).

A somewhat different picture applies in the case of an oscillating charged tip. The cantilever charge does not change when its tip moves parallel to the surface, while the sample charge varies in time at any fixed point. Thus the electric field from the oscillating tip will be the same as that from an oscillating wire located at $z=d_1$. The oscillating electric potential due to the tip, at a point $\mathbf{r}$ exterior to the tip and the sample, is

$$\varphi_1(\mathbf{r},t) = \varphi_1(\mathbf{r})e^{-i\omega t} + \text{c.c.}, \tag{132}$$

where

$$\varphi_1(\mathbf{r}) = iQu_0 \int_{-\infty}^{\infty} \frac{dq\, q}{|q|} e^{iqx} [e^{-|q||z-z_+|} - e^{-|q||z-z_-|} R_p(q,\omega)], \quad (133)$$

and $R_p(q,\omega)$ is the reflection amplitude for p-polarized electromagnetic waves. The electric field is given by $\mathbf{E}(\mathbf{r}) = -\nabla\varphi(\mathbf{r})$. The energy dissipation per unit time induced by the electromagnetic field inside the metallic substrate is determined by integrating the Poynting vector over the surface of the metal, and is

$$P = \frac{c}{4\pi} \int dS\, \hat{z} \cdot [\mathbf{E}(\mathbf{r}) \times \mathbf{B}^*(\mathbf{r})]_{z=+0} + \text{c.c.}$$
$$= -\frac{i\omega}{4\pi} \int dS \left(\varphi_1(\mathbf{r}) \frac{d}{dz} \varphi_1^*(\mathbf{r}) \right)_{z=+0} + \text{c.c.}$$
$$= 4\omega Q^2 |u_0|^2 w \int_0^{\infty} dq\, q e^{-2qd_1} \operatorname{Im} R_p(\omega,q). \quad (134)$$

Taking into account that the energy dissipation per unit time must be equal to $2\omega^2\Gamma|u_0|^2$, using Eq. (134) gives the friction coefficient

$$\Gamma = \lim_{\omega\to 0} 2C^2V^2w \int_0^{\infty} dq\, q e^{-2qd_1} \frac{\operatorname{Im} R_p(\omega,q)}{\omega}. \quad (135)$$

Now, assume that the electric potential at the surface of the tip is inhomogeneous and consists of the domains or patches. The cylinder with linear size w is "divided" into cylinder segments with the linear size w_i, $w=\Sigma_i w_i \gg w_i \gg \sqrt{dR}$, and with the surface potential $V_{is}=V+V_i$, where V is the bias voltage and V_i is the randomly fluctuating surface potential for the domain i. In the case of a cylindrical tip geometry all domains give independent contributions to the friction, which can be obtained from Eq. (135) after replacement $V\to V+V_i$ and $w\to w_i$. The contribution to friction from all domains is

$$\Gamma = \sum_i \Gamma_i = \sum_i \lim_{\omega\to 0} 2C^2(V+V_i)^2 w_i \times \int_0^{\infty} dq\, q e^{-2qd_1} \frac{\operatorname{Im} R_p(\omega,q)}{\omega}$$
$$= \lim_{\omega\to 0} 2C^2(V^2+V_0^2)w \times \int_0^{\infty} dq\, q e^{-2qd_1} \frac{\operatorname{Im} R_p(\omega,q)}{\omega}, \quad (136)$$

where we have assumed that the average value of the fluctuating surface potential $\langle V_i\rangle = \Sigma_i w_i V_i = 0$ and $V_0^2 = \Sigma_i w_i V_i^2/w$, so that V_0 is the root-mean-square variation of the surface potential. According to Eq. (136), bias voltage and patch contributions to the friction have the same dependence on d.

Many experiments use thermally evaporated thin films of gold (Stipe *et al.*, 2001). The work function of gold is 5.47, 5.37, and 5.31 eV for the ⟨100⟩, ⟨110⟩, and ⟨111⟩ directions, respectively (Lide, 2001). If the surfaces are clean and amorphous then we can assume that they consist of equal areas of these three crystallographic planes, and the root mean square $\langle\sigma_v^2\rangle^{1/2}$ of the potential distribution becomes

$$\langle\sigma_v^2\rangle^{1/2} = \sqrt{\langle (V_i - V_j)^2\rangle} = \sqrt{2(\langle V_i^2\rangle - \langle V_i\rangle^2)} \approx 90\ \text{mV}.$$

When annealed, thin gold films form mesa structures with the ⟨111⟩ crystallographic planes exposed. In this case, variations of the surface potential are presumably generated by the material lying between the mesas. The size of the mesas depends on the temperature of the substrate during the formation of the film.

Sukenik *et al.* measured the root-mean-square variation of the surface potential due to thermally evaporated gold using the Stark effect in sodium atoms (Sukenik *et al.*, 1993). The films were partially optically transparent with a thickness of 42 nm and heated at 120 °C for several hours in vacuum. They deduced that the magnitude of the fluctuating surface potential is $V_0=150$ mV, and showed that the scale of the lateral variation of the surface potential is of the order of the film thickness. The measurement of the noncontact friction between a gold tip and a gold sample gave $V_0 \sim 200$ mV (Stipe *et al.*, 2001), thus confirming the prediction of the theory that this parameter is determined by the root-mean-square variation of the surface potential.

Now, we consider a spherical tip (radius R) with (constant voltage) surface domains with the linear size R_i. If $R \gg R_i \gg \sqrt{dR}$, the domain on the apex of the tip will give the main contribution to the friction. In this case we can neglect the spatial variation of the surface potential and the electric field induced by the bias voltage is approximately the same as that which would be produced in the vacuum region between two point charges $\pm Q_i = \pm C(V+V_i)$ located at (Volokitin and Persson, 2005; Volokitin *et al.*, 2006)

$$z = \pm d_1 = \pm \sqrt{3Rd/2 + \sqrt{(3Rd/2)^2 + Rd^3 + d^4}}, \quad (137)$$

where

$$C = \frac{d_1^2 - d^2}{2d}. \quad (138)$$

It can be shown that the electrostatic force between the tip and metal surface within this approximation agrees well with the exact expression for a sphere above a metal surface (Hudlet *et al.*, 1998). The vibrations of the tip will produce an oscillating electromagnetic field, which in the vacuum region coincides with the electromagnetic field of an oscillating point charge. The friction coefficient for a point charge moving parallel to the surface due to the electromagnetic energy losses inside the sample is determined by (Persson, 1991) (see also Appendix D)

$$\Gamma_{\parallel} = \lim_{\omega\to 0} \frac{Q_i^2}{2} \int_0^{\infty} dq\, q^2 e^{-2qd_1} \frac{\operatorname{Im} R_p(\omega,q)}{\omega}. \quad (139)$$

For motion normal to the surface, $\Gamma_{\perp} = 2\Gamma_{\parallel}$. Thus, just as for the cylindrical tip geometry, for a spherical tip the friction depends quadratically on the bias voltage. How-

ever, for a spherical tip the parabola begins from zero in contrast to the cylindrical tip where the parabola begins from a finite positive value.

2. Clean surface

For clean flat surfaces the reflection amplitude is determined by the Fresnel formula (38). In this case, for a cylindrical tip with radius $R \gg d$ and a metal substrate, Eq. (136) gives

$$\Gamma_{cl}^{c} = \frac{w(V^2 + V_0^2)}{2^6 \pi \sigma d^2}. \tag{140}$$

This formula, neglecting the contribution from the spatial variation of the surface potential, was first derived by Chumak *et al.* (2004) using a different approach. With $w = 7 \times 10^{-6}$ m and $\sigma = 4 \times 10^{17}$ s^{-1} (which corresponds to gold at 300 K), and with $d = 20$ nm and $V = 1$ V, Eq. (140) gives $\Gamma = 2.4 \times 10^{-20}$ kg/s which is eight orders of magnitude smaller than the experimental value 3×10^{-12} kg/s (Stipe *et al.*, 2001).

Assuming $R \gg d$, using Eqs. (139) and (38) gives the friction between a spherical tip and a clean sample surface

$$\Gamma_{cl}^{s} = \frac{3^{1/2} R^{1/2} V^2}{2^7 d^{3/2} \pi \sigma}. \tag{141}$$

This expression is only a factor of 1.6 smaller than the result obtained independently by Chumak *et al.* (2004). For the same parameters as above and at $d = 20$ nm and $R = 1$ μm, the friction for a spherical tip is two orders of magnitude smaller than that for the cylindrical tip. The friction determined by Eq. (141) has the same distance dependence as in the experiment (Stipe *et al.*, 2001). However, the magnitude of the friction is too small to explain the experimental data.

To get insight into the possible mechanisms of enhancement of noncontact friction, it is instructive to note that Eq. (140) can be obtained qualitatively from the following simple geometrical arguments (Stowe *et al.*, 1999). The vibrating tip will induce current in the sample in a volume with the spatial dimensions L_x, L_y, and L_z. The instantaneous dissipated power in the sample is $P \sim I^2 r$, where I is the current and r is the effective resistance. The current I is proportional to the tip velocity v_x, and can be written as $I \sim v_x Q_t / L_x$, where Q_t is the charge of the tip. The effective resistance r can be approximated by the macroscopic relation $r = \rho L_x / L_y L_z$, where ρ is the resistivity. Using these simple expressions for the current I and the resistance, and using the relation $Q_t = C_t V_s$ (where C_t is the tip-sample capacitance) for the induced charge, the instantaneous power dissipation is

$$P = I^2 r \sim \rho \frac{v_x^2 C_t^2 V_s^2}{L_x L_y L_z}. \tag{142}$$

Comparing this expression with $P = \Gamma v_x^2$ we get

$$\Gamma \sim \rho \frac{C_t^2 V_s^2}{L_x L_y L_z}. \tag{143}$$

For the cylindrical tip vibrating above the clean surface, $L_y \sim w$ and $L_x \sim L_z \sim d_1$. For $d \ll R$ the tip-sample capacitance $C_t \sim w\sqrt{R/8d}$ and $d_1 \sim \sqrt{2dR}$. Substituting these expressions into Eq. (143) gives Eq. (140) to within a numerical factor of order of unity. From Eq. (143) it follows that the friction will increase when the thickness L_z of the dissipation volume decreases. This is the reason why 2D systems may exhibit higher friction than 3D systems.

3. Film on top of a higher-resistivity substrate

From the qualitative arguments given above, it follows that for a thin metal film on top of a higher resistivity substrate, e.g., a dielectric or a high-resistivity metal, the friction will be larger than for a semi-infinite sample, with the same bulk resistivity as for the film. In this case, the main part of the dissipation occurs within the film, and according to Eq. (143) this will give rise to a strong enhancement of the friction.

For a planar film with thickness d_f and dielectric constant ε_2 on top of a substrate with dielectric constant ε_3, the reflection amplitude is determined by Eq. (107). For a metallic film on a dielectric substrate, or a metallic film on a metallic substrate with $\sigma_2 \gg \sigma_3$, for $d_1 \gg d_f$ and $R \gg d$, Eqs. (136) and (107) give

$$\Gamma_f^c = \frac{w(V^2 + V_0^2) R^{1/2}}{2^{9/2} \pi \sigma_2 d_f d^{3/2}}. \tag{144}$$

This is greater by a factor of $2\sqrt{2dR}/d_f$ than the corresponding friction for a semi-infinite sample with the clean surface with the same bulk conductivity as for the film. For a thin film the effective resistivity of the substrate is increased, giving rise to additional Ohmic dissipation. Chumak *et al.* (2004) obtained Eq. (144) using a different approach and neglecting the spatial variation of the surface potential.

4. 2D system on top of a dielectric or metal substrate

We now consider a 2D system, e.g., electronic surface states or a quantum well, or an incommensurate layer of ions adsorbed on a metal surface. For example, for the Cs/Cu(100) system, experiment suggests the existence of an acoustic film mode even for the dilute phase (coverage $\theta \approx 0.1$). This implies that the Cs/Cu(100) adsorbate layer experiences a negligible surface pinning potential. The reflection amplitude for a 2D system is given by Eq. (113) and

$$\mathrm{Im}\, R_p \approx \frac{2\omega\eta q a \omega_q^2}{(\omega^2 - \omega_q^2)^2 + \omega^2 \eta^2}, \tag{145}$$

where $\omega_q^2 = 4\pi n_a e^{*2} a q^2 / M$. In the case of a 2D structure on top of a dielectric, the factor qa in Eq. (145) and in the expression for ω_q^2 must be replaced by $1/\varepsilon$, where ε

is the dielectric function of the substrate. Using Eq. (145) in Eq. (136) for $R \gg d$ we get

$$\Gamma_{ad}^{c} = \frac{w\eta M R^{1/2}(V^2 + V_0^2)}{2^{9/2} d^{3/2} \pi n_a e^{*2}}. \tag{146}$$

This friction exhibits the same distance dependence as observed experimentally (Stipe *et al.*, 2001). The same expression for the friction is valid for a 2D structure on top of a dielectric. Comparing Eqs. (140) and (146) we find that a 2D structure on top of a substrate gives the same magnitude of the friction as for a semi-infinite solid (with a clean surface) with the effective conductivity $\sigma_{\rm eff} = n_a e^{*2}/M\eta 2 d_1$. Agreement with experiment (Stipe *et al.*, 2001) for $d = 20$ nm is obtained if $\sigma_{\rm eff} \approx 4 \times 10^9$ s^{-1}. In the case of a 2D electron system, for $R = 1$ μm such an effective conductivity is obtained if $\eta_\parallel = 10^{14}$ s^{-1} and $n_a = 10^{15}$ m^{-2}. For Cs/Cu(100), for $n_a = 10^{18}$ m^{-2} ($\theta \approx 0.1$) the electric charge of the Cs ions $e^* = 0.28e$ (Senet *et al.*, 1999). Due to the similarities of Cu and Au surfaces, a similar effective charge can be expected for the Cs/Au surface. For such a 2D system agreement with experiment is obtained for $n_a = 10^{18}$ m^{-2} and $\eta_\parallel = 10^{11}$ s^{-1}. Volokitin and Persson (2005) estimated the damping parameter associated with the covalent bond for a Cs atom on Cu (100): $\eta_{\parallel \rm cov} = 3 \times 10^9$ s^{-1}. However, the collisions between ions, and between ions and other surface defects, will also contribute to η. In this case $\eta_{\rm col} \sim v_T/l$, where $v_T \sim \sqrt{k_B T/M}$ and l is the ion mean free path. For $T = 293$ K and $l \sim 1$ nm we get $\eta_{\rm col} = 10^{11}$ s^{-1}.

For a spherical tip and a 2D system on top of the substrate, from Eqs. (145) and (139) for $R \gg d$ we get the contribution to the friction from the 2D system,

$$\Gamma_{ad}^{s} = \frac{3RM\eta V^2}{2^6 d \pi n_a e^{*2}}. \tag{147}$$

At $d = 20$ nm and $R = 1$ μm this friction is approximately two orders of magnitude smaller than for the cylindrical tip.

B. Friction due to spatial fluctuations of static charge in the bulk of the sample

In this section we consider a dielectric substrate with a stationary, inhomogeneous distribution of charged defects. Such a situation was investigated experimentally (Stipe *et al.*, 2001) by employing a fused silica sample irradiated with γ rays. In the course of irradiation, positively charged centers (Si dangling bonds) are generated. Randomly distributed positive charges are compensated by randomly distributed negative charges; thus on average the sample is electrically neutral. We model the sample as consisting of microscopically small volume elements ΔV_i. Each volume element is chosen sufficiently small that no more than one charge center is present in it. Thus the electric charge q_i of each element is equal to $\pm e$ or 0, in such a way that the average $\langle q_i \rangle = 0$. We consider fluctuations of charges in different volume elements i, j to be statistically independent, so that $\langle q_i q_j \rangle = 0$ for $i \neq j$. The mean square of charge fluctuations within a given element $\langle q_i q_i \rangle \approx 2Ne^2$, where N is the average number of positive charges in one volume element. In the absence of cross terms, the average tip-sample friction coefficient is determined by adding the friction coefficient from all charges q_i. According to Eq. (139) the contribution to the friction coefficient from the charge q_i in the element ΔV_i is

$$\Delta\Gamma_{i\parallel} = \lim_{\omega \to 0} Ne^2 \int_0^\infty dq\, q^2 e^{-2qd_i} \frac{{\rm Im}\, R_p(\omega, q)}{\omega}, \tag{148}$$

where $d_i = D(x_i, y_i) - z_i$. Here the coordinates x_i, y_i, z_i give the position of the ith volume element in the substrate, and $D(x_i, y_i)$ is the distance between the sample and points x_i, y_i located on the surface of the tip. The total friction coefficient is obtained by summing over all volume elements. Replacing the sum by an integral ($N\Sigma \to n \int d^3 r$, where n is the number of positive charge centers per unit volume) and integrating over z gives

$$\Gamma_\parallel = \lim_{\omega \to 0} \frac{ne^2}{2} \int_0^\infty dq\, q \int dx \int dy\, e^{-2qD(x,y)} \times \frac{{\rm Im}\, R_p(\omega, q)}{\omega}. \tag{149}$$

For a cylindrical tip $D(x, y) = d + x^2/2R$, and we get

$$\Gamma_\parallel^c = \lim_{\omega \to 0} \frac{\sqrt{\pi R} n e^2 w}{2} \int_0^\infty dq\, q^{1/2} e^{-2qd} \frac{{\rm Im}\, R_p(\omega, q)}{\omega}. \tag{150}$$

Using the same parameters as in Sec. II.B, for a cylindrical gold tip separated by $d = 10$ nm from a dielectric sample with $n = 7 \times 10^{17}$ cm^{-3} we get $\Gamma_\parallel = 4.4 \times 10^{-20}$ kg s^{-1}.

For the tip surface with a 2D structure on it, using Eq. (145) we get

$$\Gamma_{2D\parallel}^{c} = \frac{1}{2^{5/2}} \left(\frac{e}{e^*}\right)^2 \sqrt{\frac{R}{d}} \frac{nw}{n_a} M\eta = \frac{e^2 nw}{16\sigma_{\rm eff} d}. \tag{151}$$

With $\sigma_{\rm eff} = n_a e^{*2}/2M\eta d_1 = 4 \times 10^9$ s^{-1}, $n = 7 \times 10^{17}$ cm^{-3}, and with the other parameters the same as before, we get for $d = 10$ nm, $\Gamma_{2D\parallel}^{c} = 3.5 \times 10^{-12}$ kg s^{-1}, which is nearly the same as observed experimentally (Stipe *et al.*, 2001). Thus the theory of the friction between a gold tip and silica substrate with an inhomogeneous distribution of charged defects is consistent with the theory of friction between a gold tip and gold substrate (see Sec. II.D). In both theories we have assumed that the gold surfaces are covered by a 2D structure.

The analysis above has ignored the screening of the electric field in the dielectric substrate. This can be justified in the case of small tip-sample separations (substantially smaller than the screening length), as only defects in the surface layer of thickness d contribute to the integral in Eq. (149). When screening is included, the effective electric field outside the sample will be reduced by the factor $(\varepsilon + 1)/2$ (Landau and Lifshitz, 1960) and

the friction coefficient will be reduced by the factor $[(\varepsilon+1)/2]^2$, which is equal to 6.25 in the case of silica.

VII. PHONON AND INTERNAL NONCONTACT FRICTION

A. Noncontact friction due to excitation of substrate phonons

Consider a tip which performs harmonic oscillation, $u=u_0\exp(-i\omega t)+$c.c., above an elastic body with a flat surface. This will result in a oscillating stress acting on the surface of the solid which excites acoustic waves with parallel wave number $q<\omega/c_s$, where c_s is the sound velocity. The stress σ_{iz} acting on the surface of the elastic solid can be represented through the Fourier integral

$$\sigma_{iz}(\mathbf{x},t)=\int\frac{d^2q}{(2\pi)^2}\sigma_i(\mathbf{q})u_0e^{i\mathbf{q}\cdot\mathbf{x}-i\omega t}+\text{c.c.} \tag{152}$$

Using the theory of elasticity (assuming an isotropic elastic medium for simplicity), one can calculate the displacement field u_i at the surface $z=0$ in response to the surface stress distribution σ_{iz},

$$u_i(\mathbf{x},t)=\int\frac{d^2q}{(2\pi)^2}M_{ij}(\mathbf{q},\omega)\sigma_j(\mathbf{q})u_0e^{i\mathbf{q}\cdot\mathbf{x}-i\omega t}+\text{c.c.} \tag{153}$$

The energy dissipation per unit time equals

$$P=\int d^2x\langle\dot{u}_i(\mathbf{x},t)\sigma_{iz}(\mathbf{x},t)\rangle$$

$$=2\omega\int\frac{d^2q}{(2\pi)^2}\,\mathrm{Im}\,M_{ij}(\mathbf{q},\omega)\sigma_i(\mathbf{q})\sigma_j^*(\mathbf{q})|u_0|^2, \tag{154}$$

where $\langle\cdots\rangle$ stands for time averaging. The explicit form of the stress tensor M_{ij} in the model of the elastic continuum has been given by Persson (2001) [see also Volokitin *et al.* (2006)]. The energy dissipation per unit time must be equal to $\Gamma\langle\dot{u}(t)^2\rangle=\Gamma 2\omega^2|u_0|^2$. Comparing this expression with Eq. (154) gives

$$\Gamma=\int\frac{d^2q}{(2\pi)^2}\frac{\mathrm{Im}\,M_{ij}(\mathbf{q},\omega)}{\omega}\sigma_i(\mathbf{q})\sigma_j^*(\mathbf{q}). \tag{155}$$

At typical experimental conditions we have $\omega\sim10^3$–10^6 s^{-1} and $qr^*<\omega r^*/c_s<10^{-3}\ll1$, where the effective radius of the interaction $r^*\approx\sqrt{dR}$, d is the separation between the tip and the sample, and R is the radius of curvature of the tip. Volokitin *et al.* (2006) showed that in this case the contribution to the friction from excitation of acoustic waves can be determined by calculating the energy dissipation due to an oscillating point force applied to the surface of the semi-infinite elastic continuum. These calculations were done in connection with the vibrational energy relaxation of adsorbates (Persson and Ryberg, 1985). According to this theory the friction coefficient for vibration of the tip normal to the surface is

$$\Gamma_\perp=\frac{\xi_\perp}{4\pi}\frac{K^2}{\rho c_t^3}, \tag{156}$$

where $\xi_\perp\approx1.65$, c_t is the transverse sound velocity of the solid, ρ is the mass density of the sample, and $K=\partial F/\partial d$, with $F(d)$ the static force acting on the tip due to interaction with the sample. For vibration of the tip parallel to the sample surface, the friction coefficient due to excitation of the acoustic waves is [see Volokitin *et al.* (2006)]

$$\Gamma_\parallel=\frac{\xi_\parallel}{4\pi}\frac{\omega^2}{\rho c_t^5}F^2(d), \tag{157}$$

where $\xi_\parallel\approx1.50$. Using Eqs. (156) and (157) we get $\Gamma_\parallel/\Gamma_\perp\sim(\omega d/c_t)^2\ll1$. Thus the phononic friction coefficient for parallel vibrations of the tip will be smaller by many orders of magnitude than for normal vibrations. We consider now two different contributions to the tip-sample interaction.

1. van der Waals interaction

According to the Lifshitz theory (Lifshitz, 1956; Dzyaloshinskii *et al.*, 1961) the stress $\sigma_{zz}(d)$ acting on the surfaces of two identical semi-infinite bodies due to van der Waals interaction at small separation $d\ll c/\omega_p$ (where ω_p is the plasma frequency) and $d\ll\lambda_T$ is

$$\sigma_{zz}(d)=\frac{\hbar}{8\pi^2d^3}\int_0^\infty d\xi\frac{[\varepsilon(i\xi)-1]^2}{[\varepsilon(i\xi)+1]^2}. \tag{158}$$

In the Drude model the explicit form of ε is

$$\varepsilon(i\xi)=1+\frac{\omega_p^2}{\xi(\xi+\eta)}\approx1+\frac{\omega_p^2}{\xi^2}, \tag{159}$$

where we have used that for most typical metals $\eta\ll\omega_p$. It follows from Eqs. (158) and (159) that

$$\sigma_{zz}=\frac{\hbar\omega_p}{32\sqrt{2}\pi d^3}. \tag{160}$$

For a spherical tip of radius R, using the same approximation as in Eq. (79), we get

$$F_z(d)=\frac{R\hbar\omega_p}{32\sqrt{2}d^2} \tag{161}$$

and

$$K^s=\frac{R\hbar\omega_p}{16\sqrt{2}d^3}. \tag{162}$$

Similarly, in the case of a cylindrical tip we have

$$F_z^c(d)=\frac{3wR^{1/2}\hbar\omega_p}{2^8d^{5/2}} \tag{163}$$

and

$$K^c = \frac{15wR^{1/2}\hbar\omega_p}{2^9 d^{7/2}}. \tag{164}$$

For a copper tip separated from a copper substrate by $d=10$ nm, and with $R=1$ μm, $w=7$ μm, we get for a spherical tip $\Gamma^s_\perp = 6.3\times10^{-18}$ kg s^{-1} and for a cylindrical tip $\Gamma^c_\perp = 1.3\times10^{-14}$ kg s^{-1}. The phononic friction decreases as d^{-6} and d^{-7} for the spherical and cylindrical tips, respectively.

2. Electrostatic interaction due to a bias voltage

In the presence of the bias voltage V the attractive force between the tip and sample at $d \ll R$ is

$$F^c(d) = \frac{wV^2R^{1/2}}{2^{7/2}d^{3/2}} \tag{165}$$

for a cylindrical tip, and

$$F^s(d) = \frac{RV^2}{4d} \tag{166}$$

for a spherical tip. For bias voltage $V=1$ V, and with the other parameters the same as above, we get $\Gamma^s_\perp = 8.8\times10^{-17}$ kg s^{-1} and $\Gamma^c_\perp = 1.2\times10^{-13}$ kg s^{-1} for the spherical and cylindrical tips, respectively. Note that in this case the friction depends on the bias voltage as V^4.

B. Noncontact friction due to internal friction of the substrate

In studying the phononic friction in Sec. VII.A it was assumed that the deformations of the solids are purely elastic. The deformation will be purely elastic (or adiabatic) only for infinitely small velocity, so that at every moment the system stays in the equilibrium state. However, real motion always occurs with finite velocity, and the body does not stay in equilibrium. Thus nonadiabatic "flow processes" occur, resulting in dissipation of the mechanical energy.

At least two kinds of processes result in energy dissipation: (a) heat flow resulting from the temperature gradient, and (b) some kind of internal motion, e.g., point defect flipping. These processes of energy dissipation can be denoted (as in liquids) as internal friction or viscosity.

The friction coefficient due to the internal friction is determined by Eq. (155). However, in contrast to the phononic friction, large values of $q \gg \omega/c_t$ play the most important role for the internal friction. For $q \gg \omega/c_s$ the tensor component M_{zz} is (Persson, 2001)

$$M_{zz} = \frac{2(1-\nu^2)}{Eq}, \tag{167}$$

where $E(\omega)$ is the complex elastic modulus and ν is the Poisson ratio.

1. van der Waals interaction

For $R \gg d$ only the σ_{zz} component of the stress tensor due to the van der Waals interaction is important. In this case, for vibrations of the cylindrical tip parallel to the sample surface, we get

$$\sigma_z(\mathbf{q}) = \int d^2x e^{i\mathbf{q}\cdot\mathbf{x}} \frac{\partial}{\partial x}\sigma_{zz}(\mathbf{x}) = -\frac{iq_xR^{1/2}}{2^7 d^{5/2}} \frac{\sin(q_y w/2)}{q_y}(3+\xi^2+3\xi)e^{-\xi}, \tag{168}$$

where $\xi = \sqrt{2dR}q_x$. Using Eqs. (168) and (167) in Eq. (155) we get for a cylindrical tip

$$\Gamma^c_\parallel = \frac{75\pi}{2^{16}} \frac{w\hbar^2\omega_p^2}{d^6} \frac{\mathrm{Im}[E/(1-\nu^2)]}{\omega|E/(1-\nu^2)|^2}. \tag{169}$$

For a spherical tip, similar calculations give

$$\Gamma^s_\parallel = \frac{0.25}{2^9\sqrt{2}\pi} \frac{R^{1/2}\hbar^2\omega_p^2}{d^{11/2}} \frac{\mathrm{Im}[E/(1-\nu^2)]}{\omega|E/(1-\nu^2)|^2}. \tag{170}$$

In general, Im $E(\omega)$ has many resonance peaks, corresponding to different thermally activated relaxation processes. One important source of internal friction at high frequencies is related to thermal currents: elastic compression of a material is commonly associated with heating effects. If the compression takes place sufficiently rapidly, there is no opportunity for heat to be conducted away, while for very slow compression temperature gradients are eliminated by thermal conduction. In both these cases the process of compression will be reversible. In the former case it will be adiabatic and in the latter case isothermal. In both these limiting cases the contribution from thermal current to the internal friction will be negligible. However, in the intermediate frequency regime, we expect dissipation of mechanical energy into heat. The characteristic frequency for the maximum dissipation will be of the order of $\omega_t = 1/\tau$, where, from dimensional arguments, we expect the relaxation time $\tau \sim l^2/D$, where l is the linear size of the compression region and the thermal diffusibility $D = \kappa/\rho C_p$ (where C_p is the specific heat and κ is the heat conductivity). For $l \sim 10^3$ Å this gives for gold $\omega_t \approx 10^{11}$ s^{-1}, which is much higher than the resonance frequency of the cantilever of the atomic force microscope. Another important contribution to the internal friction is point-defect flipping. This involves thermally activated transitions of point defects or loose sites in a crystalline or amorphous network. A special case is the vibrational motion of adsorbates at the surface of the substrate and/or on the tip, as was treated separately above. Another contribution to the internal friction comes from grain-boundary slip (McClintock and Argon 1966). For a copper cylindrical tip and a copper substrate using $d=10$ nm, $w=7$ μm, $R=1$ μm, $\omega=10^4$ s^{-1}, and, as is typical for metals value Im $E(\omega)/|E(\omega)| \approx 10^{-5}$ (Persson, 2000), and $E \approx 10^{11}$ N/m^2, we get $\Gamma^c_\parallel \approx 10^{-16}$ kg s^{-1}. Thus at this separation the internal friction gives a much smaller contribution to the friction coefficient than the electrostatic

friction due to bias voltage or spatial variation of the surface potential. However, internal friction can give the dominant contribution for small separations $d \lesssim 1$ nm. For a spherical tip with $R=1$ μm the friction coefficient is two orders of magnitude smaller. Finally we note that the internal friction of solids gives an important contribution to the rolling resistance of most solids (Persson, 1998), and is the main contribution to rubber friction on rough substrates, e.g., road surface (Persson, 1998), where in the transition region between the rubbery and glassy region of the rubber viscoelastic spectra, $\mathrm{Im}\, E(\omega)/|E(\omega)| \approx 1$.

VIII. SUMMARY AND OUTLOOK

All material bodies are surrounded by a fluctuating electromagnetic field due to thermal and quantum fluctuations of the current density inside them. This fluctuating electromagnetic field can be studied using the semiclassical theory due to Rytov, or quantum field theory. In the near-field zone of any body the electromagnetic field is greatly enhanced in comparison with the far-field region due to the existence of evanescent waves. This enhancement is especially large if the surface of the body can support surface modes, e.g., surface plasmon polaritons, surface phonon polaritons, or adsorbate vibrational modes of adsorbed ions. The thermal radiation emitted by surface modes is spatially and temporally coherent, which can be used for developing tunable infrared emitters with high power in a narrow spectral band, which may be used for sensing, spectroscopy, and thermophotovoltaic applications.

The fluctuating electromagnetic field is responsible for many important phenomena, e.g., the radiative heat transfer between bodies, the van der Waals interaction, and the van der Waals friction. The heat transfer between two bodies in a vacuum is strongly modified when the surfaces come closer than the characteristic wavelength of thermal radiation, $\lambda_T = c\hbar/k_B T$. For separation $d < \lambda_T$ the heat transfer is greatly enhanced in comparison with blackbody radiation, due to the contribution from evanescent waves. The latter contribution is particularly large if the conductivity of the materials is tuned to maximize the heat flow due to photon tunneling. At room temperature this implies conductivities typical for semimetals, such as carbon, or for metal-insulator composites. The radiative heat transfer can also be greatly enhanced when resonant photon tunneling between surface modes, like surface plasmon polaritons or surface phonon polaritons, can occur. In the case of resonant photon tunneling the heat flux occurs within a very narrow frequency band, which can find application in energy conversion technologies, such as thermophotovoltaic energy conversion. Adsorbates can generate evanescent waves very localized in space and in a very narrow frequency band. These phenomena can be used in scanning probe microscopy for local heating and modification of surfaces.

Similar to radiative heat transfer, the van der Waals friction can also be enhanced in the case of resonant photon tunneling between surface modes. This enhancement is especially large for surfaces which can exhibit a 2D acoustic branch in the spectrum of the elementary excitations, e.g., 2D electron systems on dielectric surfaces, or adsorbed layers of ions with acoustic vibrations parallel to the surface. For such systems the electrostatic friction can also be important. In particular, the friction observed by Stipe *et al.* (2001) and Kuehn, Loring, and Marohn (2006) can be explained by electrostatic friction. The van der Waals friction is responsible for the frictional drag between quantum wells (Gramila *et al.*, 1991, 1993; Sivan *et al.*, 1992) and can also be measured in noncontact friction experiments using state-of-the-art equipment. The noncontact friction can be technologically important for ultrasensitive force registration, and is also of great basic scientific interest.

The van der Waals friction will be even more important for 1D structures like carbon nanotubes. The 1D nature of carbon nanotubes may have profound consequences for the basic physical phenomenology for their description: single-wall carbon nanotubes have been predicted to be Luttinger liquids (Egger and Gogolin, 1997, 1998), and some experimental evidence exists (Bockrath *et al.*, 1999) even though other interpretations has been suggested (Kasumov *et al.*, 2003). Whether multiwall carbon nanotubes are Fermi or Luttinger liquids has been investigated experimentally (Tarkiainen *et al.*, 2001; Kang *et al.*, 2003; Krstić *et al.*, 2003) theoretically (Egger, 1999) and seems to depend on the situation. In carbon nanotube ropes also the situation is not yet clear (Hunger *et al.*, 2004). One hopes to get additional information on strongly correlated low-dimensional systems from the study of noncontact friction between them.

In a recent experiment (Ghosh *et al.*, 2003, 2004), it was observed that the flow of an ion-rich liquid such as water through assembles of single-walled carbon nanotubes induces a voltage in the nanotubes along the direction of the flow. Strikingly, the voltage grows logarithmically with the liquid flow velocity over nearly six decades. Several mechanisms were proposed to explain the frictionally induced voltage in the carbon nanotubes (Ghosh *et al.*, 2003, 2004; Persson *et al.*, 2004). In one proposed mechanism (Ghosh *et al.*, 2004) the induced voltage is related to the fluctuating Coulomb field created by charge density fluctuations in the moving liquid. Thus the problem of flow-induced voltage may be related to the van der Waals friction. However, the situation is not yet clear.

ACKNOWLEDGMENTS

A.I.V. acknowledges financial support from the Russian Foundation for Basic Research (Grant No. 06-02-16979-a), DFG, and the European Union Nanotribology Project. B.N.J.P. and A.I.V. acknowledge support from the European Union Smart Quasicrystals Project.

APPENDIX A: CROSS-SPECTRAL DENSITY OF THE ELECTRIC FIELDS

Using Eqs. (8)–(10) we get

$$\begin{aligned}\langle E_i(\mathbf{r})E_j^*(\mathbf{r}')\rangle_\omega &= \frac{\hbar}{8\pi^2}\coth(\hbar\omega/2k_BT)\int d\mathbf{r}''\int d\mathbf{r}'''\\ &\times \mathrm{Im}\,\varepsilon_{kl}(\mathbf{r}'',\mathbf{r}''')D_{ik}(\mathbf{r},\mathbf{r}'')D_{jl}^*(\mathbf{r}',\mathbf{r}''')\\ &= \frac{\hbar c^2}{16\pi^2 i\omega^2}\coth(\hbar\omega/2k_BT)\int dS_{1l}''\\ &\times\{D_{ik}(\mathbf{r},\mathbf{r}'')[\nabla_l''D_{jk}^*(\mathbf{r}',\mathbf{r}'')\\ &- \nabla_k''D_{jl}^*(\mathbf{r}',\mathbf{r}'')] - D_{jk}^*(\mathbf{r}',\mathbf{r}'')\\ &\times[\nabla_l''D_{ik}(\mathbf{r},\mathbf{r}'') - \nabla_k''D_{il}(\mathbf{r},\mathbf{r}'')]\},\end{aligned} \tag{A1}$$

where we have transformed an integral over the volume of the body to an integral over the surface of the body. Assume that the two points $\mathbf{r}$ and $\mathbf{r}'$ lie outside the bodies. Using that outside the body for $\mathbf{r}\neq\mathbf{r}'\neq\mathbf{r}''$,

$$D_{ik}(\mathbf{r},\mathbf{r}'')\nabla_k''D_{jl}^*(\mathbf{r}',\mathbf{r}'') = \nabla_k''[D_{ik}(\mathbf{r},\mathbf{r}'')D_{jl}^*(\mathbf{r}',\mathbf{r}'')], \tag{A2}$$

$$D_{Jk}^*(\mathbf{r}',\mathbf{r}'')\nabla_k''D_{il}(\mathbf{r},\mathbf{r}'') = \nabla_k''[D_{jk}^*(\mathbf{r}',\mathbf{r}'')D_{il}(\mathbf{r},\mathbf{r}'')], \tag{A3}$$

and performing the surface integral in Eq. (A1) gives

$$\begin{aligned}\langle E_i(\mathbf{r})E_j^*(\mathbf{r}')\rangle_\omega &= \frac{\hbar c^2}{16\pi^2 i\omega^2}\coth(\hbar\omega/2k_BT)\\ &\times\int d\mathbf{S}_1''\{D_{ik}(\mathbf{r},\mathbf{r}'')\nabla''D_{jk}^*(\mathbf{r}',\mathbf{r}'')\\ &- D_{jk}^*(\mathbf{r}',\mathbf{r}'')\nabla''D_{ik}(\mathbf{r},\mathbf{r}'')\}.\end{aligned} \tag{A4}$$

For the plane surface it is convenient to decompose the electromagnetic field into s- and p-polarized plane waves. In this representation with $\hat{q}=\mathbf{q}/q$ and $\hat{n}=[\hat{z}\times\hat{q}]$, where $\mathbf{q}$ is the surface component of the wave vector, the Green's tensor is given by

$$\begin{aligned}\vec{\mathbf{D}}(\mathbf{r},\mathbf{r}') = \int\frac{d^2q}{(2\pi)^2}[&\hat{n}D_{nn}(z,z',\mathbf{q})\hat{n} + \hat{q}D_{qq}(z,z',\mathbf{q})\hat{q}\\ &+ \hat{z}D_{zz}(z,z',\mathbf{q})\hat{z} + \hat{z}D_{zq}(z,z',\mathbf{q})\hat{q}\\ &+ \hat{q}D_{qz}(z,z',\mathbf{q})\hat{z}]e^{i\mathbf{q}\cdot(\mathbf{x}-\mathbf{x}')},\end{aligned} \tag{A5}$$

where we have taken into account that $D_{nz}=D_{nq}=0$ (see Appendix B). The cross-spectral density of the electric field is given by

$$\begin{aligned}\langle\mathbf{E}(\mathbf{r})\mathbf{E}^*(\mathbf{r}')\rangle_\omega = \frac{\hbar c^2}{16\pi^2 i\omega^2}\coth(\hbar\omega/2k_BT)\int\frac{d^2q}{(2\pi)^2}\Big(&\hat{n}D_{nn}(z,z'',\mathbf{q})\frac{\partial}{\partial z''}D_{nn}^*(z',z'',\mathbf{q})\hat{n} + \hat{q}D_{qq}(z,z'',\mathbf{q})\frac{\partial}{\partial z''}D_{qq}^*(z',z'',\mathbf{q})\hat{q}\\ &+ \hat{q}D_{qz}(z,z'',\mathbf{q})\frac{\partial}{\partial z''}D_{qz}^*(z',z'',\mathbf{q})\hat{q} + \hat{z}D_{zz}(z,z'',\mathbf{q})\frac{\partial}{\partial z''}D_{zz}^*(z',z'',\mathbf{q})\hat{z} + \hat{z}D_{zq}(z,z'',\mathbf{q})\frac{\partial}{\partial z''}D_{zq}^*(z',z'',\mathbf{q})\hat{z}\\ &+ \hat{z}D_{zq}(z,z'',\mathbf{q})\frac{\partial}{\partial z''}D_{qz}^*(z',z'',\mathbf{q})\hat{q} + \hat{z}D_{zz}(z,z'',\mathbf{q})\frac{\partial}{\partial z''}D_{qz}^*(z',z'',\mathbf{q})\hat{q} + \hat{q}D_{qq}(z,z'',\mathbf{q})\frac{\partial}{\partial z''}D_{zz}^*(z',z'',\mathbf{q})\hat{z}\\ &+ \hat{q}D_{qz}(z,z'',\mathbf{q})\frac{\partial}{\partial z''}D_{zz}^*(z',z'',\mathbf{q})\hat{z} - [D_{ik}(z,z'',\mathbf{q})\leftrightarrow D_{jk}^*(z',z'',\mathbf{q})]\Big)_{z''=+0}e^{i\mathbf{q}\cdot(\mathbf{x}-\mathbf{x}')},\end{aligned} \tag{A6}$$

$[\cdots\leftrightarrow\cdots]$ denotes the terms that can be obtained from the first terms by permutation of $D_{ik}(z,z'',\mathbf{q})$ and $D_{jk}^*(z',z'',\mathbf{q})$. The Green's functions in Eq. (A6) can be obtained from the Green's functions calculated in Appendix B for $R_{2p(s)}=0$. Substituting this in Eq. (A6) gives Eq. (13).

APPENDIX B: HEAT FLUX BETWEEN TWO PLANE SURFACES

Suppose that the half space $z<0$ is occupied by a solid at temperature T_1 with the reflection amplitudes $R_{1p}(\mathbf{q},\omega)$ and $R_{1s}(\mathbf{q},\omega)$ for s- and p-electromagnetic fields, respectively. Similarly, the half space $z>d$ is occupied with a solid at temperature T_2 with the reflection amplitudes $R_{2p}(\mathbf{q},\omega)$ and $R_{2s}(\mathbf{q},\omega)$. The region $0<z<d$ is assumed to be vacuum. Here $\mathbf{q}$ is the surface component of wave vector $\mathbf{k}=(\mathbf{q},\gamma)$ and

$$\gamma = \sqrt{\left(\frac{\omega}{c}\right)^2 - q^2}. \tag{B1}$$

Since the system is uniform in the $\mathbf{x}=(x,y)$ directions, the Green's function $D_{ij}(\mathbf{r},\mathbf{r}')$ can be represented by the Fourier integral

$$D_{ij}(\mathbf{r},\mathbf{r}') = \int\frac{d^2q}{(2\pi)^2}e^{i\mathbf{q}\cdot(\mathbf{x}-\mathbf{x}')}D_{ij}(z,z',\mathbf{q},\omega). \tag{B2}$$

In the x-y plane it is convenient to choose the coordinate axes along the vectors $\hat{q}=\mathbf{q}/q$ and $\hat{n}=\hat{z}\times\hat{q}$. In this coordinate system the equations (9) and (10) for the Green's functions become

$$\left(\gamma^2+\frac{\partial^2}{\partial z^2}\right)D_{nn}(z,z')=-\frac{4\pi\omega^2}{c^2}\delta(z-z'), \tag{B3}$$

$$\left(\frac{\omega^2}{c^2}+\frac{\partial^2}{\partial z^2}\right)D_{qq}(z,z')-iq\frac{\partial}{\partial z}D_{zq}(z,z') =-\frac{4\pi\omega^2}{c^2}\delta(z-z'), \tag{B4}$$

$$\gamma^2 D_{zq}(z,z')-iq\frac{\partial}{\partial z}D_{qq}(z,z')=0, \tag{B5}$$

$$\gamma^2 D_{zz}(z,z')-iq\frac{\partial}{\partial z}D_{qz}(z,z')=-\frac{4\pi\omega^2}{c^2}\delta(z-z'), \tag{B6}$$

$$\gamma^2 D_{qz}(z,z')+iq\frac{\partial}{\partial z'}D_{qq}(z,z')=0. \tag{B7}$$

The components D_{qn} and D_{zn} of the Green's function vanish, since the equations for them turn out to be homogeneous. Solving the system of Eqs. (B3)–(B7) amounts to solving two equations: Eq. (B3) for D_{nn} and the equation for D_{qq} which follows from Eqs. (B4) and (B5),

$$\left(\gamma^2+\frac{\partial^2}{\partial z^2}\right)D_{qq}(z,z')=-4\pi\gamma^2\delta(z-z'), \tag{B8}$$

after which D_{qz}, D_{zq}, and D_{zz} for $z\neq z'$ are obtained as

$$D_{qz}=-\frac{iq}{\gamma^2}\frac{\partial}{\partial z'}D_{qq},\quad D_{zq}=\frac{iq}{\gamma^2}\frac{\partial}{\partial z}D_{qq}, \tag{B9}$$

$$D_{zz}=\frac{q^2}{\gamma^4}\frac{\partial^2}{\partial z\partial z'}D_{qq}. \tag{B10}$$

In the vacuum gap $0<z<d$ the solution of Eq. (B3) has the form

$$D_{nn}(z,z')=\frac{2\pi i\omega^2}{\gamma c^2}e^{i\gamma|z-z'|}+v_n e^{i\gamma z}+w_n e^{-i\gamma z}. \tag{B11}$$

At the boundaries $z=0$ and $z=d$ the amplitude of the scattered wave is equal to the amplitude of the incident wave times the corresponding reflection amplitude. The Green's function D_{nn} satisfies the same boundary conditions as the s-polarized electromagnetic field, and the boundary conditions for it give

$$v_n=R_{1s}\left(w_n+\frac{2\pi i\omega^2}{\gamma c^2}e^{ipz'}\right)\quad \text{for } z=0, \tag{B12}$$

$$w_n=R_{2s}e^{2i\gamma d}\left(v_n+\frac{2\pi i\omega^2}{\gamma c^2}e^{-ipz'}\right)\quad \text{for } z=d. \tag{B13}$$

Using Eqs. (B11)–(B13) we get

$$D_{nn}(z,z')=\frac{2\pi i\omega^2}{\gamma c^2}\left\{e^{i\gamma|z-z'|}+\frac{R_{1s}R_{2s}e^{2i\gamma d}(e^{i\gamma(z-z')}+e^{-i\gamma(z-z')})}{\Delta_s}+\frac{R_{1s}e^{i\gamma(z+z')}+R_{2s}e^{2i\gamma d}e^{-i\gamma(z+z')}}{\Delta_s}\right\}, \tag{B14}$$

$$\Delta_s=1-e^{2i\gamma d}R_{2s}R_{1s}. \tag{B15}$$

Equation (B8) for D_{qq} is similar to Eq. (B3) for D_{nn}, and the equation for D_{qq} can be obtained from Eq. (B14) by replacement of the reflection amplitude

$$D_{qq}=\left(\frac{\gamma c}{\omega}\right)^2 D_{nn}[R_s\to -R_p]. \tag{B16}$$

In our approach, calculation of the reflection amplitude for s- and p-polarized waves constitutes a separate problem, which can be solved taking into account nonlocal effects. For the local optical case the reflection amplitudes are determined by the well-known Fresnel formulas

$$R_{ip}=\frac{\varepsilon_i\gamma-\gamma_i}{\varepsilon_i\gamma+\gamma_i},\quad R_{is}=\frac{\gamma-\gamma_i}{\gamma+\gamma_i}, \tag{B17}$$

where ε_i is the complex dielectric constant for body i:

$$\gamma_i=\sqrt{\frac{\omega^2}{c^2}\varepsilon_i-q^2}. \tag{B18}$$

For a body that is homogeneous in the x-y plane, the second term in Eq. (20) can be written as

$$\nabla'_k\langle E_k(\mathbf{r})E_z^*(\mathbf{r}')\rangle_{\mathbf{r}=\mathbf{r}'}=\nabla_k\langle E_k(\mathbf{r})E_z^*(\mathbf{r})\rangle=\nabla_z\langle E_z(\mathbf{r})E_z^*(\mathbf{r})\rangle. \tag{B19}$$

This term is purely real and does not give any contribution to the z component of the Poynting vector. Using Eqs. (B9), (B10), and (21) in Eq. (20) we get

$$\langle S_z\rangle_\omega=\frac{c^4[\Pi_1(\omega)-\Pi(\omega)]}{64\pi^3\omega^4}\int\frac{d^2\mathbf{q}}{(2\pi)^2}\times\left\{\left(D_{nn}\frac{\partial^2}{\partial z\partial z'}D_{nn}^*(z,z')-\frac{\partial}{\partial z}D_{nn}^*\frac{\partial}{\partial z'}D_{nn}(z,z')\right)+\left(\frac{\omega}{\gamma c}\right)^4([n\to q])+\text{c.c.}\right\}_{z\to z'}. \tag{B20}$$

Using Eqs. (B14) and (B16), in Eq. (B20) we finally get Eq. (23).

APPENDIX C: REFLECTION AMPLITUDES FOR A 2D QUANTUM WELL

The reflection amplitudes for a 2D electron system are determined by (Volokitin and Persson, 2001c)

$$R_{1s(p)} = \frac{\varepsilon_{1s(p)} - 1}{\varepsilon_{1s(p)} + 1},$$

$$\varepsilon_{1s} = \frac{4\pi\omega\sigma_t}{\gamma c^2} + 1, \quad \varepsilon_{1p} = \frac{4\pi\gamma\sigma_l}{\omega\varepsilon} + 1, \tag{C1}$$

where σ_l and σ_t are the transverse and longitudinal conductivities of the layer. The longitudinal conductivity can be written as

$$\sigma_l(\omega,q) = \frac{-i\omega}{q^2}\chi_l(\omega,q), \tag{C2}$$

where χ_l is the finite-lifetime generalization of the longitudinal 2D Lindhard response function, which according to Mermin (1970) can be written as

$$\chi_l(\omega,Q) = \frac{(1+i/\omega\tau)\chi_l^0(\omega+i/\tau,Q)}{1+(i/\omega\tau)\chi_l^0(\omega+i/\tau,Q)/\chi_l^0(0,Q)}, \tag{C3}$$

where for a degenerate electron gas

$$\chi_l^0(\omega,q) = \frac{n_s e^2}{z m^* v_F^2}\{2z + \sqrt{(u-z)^2-1} - \sqrt{(u+z)^2-1}\}, \tag{C4}$$

with τ the relaxation time, $z=q/2k_F$, $u=\omega/qv_F$, and k_F and v_F the Fermi wave vector and Fermi velocity, respectively, and n_s the 2D electron density in the layer. The transverse conductivity of the layer is

$$\sigma_t(\omega,q) = -\frac{in_s e^2}{3(\omega+i\tau^{-1})m^* z}\{[(u'+z)^2-1]^{3/2} - [(u'-z)^2-1]^{3/2} - 2z[3u'^2+z^2]\}, \tag{C5}$$

where $u'=(\omega+i\tau^{-1})/qv_F$. For a nondegenerate electron gas the longitudinal conductivity is determined by Eq. (C2) with

$$\chi_l^0(\omega,q) = \frac{n_s e^2}{k_B T}\left[1 + F\left(\frac{\omega}{\sqrt{2}qv_T}\right)\right], \tag{C6}$$

and the transverse conductivity is

$$\sigma_t(\omega,q) = -\frac{in_s e^2}{m^*(\omega+i\tau^{-1})}F\left(\frac{\omega+i\tau^{-1}}{\sqrt{2}qv_T}\right), \tag{C7}$$

where $v_T=\sqrt{k_B T/m^*}$ and m^* is the effective electron mass, and the function $F(x)$ is defined by the integral

$$F(x) = \frac{x}{\sqrt{\pi}}\int_{-\infty}^{+\infty} dz \frac{e^{-z^2}}{z-x-i0}. \tag{C8}$$

APPENDIX D: FRICTION COEFFICIENT FOR POINT CHARGES MOVING RELATIVE TO A PLANE SURFACE

Consider a semi-infinite metal having a flat surface which coincides with the x-y coordinate plane, and with the z axes pointed along the upward normal. The electric field above the flat surface can be represented by the Fourier integral

$$\mathbf{E}(\mathbf{r}) = \int \frac{d^2q}{(2\pi)^2} e^{i\mathbf{q}\cdot\mathbf{r}-i\omega t}\mathbf{E}(\mathbf{q},z), \tag{D1}$$

with a similar expression for the magnetic induction field $\mathbf{B}(\mathbf{r})$. For $q \gg \omega/c$ the electric and magnetic induction fields at $z>0$ can be written as

$$\mathbf{E}(\mathbf{q},z) = v_{0q}[\hat{\mathbf{z}}(e^{qz} + R_p e^{-qz}) + \hat{\mathbf{q}}i(e^{qz} - R_p e^{-qz})], \tag{D2}$$

$$\mathbf{B}(\mathbf{q},z) = -\frac{\omega}{cq}\hat{\mathbf{n}}E_z(\mathbf{q},z), \tag{D3}$$

where $\hat{n}=\hat{z}\times\hat{q}$ and R_p is the reflection amplitude for the p-polarized electromagnetic field. The energy dissipation induced by the electromagnetic field in the bulk of the metal is determined by integrating the Poynting vector over the surface of the metal, and is

$$\dot{Q} = -\frac{c}{4\pi}\int \frac{d^2q}{(2\pi)^2}(E_{\mathbf{q}}B_{\mathbf{n}}^* + \text{c.c.}) = \frac{\omega}{\pi}\int \frac{d^2q}{(2\pi)^2 q}\,\text{Im}\,R(\omega)|v_{0q}|^2. \tag{D4}$$

Consider now a point charge e_i located at $(\mathbf{r}_i, d+z_i)$, and performing small-amplitude vibrations with the vibrational coordinate $\mathbf{u}(t)=\hat{\mathbf{z}}u_0 e^{-i\omega t}$. In this case

$$v_{0q} = -2\pi i u_0 \sum_i e_i e^{i\mathbf{q}\cdot\mathbf{r}_i - q(d+z_i)} q_x. \tag{D5}$$

Taking into account that the energy dissipation per unit time must be equal to $2\omega^2\Gamma|u_0|^2$, using Eqs. (D4) and (D5) gives the friction coefficient

$$\Gamma_\parallel = \lim_{\omega\to 0}\int_0^\infty \frac{d^2q}{\pi q} q_x^2 e^{-2qd}\frac{\text{Im}\,R_p(\omega,q)}{\omega}\left|\sum_i e_i e^{i\mathbf{q}\cdot\mathbf{r}_i - qz_i}\right|^2. \tag{D6}$$

For a uniformly charged wire with the length w passing through point $z=d$ along the y axis, from Eq. (D6) we get

$$\Gamma_\parallel = \lim_{\omega\to 0} Q^2\int_{-\infty}^{\infty} dq_x \int_{-\infty}^{\infty} dq_y \frac{q_x^2}{2\pi q} e^{-2qd} \times \frac{\text{Im}\,R(q,\omega)}{\omega}\left|\int_{-w/2}^{w/2} dy e^{iq_y y}\right| = \lim_{\omega\to 0} Q^2 w\int_{-\infty}^{\infty} dq_x \int_{-\infty}^{\infty} dq_y \frac{q_x^2}{q} e^{-2qd}\frac{\text{Im}\,R(q,\omega)}{\omega}\delta(q_y) = \lim_{\omega\to 0} 2Q^2 w\int_0^\infty dq_x q_x e^{-2q_x d}\frac{\text{Im}\,R(q_x,\omega)}{\omega}. \tag{D7}$$

REFERENCES

Abrikosov, A. A., L. P. Gor'kov, and I. Y. Dzyaloshinskii, 1965, *Quantum Field Theoretical Methods in Statistical Physics* (Pergamon, Oxford).
Agarwal, G. S., 1975, Phys. Rev. A **11**, 230.
Arkani-Hamed, N., S. Dimopoulos, and G. Dvali, 1998, Phys.

Lett. B **429**, 263.
Barnes, J. R., R. J. Stephenson, M. E. Welland, C. Gerber, and J. K. Gimzewski, 1994, Nature (London) **372**, 79.
Beckerle, J. D., M. P. Casassa, E. J. Heilweil, R. R. Cavanagh, and J. C. Stephenson, 1990, in *Vibrations at Surfaces 1990*, edited by Y. T. Chabal, F. M. Hoffmann, and G. P. Williams (Elsevier, New York), p. 17.
Berman, G. P., G. D. Doolen, P. C. Hammel, and V. I. Tsifrinovich, 2000, Phys. Rev. B **61**, 14694.
Bockrath, M., D. H. Gobden, J. Lu, A. G. Rinzler, R. E. Smalley, L. Balents, and P. L. McEuen, 1999, Nature (London) **397**, 598.
Callen, H. R., and T. A. Welton, 1951, Phys. Rev. **83**, 34.
Carminati, R., and J. J. Greffet, 1999, Phys. Rev. Lett. **82**, 1660.
Chang, H. C., and G. E. Ewing, 1990, in *Vibrations at Surfaces 1990*, edited by Y. Chabal, F. Hoffmann, and G. Williams (Elsevier, New York), p. 39.
Chang, H. C., H. H. Richardson, and G. E. Ewing, 1988, J. Chem. Phys. **89**, 7561.
Chumak, A. A., P. W. Milonni, and G. P. Berman, 2004, Phys. Rev. B **70**, 085407.
Cleland, A. N., 2002, *Foundations of Nanomechanics: From Solid State Theory to Device Applications* (Springer-Verlag, New York).
d'Agliano, E. G., P. Kumar, W. Schaich, and H. Suhl, 1975, Phys. Rev. B **11**, 2122.
Debye, P., 1929, *Polar Molecules* (Chemical Catalog, New York).
Dedkov, G. V., and A. A. Kyasov, 1999, Phys. Lett. A **259**, 38.
Dedkov, G. V., and A. A. Kyasov, 2000, Surf. Sci. **259**, 38.
Domingues, G., S. Volz, K. Joulain, and J. J. Greffet, 2005, Phys. Rev. Lett. **94**, 085901.
Dorofeyev, I., H. Fuchs, G. Wenning, and B. Gotsmann, 1999, Phys. Rev. Lett. **83**, 2402.
Dzyaloshinskii, I. E., E. M. Lifshitz, and L. P. Pitaevskii, 1961, Adv. Phys. **10**, 165.
Ederth, T., 2000, Phys. Rev. A **62**, 062104.
Egger, R., 1999, Phys. Rev. Lett. **83**, 5547.
Egger, R., and A. O. Gogolin, 1997, Phys. Rev. Lett. **79**, 5082.
Egger, R., and A. O. Gogolin, 1998, Eur. Phys. J. B **3**, 281.
Forster, T. H., 1948, Ann. Phys. **6**, 55.
Ghosh, S., A. K. Sood, and N. Kumar, 2003, Science **299**, 1042.
Ghosh, S., A. K. Sood, S. Ramaswamy, and N. Kumar, 2004, Phys. Rev. B **70**, 205423.
Gotsmann, B., and H. Fuchs, 2001, Phys. Rev. Lett. **86**, 2597.
Gramila, T. J., J. P. Eisenstein, A. H. MacDonald, L. N. Pfeiffer, and K. W. West, 1991, Phys. Rev. Lett. **66**, 1216.
Gramila, T. J., J. P. Eisenstein, A. H. MacDonald, L. N. Pfeiffer, and K. W. West, 1992, Surf. Sci. **263**, 446.
Gramila, T. J., J. P. Eisenstein, A. H. MacDonald, L. N. Pfeiffer, and K. W. West, 1993, Phys. Rev. B **47**, 12957.
Gramila, T. J., J. P. Eisenstein, A. H. MacDonald, L. N. Pfeiffer, and K. W. West, 1994, Physica B **197**, 442.
Greffet, J. J., R. Carminati, K. Joulain, J. P. Mulet, S. Mainguy, and Y. Chen, 2002, Nature (London) **416**, 61.
Hahn, J. R., and W. Ho, 2001, Phys. Rev. Lett. **87**, 166102.
Hargreaves, C. M., 1969, Phys. Lett. **30A**, 491.
Hartmann, U., 1990, Phys. Rev. B **42**, 1541.
Hartmann, U., 1991, Phys. Rev. B **43**, 2404.
Henkel, C., and K. Joulain, 2006, Appl. Phys. B: Lasers Opt. **84**, 61.
Hu, B.-K., A. P. Jauho, and J. M. Kinaret, 1995, Phys. Rev. B **52**, 14761.
Hudlet, S., M. S. Jean, C. Guthmann, and J. Berger, 1998, Eur. Phys. J. B **2**, 5.
Hunger, T., B. Lengeler, and J. Appenzeller, 2004, Phys. Rev. B **69**, 195406.
Jauho, A. P., and H. Smith, 1993, Phys. Rev. B **47**, 4420.
Johansson, P., and P. Apell, 1997, Phys. Rev. B **56**, 4159.
Joulain, K., J. P. Mulet, F. Marquier, R. Carminati, and J. J. Greffet, 2005, Surf. Sci. Rep. **57**, 59.
Kamenev, A., and Y. Oreg, 1995, Phys. Rev. B **52**, 7516.
Kang, N., L. Lu, W. J. Kong, J. S. Hu, W. Yi, Y. P. Wang, D. L. Zhang, Z. W. Pan, and S. S. Xie, 2003, Phys. Rev. B **67**, 033404.
Kasumov, A., M. Kociak, M. Ferrier, R. Deblock, S. Guéron, B. Reulet, I. Khodos, O. Stéphan, and H. Bouchiat, 2003, Phys. Rev. B **68**, 214521.
Kittel, A., W. Müller-Hirsch, J. Parisi, S. Biehs, D. Reddig, and M. Holthaus, 2005, Phys. Rev. Lett. **95**, 224301.
Kliewer, K. L., and R. Fuchs, 1968, Phys. Rev. **172**, 607.
Kliewer, K. L., and R. Fuchs, 1969, Phys. Rev. **186**, 905.
Komeda, T., Y. Kim, M. Karai, B. N. J. Persson, and H. Ueba, 2002, Science **295**, 2055.
Kovac, J. M., E. M. Leitch, C. Pryke, J. E. Carlstom, N. W. Halverson, and W. L. Holzapfel, 2002, Nature (London) **420**, 772.
Kreiter, M., J. Oster, R. Sambles, S. Herminghaus, S. Mittler-Neher, and W. Knoll, 1999, Opt. Commun. **168**, 117.
Krishnan, A., T. Thio, T. J. Kim, H. J. Lezec, T. W. Ebbesen, P. A. Wolf, J. Pendry, L. Martin-Moreno, and F. J. Garcia-Vidal, 2001, Opt. Commun. **200**, 1.
Krstić, V., S. Blumentritt, J. Muster, S. Roth, and A. Rubio, 2003, Phys. Rev. B **67**, 041401.
Kuehn, S., R. F. Loring, and J. A. Marohn, 2006, Phys. Rev. Lett. **96**, 156103.
Kuehn, S., J. A. Marohn, and R. F. Loring, 2006, J. Phys. Chem. B **110**, 14525.
Landau, L. D., and E. M. Lifshitz, 1960, *Electrodynamics of Continuous Media* (Pergamon, Oxford).
Landau, L. D., and E. M. Lifshitz, 1970, *Statistical Physics* (Pergamon, Oxford).
Lang, N. D., and W. Kohn, 1971, Phys. Rev. B **3**, 1215.
Langreth, D. C., 1989, Phys. Rev. B **39**, 10020.
Laroche, M., C. Arnold, F. Marquier, R. Carminari, J. J. Greffet, S. Collin, N. Bardou, and J. L. Pelouard, 2005, Opt. Lett. **30**, 2623.
Levin, M. L., V. G. Polevoy, and S. M. Rytov, 1980, Sov. Phys. JETP **52**, 1054.
Levin, M. L., and S. M. Rytov, 1967, *Theory of Eqilibrium Thermal Fluctuations in Electrodynamics* (Science, Moscow).
Levitov, L. S., 1989, Europhys. Lett. **8**, 499.
Lide, C. R., 2001, Ed., *CRC Handbook of Chemistry and Physics* (CRC, Boca Raton, FL).
Lifshitz, E. M., 1956, Sov. Phys. JETP **2**, 73.
Lifshitz, E. M., and L. P. Pitaevskii, 1980, *Statistical Physics: Theory of the Condensed State* (Pergamon, Oxford).
Lifshitz, E. M., and L. P. Pitaevskii, 1981, *Physical Kinetics* (Pergamon, Oxford).
Liu, Z. H., N. M. D. Brown, and A. McKinley, 1997, J. Phys.: Condens. Matter **9**, 59.
Loomis, J. J., and H. J. Maris, 1994, Phys. Rev. B **50**, 18517.
Mahan, G., 1990, *Many-Particle Physics* (Plenum, New York).
Mahanty, J., 1980, IBM J. Res. Dev. **13**, 4391.
Majumdar, A., 1999, Annu. Rev. Mater. Sci. **29**, 505.
Mamin, H. J., and D. Rugar, 2001, Appl. Phys. Lett. **79**, 3358.

Marquier, F., K. Joulain, J. P. Mulet, R. Carminati, and J. J. Greffet, 2004, Opt. Commun. **237**, 379.
McClintock, F.A., and A. S. Argon, 1966, *Mechanical Behavior of Material* (Addison-Wesley, Reading, MA).
Mermin, N. D., 1970, Phys. Rev. B **1**, 2362.
Mkrtchian, V. E., 1995, Phys. Lett. A **207**, 299.
Mkrtchian, V., V. A. Parsegian, R. Podgornik, and W. M. Saslow, 2003, Phys. Rev. Lett. **91**, 220801.
Mohideen, U., and A. Roy, 1998, Phys. Rev. Lett. **81**, 4549.
Mulet, J. P., K. Joulin, R. Carminati, and J. J. Greffet, 2001, Appl. Phys. Lett. **78**, 2931.
Mulet, J. P., K. Joulin, R. Carminati, and J. J. Greffet, 2002, Microscale Thermophys. Eng. **6**, 209.
Müller-Hirsch, W., A. Kraft, M. Hirsch, J. Parisi, and A. Kittel, 1999, J. Vac. Sci. Technol. A **17**, 1205.
Nourtier, A., 1977, J. Phys. (Paris) **38**, 479.
Palik, E. D., 1985, *Handbook of Optical Constants of Solids* (Academic, San Diego, CA).
Pascual, J. I., N. Lorente, Z. Song, H. Conrad, and H.-P. Rust, 2003, Nature (London) **432**, 525.
Peebles, P. J. E., 1993, *Principles of Physical Cosmology* (Princeton University Press, Princeton, NJ).
Pendry, J. B., 1983, J. Phys. A **16**, 2161.
Pendry, J. B., 1997, J. Phys.: Condens. Matter **9**, 10301.
Pendry, J. B., 1999, J. Phys.: Condens. Matter **11**, 6621.
Persson, B. N. J., 1991, Phys. Rev. B **44**, 3277.
Persson, B. N. J., 1998, Surf. Sci. **401**, 445.
Persson, B. N. J., 2000, *Sliding Friction: Physical Principle and Applications* (Springer, Heidelberg).
Persson, B. N. J., 2001, J. Chem. Phys. **115**, 3840.
Persson, B. N. J., T. Kato, H. Ueba, and A. I. Volokitin, 2001, Phys. Rev. B **75**, 193404.
Persson, B. N. J., and M. Persson, 1980, Solid State Commun. **36**, 175.
Persson, B. N. J., and R. Ryberg, 1985, Phys. Rev. B **32**, 3586.
Persson, B. N. J., U. Tartaglino, E. Tosatti, and H. Ueba, 2004, Phys. Rev. B **69**, 235410.
Persson., B. N. J., and A. I. Volokitin, 2000, Phys. Rev. Lett. **84**, 3504.
Persson, B. N. J., and Z. Zhang, 1988, Phys. Rev. B **57**, 7327.
Pogrebinskii, M. B., 1977, Sov. Phys. Semicond. **11**, 372.
Polder, D., and M. Van Hove, 1971, Phys. Rev. B **4**, 3303.
Polevoi, V. G., 1990, Sov. Phys. JETP **71**, 1119.
Pralle, M. U., 2002, Appl. Phys. Lett. **81**, 4685.
Price, P. J., 1983, Physica B & C **117**, 750.
Rast, S., U. Gysin, E. Meyer, and D. W. Lee, 2007, in *Fundamentals of Friction and Wear on the Nanoscale*, edited by E. Gnecco and E. Meyer (Springer, Berlin), pp. 437–451.
Rossi, F., and G. I. Opat, 1992, J. Phys. D **25**, 1349.
Rugar, D., R. Budakian, H. J. Mamin, and B. W. Chui, 2004, Nature (London) **430**, 329.
Rytov, S. M., 1953, *Theory of Electrical Fluctuation and Thermal Radiation* (Academy of Science of USSR, Moscow).
Rytov, S. M., Y. A. Kravtsov, and V. I. Tatarskii, 1989, *Principles of Statistical Radiophyics* (Springer, New York), Vol. 3.
Schaich, W. L., 1974a, J. Chem. Phys. **60**, 1087.
Schaich, W. L., 1974b, Solid State Commun. **60**, 1087.
Schaich, W. L., and J. Harris, 1981, J. Phys. F: Met. Phys. **11**, 65.
Schmid, H., H. Biebuyck, B. Michel, and O. J. F. Martin, 1998, Appl. Phys. Lett. **72**, 2379.
Senet, P., J. P. Toennis, and G. Witte, 1999, Chem. Phys. Lett. **299**, 389.
Sernelius, B. E., 2001, *Surface Modes in Physics* (Wiley-VCH Verlag, Berlin).
Shchegrov, A. V., K. Joulain, R. Carminati, and J. J. Greffet, 2000, Phys. Rev. Lett. **85**, 1548.
Sidles, J. A., J. L. Carbini, K. J. Bruland, D. Rugar, O. Zuger, S. Hoen, and C. S. Yannoni, 1995, Rev. Mod. Phys. **67**, 249.
Sivan, U., P. M. Solomon, and H. Shtrikman, 1992, Phys. Rev. Lett. **68**, 1196.
Speake, C. C., and C. Trenkel, 2003, Phys. Rev. Lett. **90**, 160403.
Stipe, B. C., H. J. Mamin, T. D. Stowe, T. W. Kenny, and D. Rugar, 2001, Phys. Rev. Lett. **87**, 096801.
Stowe, T. D., D. J. T., W. Kenn, and D. Rugar, 1999, Appl. Phys. Lett. **75**, 2785.
Sukenik, C. I., M. G. Boshier, V. S. D. Cho, and E. A. Hinds, 1993, Phys. Rev. Lett. **70**, 560.
Tarkiainen, R., M. Ahlskog, J. Penttilä, L. Roschier, P. Hakonen, M. Paalanen, and E. Sonin, 2001, Phys. Rev. B **64**, 195412.
Teodorovitch, E. V., 1978, Proc. R. Soc. London, Ser. A **362**, 71.
Tomassone, S., and A. Widom, 1997, Phys. Rev. B **56**, 4938.
Tso, H. C., and P. Vasilopoulos, 1992, Phys. Rev. B **45**, 1333.
Volokitin, A. I., and B. N. J. Persson, 1993, in *Inelastic Energy Transfer in Interactions with Surfaces and Adsorbates*, edited by B. Gumhalter, A. C. Levi, and F. Flores (World Scientific, Singapore), pp. 217–248.
Volokitin, A. I., and B. N. J. Persson, 1998, Phys. Low-Dimens. Struct. **7/8**, 17.
Volokitin, A. I., and B. N. J. Persson, 1999, J. Phys.: Condens. Matter **11**, 345.
Volokitin, A. I., and B. N. J. Persson, 2001a, Phys. Rev. B **63**, 205404.
Volokitin, A. I., and B. N. J. Persson, 2001b, Phys. Low-Dimens. Struct. **5/6**, 151.
Volokitin, A. I., and B. N. J. Persson, 2001c, J. Phys.: Condens. Matter **13**, 859.
Volokitin, A. I., and B. N. J. Persson, 2002, Phys. Rev. B **65**, 115419.
Volokitin, A. I., and B. N. J. Persson, 2003a, JETP Lett. **78**, 457.
Volokitin, A. I., and B. N. J. Persson, 2003b, Phys. Rev. Lett. **91**, 106101.
Volokitin, A. I., and B. N. J. Persson, 2003c, Phys. Rev. B **68**, 155420.
Volokitin, A. I., and B. N. J. Persson, 2004, Phys. Rev. B **69**, 045417.
Volokitin, A. I., and B. N. J. Persson, 2005, Phys. Rev. Lett. **94**, 086104.
Volokitin, A. I., and B. N. J. Persson, 2006, Phys. Rev. B **74**, 205413.
Volokitin, A. I., B. N. J. Persson, and H. Ueba, 2006, Phys. Rev. B **73**, 165423.
Wilde, Y. D., F. Formanek, R. Carminati, B. Gralak, P. A. Lemoire, K. Joulain, J. P. Mulet, Y. Chen, and J. J. Greffet, 2006, Nature (London) **444**, 740.
Xu, J.-B, K. L., R. Möller, K. Dransfeld, and I. H. Wilson, 1994, J. Appl. Phys. **76**, 7209.
Zheng, L., and A. H. MacDonald, 1993, Phys. Rev. B **48**, 8203.
Zurita-Sánchez, R., J. J. Greffet, and L. Novotny, 2004, Phys. Rev. A **69**, 022902.